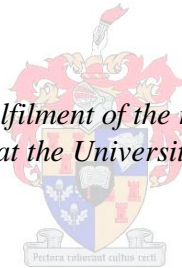


**Experimental supply demand analysis of
yeast fermentative free energy metabolism:
an *in vivo* and *in situ* investigation**

by
Justin Alan Smith

*Thesis presented in partial fulfilment of the requirements for the degree
Master of Science at the University of Stellenbosch*



Supervisor: Prof. Johann M. Rohwer
Co-supervisor: Prof. Jacky L. Snoep
Faculty of Natural Sciences
Department of Biochemistry

December 2010

Declaration

By submitting this thesis/dissertation electronically, I declare that the entirety of the work contained therein is my own, original work, and that I have not previously in its entirety or in part submitted it for obtaining any qualification.

December 2010

Acknowledgements

I would like to give special thanks the following people and organizations:

My supervisors Professor Johann Rohwer and Professor Jacky Snoep. Thank you for giving me the opportunity to further my studies in the field of biochemistry and for all guidance and advice.

My lab manager Arrie Arends. Thank you for all the technical support and for managing the lab efficiently.

To Arno Hanekom, for teaching me the ropes and being a mentor.

To Dr. Jaco Brand, Jean McKenzie and Elsa Malherbe, for all the help with the practical aspects of NMR spectroscopy.

To all my colleagues and fellow students for all the after hour conversations and for creating a positive atmosphere to work in.

The South African National Research Foundation, for funding my work.

Abstract

Yeast glycolytic flux control has been much debated in the past, with both the classical approach as well as metabolic control analysis (MCA) postulating total flux control by enzymes intrinsic to the pathway; however, with the advent of supply demand analysis the notion of extrinsic flux control by the demand for pathway product is gaining acceptance. This study aims to quantify the extent to which glycolytic flux control is distributed between the supply of and demand for free energy (expressed as the [ATP] / [ADP]) ratio in the yeast *Saccharomyces cerevisiae*.

Batch fermentations were assessed under non-growing conditions in both intact and permeabilized (*in situ*) yeast cell suspensions. Free energy supply (glycolysis) and demand (cell maintenance) were independently modulated in whole cells by titrating with maltose (glucose uptake inhibitor) and benzoic acid (un-coupler) respectively. The *in situ* [ATP] / [ADP] ratio was perturbed by varying the initial concentrations of ATP and ADP added to the system prior to the start of fermentation. Glycolytic fluxes were measured using ¹³C NMR (nuclear magnetic resonance) spectroscopy and the [ATP] / [ADP] ratio was quantified by means of ³¹P NMR spectroscopy.

Under the prevailing conditions (energy excess), the majority of glycolytic flux control was situated in the supply block ($C_{supply}^J = 0.75$, $C_{demand}^J = 0.25$). Abnormal glycolytic behavior was displayed during fermentation in permeabilized yeast, characterized by elevated sugar phosphates (FBP) and low internal ATP. This phenomenon, termed the “turbo effect” is analogous to the conduct observed in $\Delta TPS1$ yeast mutants (lacking the enzyme *trehalose-6-phosphate-synthase*) and is caused by the unregulated flow of glucose into glycolysis. The *in situ* ethanol production rate was shown to be sensitive to varying [ATP] / [ADP], yielding a response coefficient ($R_{[ATP]/[ADP]}^{J_{EtOH}}$) of 0.74.

Intrinsic control by the supply block points to the significance of steps such as glucose transport in determining the steady state glycolytic flux. The “turbo” like behavior observed in permeabilized yeast emphasizes the importance of a functional regulatory feedback loop that restricts the flow of glucose into glycolysis.

Opsomming

Die beheer van glikolitiese fluksie in gis is al lank 'n onderwerp van wetenskaplike debat. Die klassieke siening asook metaboliese kontrole-analise (MKA) postuleer dat die fluksie beheer word deur ensieme in die pad self. Die ontwikkeling van vraag-aanbod analise het egter beklemtoon dat ekstrinsieke fluksie-beheer (deur die vraag na die metaboliese pad se produk) nie geïgnoreer mag word nie. Hierdie studie poog om die beheer oor glikolitiese fluksie in terme van die vraag na en aanbod van vrye energie (gemeet in terme van die $[ATP] / [ADP]$ verhouding) in die gis *Saccharomyces cerevisiae* te bepaal.

Lot-fermentasies is onder nie-groeiende kondisies in intakte sowel as membraan-gepermeabiliseerde (*in situ*) gissuspensies uitgevoer. Die vraag na vrye energie (deur selonderhoudsreaksies) asook die aanbod daarvan (deur glikolise) is in heel selle onafhanklik gemoduleer d.m.v. titrasie met bensoësuur (onkopleaar) en maltose (glukosetransport-inhibitor). Die *in situ* $[ATP] / [ADP]$ verhouding is geperturbeer deur die beginkonsentrasies van ATP en ADP voor die aanvang van fermentasie te varieer. Die glikolitiese fluksie en $[ATP] / [ADP]$ verhouding is bepaal met behulp van onderskeidelik ^{13}C en ^{31}P -KMR (kernmagnetiese resonansie) spektroskopie.

Onder die gegewe kondisies (energie-oormaat), het die aanbod-blok die grootste deel van die glikolitiese fluksie beheer ($C_{aanbod}^J = 0.75$ & $C_{vraag}^J = 0.25$). Die gepermeabiliseerde gis het abnormale gedrag tydens fermentasie getoon, wat gekenmerk is deur groot hoeveelhede suikerfosfate en lae $[ATP]$. Hierdie fenomeen, bekend as die “turbo-effek,” is vergelykbaar met die metaboliese gedrag wat in $\Delta TPS1$ gismutante (wat die ensiem *trehalose-6-fosfaat-sintase* kort) waargeneem word, en veroorsaak word deur die ongereguleerde vloeï van glukose na glikolise. Die *in situ* etanolproduksiesnelheid is beïnvloed deur veranderings in die $[ATP] / [ADP]$ verhouding met 'n responskoëffisiënt ($R_{[ATP]/[ADP]}^{J_{EtOH}}$) van 0.74.

Intrinsieke fluksiebeheer deur die aanbodblok dui op die belang van stappe soos glukosetransport om die glikolitiese fluksie te bepaal. Die waargenome “turbo-effek” in gepermeabiliseerde giste beklemtoon verder die noodsaaklikheid van 'n regulatoriese terugvoerstelsel wat die vloeï van glukose in glikolise in beperk.

Acronyms

Miscellaneous

NMR	nuclear magnetic resonance
EMR	electromagnetic radiation
TEP	triethyl-phosphate
SDA	supply demand analysis
ESDA	experimental supply demand analysis
GC	gas chromatography
MS	mass spectrometry
MCA	metabolic control analysis
PCA	perchloric acid
PIPES	piperazine-1,4-bis(2-ethanesulfonic acid)
MES	2-(N-morpholino) ethanesulfonic acid
TMS	tetramethylsilane
c/u	charged to uncharged nucleotide ratio

Enzymes

HK	hexokinase (EC: 2.7.1.1)
PGI	phosphoglucoisomerase (EC: 5.3.1.9)
PFK	phosphofructokinase (EC: 2.7.1.146)
ALD	aldolase (EC: 2.1.2.1)
TPI	triosephosphate isomerase (EC: 5.3.1.1)
GAPDH	glyceraldehyde 3 phosphate dehydrogenase (EC: 1.2.1.12)
PGK	phosphoglycerokinase (EC: 2.7.2.3)
PGM	phosphoglyceromutase (EC: 5.4.2.2)
ENO	enolase (EC: 4.2.1.11)
PK	pyruvate kinase (EC: 2.7.1.40)
PDC	pyruvate decarboxylase (EC 4.1.1.1)
ADH	alcohol dehydrogenase (EC: 1.1.1.1)
CrK	creatine kinase (EC: 2.7.3.2)

Metabolites

Glc	D-glucose
GP	glycero-phosphates
G6P	glucose-6-phosphate
F6P	fructose-6-phosphate
FBP	fructose-1,6-bisphosphate
F1,6 BP	fructose-1,6-bisphosphate
GAP	glyceraldehyde-3-phosphate
DHAP	dihydroxyacetone phosphate
1, 3 BPG	1, 3-bisphosphoglyceric acid
3PG	3-phosphoglyceric acid
2PG	2-phosphoglyceric aid
PEP	phosphoenol pyruvate
PYR	pyruvate
AcAld	acetaldehyde
EtOH	ethanol
TPP	thiamine pyrophosphate

Contents

Preface	1
Aims and outline	3
Chapter one: Literature Study and Background	5
1.1 Overview of metabolism with specific focus on yeast glycolysis	5
1.1.1 <i>Metabolism and its principles</i>	5
1.1.2 <i>Yeast glycolysis</i>	6
1.1.3 <i>Energetics of alcoholic fermentation</i>	9
1.1.4 <i>Metabolic regulation and control</i>	10
1.1.5 <i>Allosteric regulation of yeast glycolysis</i>	11
1.2 Metabolic Control Analysis	12
1.2.1 <i>Local Properties</i>	13
1.2.2 <i>Global Properties</i>	14
1.2.3 <i>Summation theorems</i>	15
1.2.4 <i>Connectivity Theorems</i>	16
1.3 Supply-demand Analysis	16
1.3.1 <i>Theoretical background</i>	17
1.3.2 <i>Experimental supply-demand analysis</i>	21
1.4 Kinetic modeling	22
1.4.1 <i>The kinetic model for yeast glycolysis as developed by Teusink et al.</i>	23
1.5 Chemical differences between the test-tube and the cytoplasm	26
1.5.1 <i>Chemical differences and similarities</i>	26
1.5.2 <i>Implications for cellular thermodynamics and reaction kinetics</i> ..	28
1.6 Nuclear Magnetic Resonance Spectroscopy	29
1.6.1 <i>Theoretical background</i>	29
1.6.2 <i>Quantitative applications</i>	32
1.6.3 <i>NMR spectroscopy in metabolic profiling and biology</i>	33
1.7 Creatine kinase as an artificial free energy buffering system in yeast	37
1.7.1 <i>Apparent equilibrium constant of the creatine kinase reaction</i>	38

Chapter 2: Experimental supply demand analysis of anaerobic yeast glycolysis.....	40
2.1 In vivo NMR spectroscopy	40
2.1.1 Characterization of <i>Saccharomyces cerevisiae</i> cell growth	40
2.1.2 ³¹ P NMR resonance assignments	41
2.1.3 Determination of intracellular pH with ³¹ P NMR spectroscopy .	44
2.1.4 Determination of glycolytic flux with ¹³ C NMR spectroscopy.....	47
2.2 In situ metabolic analysis	51
2.2.1 In situ enzyme activity determination.....	52
2.2.2 In situ glycolytic flux determination with ¹³ C NMR spectroscopy.....	53
2.2.3 In situ ³¹ P NMR spectroscopy	55
2.2.4 Perturbing the [ATP] / [ADP] ratio in situ	59
2.3 Creatine kinase as an artificial means for clamping the [ATP] / [ADP] ratio in permeabilized yeast	64
2.3.1 Determination of the apparent equilibrium constant for the reaction catalyzed by creatine kinase by means of ³¹ P NMR spectroscopy.....	65
2.3.2 Clamping [ATP] / [ADP] ratio in situ	65
2.4 Whole cell experimental supply demand analysis.....	67
2.4.1 ³¹ P NMR determination of the steady state [ATP] / [ADP] ratio in yeast perchloric acid cell extracts	68
2.4.2 Demand perturbations by the addition of the un-coupler benzoic acid	70
2.4.3 Perturbing glycolytic supply by addition of maltose a competitive inhibitor of glucose uptake.....	72
2.4.4 Rate characteristics of supply and demand	74
Chapter 3: General discussion.....	77
3.1 Synopsis.....	77
3.2 Critique and discussion	80
3.3 Future Work.....	82
3.4 Conclusion and Perspective.....	83
Chapter 4: Materials & Experimental Procedures.....	85
4.1 Cell Growth.....	85

4.1.1	<i>Cell growth and harvesting procedures</i>	85
4.2	Permeabilized yeast	87
4.2.1	<i>In situ glycolytic enzyme activity determination</i>	87
4.3	NMR assays	89
4.3.1	<i>³¹P In Vivo NMR Assays</i>	90
4.3.2	<i>¹³C In Vivo NMR assays</i>	91
4.3.3	<i>In Situ NMR Assays</i>	92
4.3.4	<i>Perchloric acid cell extracts</i>	93
4.4	Whole cell supply and demand perturbations	94
4.4.1	<i>Demand Perturbations</i>	94
4.4.2	<i>Supply perturbations</i>	94
4.5	Creatine kinase assays	95
4.5.1	<i>Determination of the apparent equilibrium constant for the creatine kinase reaction</i>	95
4.5.2	<i>Clamping the [ATP] / [ADP] ratio in situ with creatine kinase</i>	95
4.6	Experimental controls and data analysis	96
4.6.1	<i>Flux normalization</i>	96
4.6.2	<i>Data analysis</i>	96
	References	98

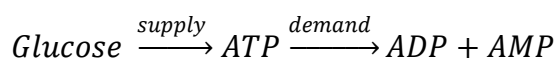
Preface

The classical view concerning metabolic flux control, states that the pathway enzyme with the slowest rate of catalysis is responsible for determining the flux through the system [1 & 2]. These so called rate limiting enzymes catalyze irreversible reactions that yield large free energy changes and operate far from equilibrium [1, 2 & 3]. With the advent of metabolic control analysis (MCA) this traditional stance has however been shown to be flawed; instead MCA has shown that flux control can be shared amongst all the constituent enzymes of the pathway [4 & 5]. In spite of this partitioned nature of flux control, the theorems of MCA do not preclude these so called "rate limiting" steps from playing a major role in shaping the flux through the network [4 & 5]. MCA in combination with kinetic modeling has proved extremely useful for identifying key flux control points in pathways of industrial and medicinal importance; these reactions are usually targeted for metabolic engineering purposes or drug delivery [6 & 7].

To effectively study metabolism, reaction blocks cannot be viewed as acting in isolation but instead a broader approach should be followed so as to include system wide behavior; where MCA focuses on calculating the control coefficients for individual enzymatic steps, modular versions such as top-down control analysis (Brown et al. [8]) and supply demand analysis (SDA) (Hofmeyr and Cornish-Bowden [9]) take into account the effects of metabolic supply (production) and demand (consumption) for pathway product on determining the flux through the system. SDA is based on the theory of MCA, but instead divides metabolism into two blocks, the producing block (called supply) and the consuming block (called demand), which are centered around a common linking metabolite or moiety [9]. The degree of flux control assigned to the metabolic supply or demand may be experimentally determined through application of the double modulation method as originally described by Kacser and Burns [10], in which the result of independent perturbations in both the supply and demand blocks are measured as changes in the linking metabolite concentration and pathway flux [11]. Through plotting rate characteristics that depict the relationship between the supply-demand flux and the linking metabolite or moiety, the sensitivities of supply and demand may be calculated (gradient of the respective rate characteristic at the steady state intercept) [9 & 10]. These sensitivities or elasticities can then be used to determine

the flux and concentration control structure of the system in terms of supply and demand [10].

This thesis presents a direct experimental application of supply demand analysis to free energy metabolism in fermenting yeast, both on a whole cell scale as well as *in situ*. The conserved adenylate moiety expressed as the $[ATP] / [ADP]$ ratio will be used to quantify the free-energy state of these yeasts. If yeast cultures are allowed to ferment in batch (high [glucose] and oxygen limited), glycolysis can be viewed as the sole pathway responsible for the supply of ATP, and as J_{supply} must equal J_{demand} at steady state, glycolytic flux can be used to quantify both supply and demand. By arresting cell growth (nitrogen deprivation), cell maintenance can be regarded as the only source of free energy demand.



In simpler terms the question addressed in this thesis, is whether the majority of yeast glycolytic flux control resides within the pathway itself (supply) or in the demand for ATP, the product of glycolysis?

Glycolytic flux control by either the supply or demand has led to much debate: on the one hand, failure to increase flux through the over-expression of key yeast glycolytic enzymes points to flux control by the demand [12 & 9], whilst a previous study performed on growing yeast under oxygen and energy limitation reported flux control by the supply block [11]. Ultimately unraveling the flux control structure of yeast glycolysis in terms of supply and demand will help clarify these discrepancies. Furthermore the metabolite time courses obtained during this study should also provide a reliable quantitative data set from which kinetic models may be refined and validated. With yeast alcoholic fermentation being an industrially important process regarding its application in the wine and alternative fuel sectors, SDA could contribute to the optimization of current metabolic engineering strategies focused on increasing glycolytic flux, by identifying key flux control points with respect to supply and demand.

Aims and outline

In this study we aim to experimentally determine the distribution of glycolytic flux control with respect to supply and demand, in the yeast *Saccharomyces cerevisiae*. The main goals for this project are listed below:

1. Setting up a protocol for quantification of the metabolic intermediates, ATP and ADP (preferably *in vivo*) using ^{31}P NMR spectroscopy.
2. Determining glycolytic flux with ^{13}C NMR spectroscopy.
3. Perturbing the glycolytic supply and demand for free energy, and correlating the change caused in the steady state $[\text{ATP}] / [\text{ADP}]$ ratio to changes in glycolytic flux.
4. Calculating the elasticities of supply and demand for elucidating the control structure of yeast glycolysis.

Chapter 1 of this thesis provides the appropriate background information and review of the relevant literature, and is divided into seven sections. A general overview on yeast physiology and metabolism (1.1) is presented first, followed by a discussion on the theoretical principles of MCA (1.2). Next the concept of SDA, as well as an example of its experimental application to yeast anaerobic free energy metabolism is presented (1.3). This is followed by a critical comparison between the *in vitro* and *in vivo* environments in terms of their respective physico-chemical attributes and the implications thereof for calculating kinetic parameters (1.4). Next the analytical application of NMR spectroscopy (1.5) regarding the study of microbial metabolism is discussed. This is followed by a brief review on kinetic modeling (1.6) in which the importance of computational approaches in the post genomic era is highlighted. As an example the glycolytic model developed by Teusink et al. [13] is also presented in this section. The phospho-creatine system (1.7) and its ability to function as a free energy reservoir, along with a thermodynamic review on the reaction catalyzed by creatine kinase, are assessed in the final section.

Experimental results are presented in *Chapter 2*, which is divided into four main sections: *in vivo* NMR spectroscopy (2.1), *in situ* glycolysis (2.2), the application of the

free-energy buffering capacity of the phospho-creatine system in permeabilized yeast (2.3) and a whole cell supply demand analysis on yeast fermentative free energy metabolism (2.4).

The general discussion is presented in *Chapter 3* and is divided into four sections: Synopsis (3.1) contains a summary of the experimental results presented in *Chapter 2*, Critique and discussion (3.2) focuses on discussing the findings of this thesis with respect to literature in a critical manner, followed by suggestions for future studies (3.3), and lastly some concluding remarks and perspectives (3.4).

Methodology and experimental procedures are described in *Chapter 4*.

Chapter One

Literature Study and Background

1.1 Overview of metabolism with specific focus on yeast glycolysis

A comprehensive background study on yeast metabolism and physiology is beyond the scope of the work presented in this thesis, which deals primarily with the control and regulatory structure of yeast glycolysis and more specifically free energy metabolism. Hence this section will only touch on those parts of yeast metabolism (glycolysis) and physiology applicable to the work presented here, in addition to a brief overview of some of the more general concepts of metabolic regulation.

1.1.1 Metabolism and its principles

Metabolism can be defined as the sum of all the chemical reactions that take place in a living cell or organism for obtaining and using the free energy required for life [1]. This is achieved by linking the exergonic reactions of nutrient oxidation to the endergonic processes essential for maintenance of life [1]. Organisms can ultimately be divided into two categories: phototrophs, which acquire free energy via photosynthetic reactions and chemotrophs, where free energy is obtained via the oxidation of organic compounds [1]. In these chemotrophs the free energy obtained is coupled to the synthesis of high-energy phospho-monoesters such as ATP, which in turn supply the energy that drives endergonic reactions. During the complete oxidation of food sources, nutrients are chemically or enzymatically degraded to metabolic intermediates, which ultimately serve as the precursors for other biologically important molecules [1].

Metabolic pathways form a ordered series of enzymatically catalyzed reactions that produce specific end products [1]. The substrates, intermediates as well as the end products are referred to as metabolites. Metabolism can be divided into two distinct categories: catabolism, in which larger and more complex molecules are broken down into smaller molecules with the subsequent release of energy and heat, and anabolism-

the synthesis of larger more complex molecules with the concomitant input of free-energy. Almost all of the free energy produced during catabolism is preserved through the generation of ATP from ADP and inorganic phosphate as well as the transfer of electrons to NAD^+ and NADP^+ to form NADH and NADPH [1]. It is these cofactors, ATP and NADPH that supply the energy for driving anabolic reactions. A wide array of substrates may act as energy sources for the cell, but metabolism converts these nutrients to a limited number of common metabolic intermediates [1]. These intermediates are then further oxidized via a central oxidative pathway which terminates in the final end products $\text{H}_2\text{O} + \text{CO}_2$ [1]. It is these common intermediates that also feed into most of the anabolic reactions responsible for the biosynthetic production of all cellular polymers [1]. Below some of the basic principles concerning the organization of metabolic pathways are listed [1].

1. Metabolic pathways are irreversible and hence directional.
2. Catabolic and anabolic processes must differ.
 - This allows for the independent regulation of the two processes.
3. Metabolic pathways have a committing step.
4. Metabolic pathways are regulated. (see Section 1.1.4)
 - Metabolism is regulated by the laws of supply and demand.
5. Metabolic pathways have specific cellular locations.
 - Eukaryotic cells are compartmentalized, therefore membrane transporters and various shuttles are required to import and export metabolites.

1.1.2 Yeast glycolysis

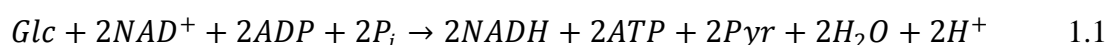
Glycolysis, as the Greek name suggests, means the “loosening of glucose”. Glycolysis is the pathway by which glucose is converted to pyruvate, with a stoichiometric equivalent of two mol pyruvate produced per mole of glucose consumed. The glycolytic pathway is a linear sequence of ten enzymatic reactions, is the best characterized of all metabolic networks and plays an integral role in yeast fermentative free energy metabolism (see Fig. 1.1) [1].

Glucose enters the cell from the exterior environment via hexose transporters located in the cell membrane. The glycolytic enzymes are located in the cytosol, with a minimal

degree of association with the cell membrane and other cellular structures [1]. Circumstantial evidence points to the formation of glycolytic enzyme complexes or metabolons, which facilitate the phenomenon of metabolite channeling, although such complexes have yet to be isolated in yeast [1, 14 & 15]. Essentially yeast glycolysis converts a six carbon molecule of glucose to two molecules of lower energy, i.e. pyruvate, or ethanol and CO₂ during alcoholic fermentation. The energy released during the catabolic breakdown of glucose is linked to the substrate-level phosphorylation of ATP. Chemically speaking the glycolytic strategy can be summed up in three key points [1].

1. Phosphorylation of glucose.
2. Conversion of phosphorylated intermediates into compounds with high phosphate group transfer potentials.
3. Coupling the hydrolysis of these high energy intermediates to the synthesis of ATP.

Glycolysis is divided into two stages, with the first five reactions or top half being a priming stage where an energy investment is required (two moles ATP) and reactions six to ten (lower half), where the energy being released is coupled to the synthesis of ATP (four moles ATP) [1]. Equation 1.1 shows the overall reaction for the glycolytic conversion of glucose to pyruvate.



Under anaerobic conditions where the NADH formed during glycolysis cannot donate its electrons to oxygen as an external electron acceptor, NAD⁺ will eventually become limiting and glycolysis will cease if NAD⁺ is not recycled. Recycling is primarily achieved through a series of additional steps following the formation of pyruvate which results in the regeneration of NAD⁺ and is termed fermentation [1]. As a byproduct to redox homeostasis, fermentation also results in the formation of various metabolic end products, i.e. ethanol, lactic acid or mixed acids, and is often used as a basis for microbial classification [1].

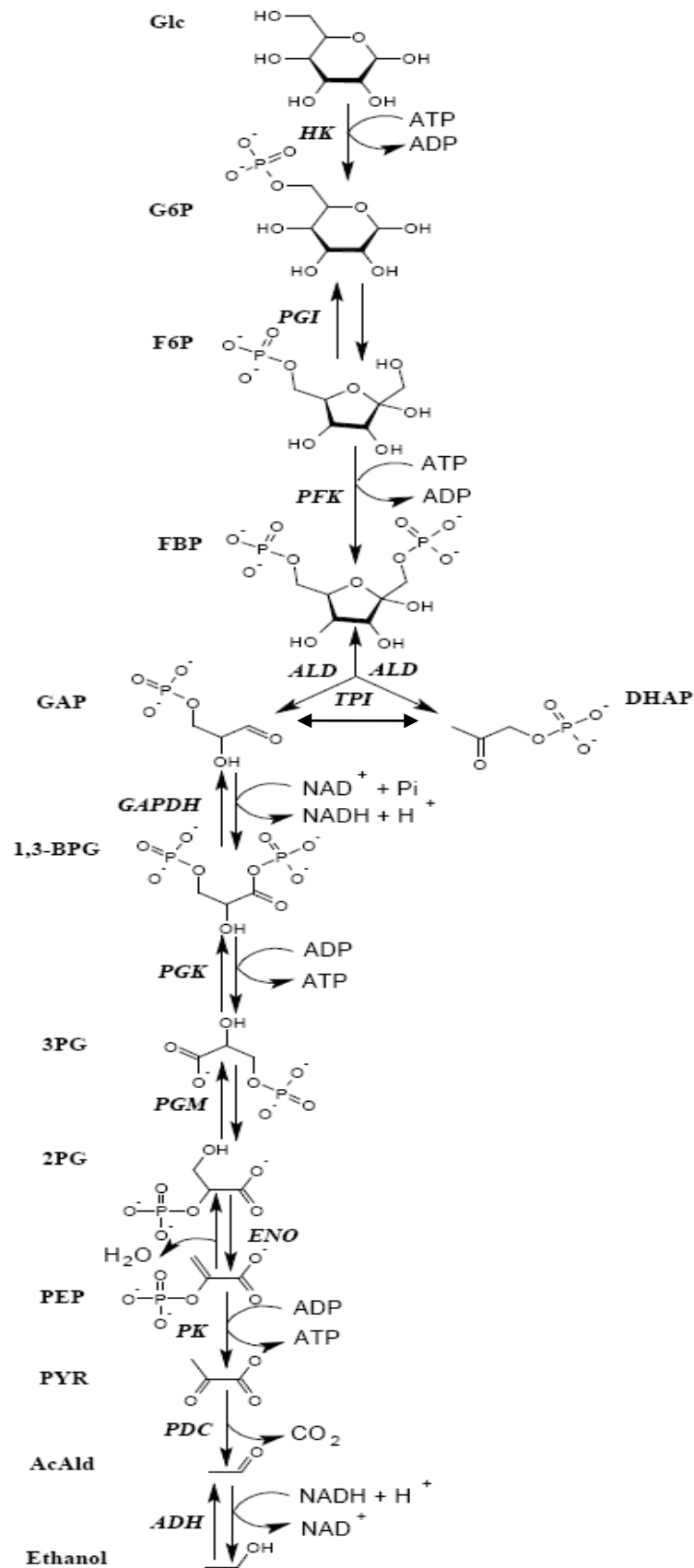


Figure 1.1: Schematic representation of yeast glycolysis, in which glucose gets converted to ethanol (referred to as alcoholic fermentation) with the production of two mol ATP per mol of glucose consumed. Abbreviations are defined on page vi and vii.

During alcoholic fermentation (Fig. 1.1) in yeast, pyruvate is decarboxylated by the enzyme pyruvate decarboxylase, with formation of acetaldehyde and CO₂ as products [1]. Acetaldehyde is then reduced in the second step by the enzyme alcohol dehydrogenase, with NADH acting as electron donor leading to the regeneration of NAD⁺ and the formation of ethanol as end product [1].

1.1.3 Energetics of alcoholic fermentation

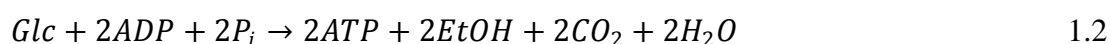
The overall reaction for the glycolytic conversion of glucose to ethanol is displayed below in equation 1.2.

Figure 1.1: Schematic representation of yeast glycolysis, in which glucose gets converted to ethanol (referred to as alcoholic fermentation) with the production of two mol ATP per mol of glucose consumed. Abbreviations are defined on page vi and vii.

During alcoholic fermentation (Fig. 1.1) which is most common in yeast, pyruvate is decarboxylated by the enzyme pyruvate decarboxylase, with formation of acetaldehyde and CO₂ as products [1]. Acetaldehyde is then reduced in the second step via the enzyme alcohol dehydrogenase, with NADH acting as electron donor leading to the regeneration of NAD⁺ and the formation of ethanol as end product [1].

1.1.3 Energetics of alcoholic fermentation

The overall reaction for the glycolytic conversion of glucose to ethanol is displayed below in equation 1.2.



Under standard biochemical conditions, the Gibbs free energy difference for the conversion of glucose to ethanol is -235kJ/mol of glucose [1]. As the conversion is coupled to the net production of two mol ATP ($\Delta G^{\circ} = + 61 \text{ kJ} / 2 \text{ mol ATP formed}$), alcoholic fermentation is only 26% efficient in terms of energy conversion with the rest being dissipated as heat [1]. Under physiologically relevant conditions, however, the free energy efficiency is in excess of 50% [(1)].

The complete oxidation of glucose to CO₂ and H₂O produces far more free energy than the glycolytic conversion to ethanol, yielding a net total of between 32 and 38 mol ATP/mol glucose consumed, in comparison to two molecules of ATP formed during fermentation. In the absence of oxygen or in the presence of high concentrations of

glucose, non-dividing yeast cells consume glucose at a prolific rate in comparison to that observed during oxidative phosphorylation; this phenomenon is known as the Pasteur effect [16]. Observation of the Pasteur effect may be ascribed to the fact that under these conditions yeast predominantly ferment their substrate whereas resting yeast usually respire a large percentage (25-100%) of the glucose they consume [16], as a result these yeast will face a deleterious energy shortage upon switching over to fermentative metabolism if $J_{glycolysis}$ is not significantly increased [17].

1.1.4 Metabolic regulation and control

The homeostasis of intermediate concentrations must be maintained in light of variations in metabolic flux caused by alterations in either the supply or demand of certain key metabolites [9]. Metabolic regulation can be viewed as the manner in which the steady state flow of metabolites through a pathway is sustained in light of changes in the environment and how this response is affected by pathway design [1, 3 & 18]. By contrast, metabolic control refers to a lower level of containment concerned with the management of (effect and mechanism) individual enzymatic steps and system parameters and their influence on the steady state variables [1, 3 & 18].

Metabolism is regulated through balancing the supply of product with the demand thereof so as to prevent unnecessary uncoupling of metabolism (energy wasting) and to maintain intermediates within a narrow range (homeostasis) [9]. Homeostasis is maintained in organisms for the following reasons [1 & 3]:

- i. In open metabolic systems steady state is the most thermodynamically efficient state.
- ii. Intermediates form part of more than one pathway so variations in concentration may disturb the metabolic balance.
- iii. To ensure that metabolism responds quickly to external signals only minor variations in intermediate concentration are permitted.
- iv. Large changes in metabolite concentrations may have disastrous implications for the osmotic properties of the cell.

The classical view of pathway regulation states that the flux through a pathway is entirely dictated by the enzyme with the lowest catalytic activity (rate determining step) [1 & 2]. Such a rate determining step operates far from equilibrium, with its products being removed by the downstream enzymes before equilibration is achieved and subsequently it has a comparatively large free energy change [1, 2 & 3]. It is these rate limiting steps that serve as the primary sites through which metabolism may be regulated. The net flux through the rate determining steps may be altered by various mechanisms [3]:

- i. *Allosteric regulation* of enzymes by effectors that may serve as substrates, cofactors as well as products of the pathway,
- ii. *Covalent modification* of pathway enzymes whereby the modifiers themselves are subject to a degree of control,
- iii. *Formation of substrate cycles*, which allows for a finer degree of metabolic tuning, as it allows for independent control over rates of synthesis and consumption, and
- iv. *Genetic control* where enzyme activities can be regulated on a more long term basis by means of their concentrations.

1.1.5 *Allosteric regulation of yeast glycolysis*

Phospho-fructokinase (PFK) catalyzes the reaction, $F6P + ATP \rightarrow F1,6BP + ADP$. It is an important site for allosteric control in glycolysis and has evolved a complex regulatory scheme [19]. This enzyme operates far from equilibrium and the reaction has a large overall negative ΔG° making it an obvious candidate for imparting a degree of control over glycolytic flux [19]. When yeasts are given a glucose pulse, PFK activity is initially increased due to the cooperative binding of its substrates F6P and ATP in addition to increasing concentrations of the main allosteric activator F2,6 BP [19 & 20]. The adenylates AMP and ATP also impact on the kinetic regulation of PFK [20]. ATP acts as both a substrate and an allosteric inhibitor at high concentrations whilst AMP is known to function as an allosteric activator [20].

Pyruvate kinase (PK) serves as the second main target for allosteric regulation in yeast glycolysis [19]. PK essentially catalyzes an irreversible reaction whereby the activated

metabolite PEP is converted to pyruvate with the simultaneous substrate-level phosphorylation of ADP to ATP. Pyruvate kinase is allosterically activated by the upstream glycolytic intermediate F1,6 BP which is also the product of the PFK reaction [21]. Hence initially in the presence of glucose, glycolysis is activated by increasing substrate and allosteric activator concentrations [22].

With the advent of metabolic control analysis (MCA) the notion of exclusive flux control by rate limiting steps was dismissed as it was shown that flux control can be shared (although not equally) amongst all the pathway enzymes [4, 5 & 9]. However, the separate and simultaneous over-expression of yeast PFK, HK and PYK, all key glycolytic enzymes catalyzing reactions with comparatively large free energy changes ($-\Delta G^\circ$), failed to increase the flux through glycolysis [12]. This finding led to the hypothesis of pathway flux control residing outside the network, implicating the importance of the demand for metabolic intermediates in determining steady state flux [9]. Not only is the control of flux shared to a varying degree by all the constituent enzymes in a biochemical pathway, but a degree of control may be intrinsic to the demand for pathway end product [4, 5, 9 & 10].

1.2 Metabolic Control Analysis

Supply-demand analysis is based on the theory of metabolic control analysis; therefore MCA will be addressed first providing an introduction to key concepts and definitions that will be used throughout this thesis.

The purpose of MCA [4, 5 & 10] is to provide a quantitative and hence mathematical framework for describing and elucidating the control and regulatory structure of metabolic pathways and other biological processes [23]. The biological function of a metabolic network as a whole is not just purely an additive feature of all the individual enzymatic reactions, but indeed it has its own unique global or systemic properties [4]. Metabolic pathways may be understood through determination of their systemic properties, such as the sensitivity of the steady state variables (fluxes and metabolic intermediate concentrations) in response to parameter variations, and relating these system characteristics to the properties of individual enzymes [23]. First developed in the 1970s by Kacser and Burns [10] and Heinrich and Rapoport [5], MCA has further

been modified and its application refined. MCA is applicable to any system no matter how complex and it does not require detailed kinetic knowledge of all the systems components, making it an important tool in the post genomic era [10 & 23].

MCA uses a linearization approach around the steady state, and because the relationship between the steady-state variables, i.e. fluxes and metabolite concentrations, and the parameters that influence enzyme activity is not per definition linear [4], MCA is only applicable when small perturbations in system parameters are analyzed [4]. This is similar to zooming in on a small segment of any function (logarithmic, polynomial, etc.) until it can be perceived as a straight line. MCA makes use of fractional or relative changes represented as dimensionless ratios, for expressing both systemic and local properties [4].

1.2.1 Local Properties

Local properties or elasticity coefficients refer to the functional steps of a large metabolic network which include the enzyme catalyzed reactions and transport steps [4 & 5]. The elasticity coefficients for an individual step can be described as the sensitivity of the rate through the enzyme (v_i) in response to infinitely small perturbations in the concentration of a substrate, product, effector molecule or any parameter (p) that will influence enzyme activity [4]. In mathematical terms elasticity coefficients are expressed as follows [4 & 5]:

$$\varepsilon_p^{v_i} = \partial \ln v_i / \partial \ln p \quad 1.3$$

In a more graphical interpretation, this is equal to the slope of the curve, obtained by plotting the logarithm of the reaction rate versus the logarithm of the concentration of the effector being perturbed [4]. Elasticities are defined as partial derivatives, with the concentrations of all the other interacting metabolites being kept constant at their respective steady-state values [4 & 5]. The elasticity coefficients for an individual step can be derived with respect to all the metabolites that appear in the enzyme's rate equation [4]. As the rate of an enzyme catalyzed reaction is usually proportional to the concentration of the enzyme (multiplier in the rate equation), the elasticity coefficient

with regard to perturbations in enzyme concentration (e) yields a value of one ($\varepsilon_{e_i}^{v_i} = \frac{\partial \ln v_i}{\partial \ln e_i} = 1$) [4].

1.2.2 Global Properties

How the system variables, i.e. the pathway flux (J) and steady-state metabolite concentrations (s), respond to perturbations in the local rate of an enzyme is of critical importance in ultimately characterizing the control structure of a metabolic network [4]. The response coefficient is defined as the sensitivity of the steady state variable in response to a fractional change in a parameter (p) affecting the local rate (v_i) through a specific enzyme (e_i) [4], and is mathematically expressed as follows:

$$R_p^J = \partial \ln J / \partial \ln p \quad 1.4$$

$$R_p^s = \partial \ln s / \partial \ln p \quad 1.5$$

Similar to the expression for elasticity coefficients, the response coefficient is equal to the slope of the curve produced when plotting $\ln J$ or $\ln s$ versus $\ln p$, at steady-state [4].

Through use of the mathematical expressions for the local sensitivity of an enzyme with regard to a parameter perturbation (see Equation 1.3) and the sensitivity of the system variables in response to a parameter perturbation (see Equations 1.4 and 1.5) the control coefficients can be derived [4].

I. Flux-control coefficient:

$$C_{v_i}^J = \frac{\partial \ln J}{\partial \ln v_i} = R_p^J / \varepsilon_p^{v_i} \quad 1.6$$

II. Concentration-control coefficient:

$$C_{v_i}^s = \frac{\partial \ln s}{\partial \ln v_i} = R_p^s / \varepsilon_p^{v_i} \quad 1.7$$

Control coefficients represent the degree of control a specific enzymatic step has over the steady state variables [4]. The expression of control coefficients in terms of elasticities and response coefficients is called the combined response relationship [4].

The numerical values for both the control coefficients and local elasticities of a metabolic network are subject to a series of restrictions and inter-dependencies which form the basis for the theorems of MCA [24].

1.2.3 *Summation theorems*

The flux summation theorem states that the flux control coefficients for all the n enzymes in a metabolic network, with respect to a particular flux must add up to unity [4]. Effectively this means that all the enzymes within a pathway have some degree of control over the steady state flux (flux control is shared amongst constituent enzymes). This of course does not exclude the possibility that certain enzymes have larger coefficients and hence exert more control over flux than others [4].

I. The flux control summation theorem:

$$\sum_{i=1}^n C_{v_i}^J = 1 \quad 1.8$$

The summation theorem of concentration control states that the concentration control coefficients for all the n enzymes in a metabolic network must add up to zero [4 & 24]. The biological interpretation is that some enzymes act to increase the concentration of intermediates (producers) and others act to decrease these metabolite concentrations (consumers) [4 & 24]. Similarly to flux control, concentration control is also shared amongst the constituent enzymes of a pathway.

II. The concentration control summation theorem:

$$\sum_{i=1}^n C_{v_i}^s = 0 \quad 1.9$$

1.2.4 Connectivity Theorems

Just as the combined response relationship (Section 1.2.2) expresses the link between the local and global properties, the connectivity theorems describe the relationship between the elasticity and control coefficients with respect to metabolic intermediates [4, 5 & 10]. The connectivity theorem of flux control states (Equation 1.10) that for a metabolic intermediate (s), the sum of the product of all the flux control coefficients effected by the metabolite and their elasticities is equals to zero [4, 5 & 10]. This theorem provides insight into how reaction kinetics affects the enzymatic steps degree of flux control [24].

I. Connectivity theorem of flux control:

$$\sum_{i=1}^n C_{v_i}^J \varepsilon_s^{v_i} = 0 \quad 1.10$$

The connectivity relationships for the concentration control coefficients are stated below. Equation 1.11 applies to the situation where the reference metabolite (x) is different from the metabolite (s) [4, 5 & 10]. Equation 1.12 refers to the case in which the reference metabolite and metabolite (s) are identical [4, 5, 10, & 24].

II. Connectivity theorems of concentration control:

$$\sum_{i=1}^n C_{v_i}^x \varepsilon_s^{v_i} = 0, x \neq s \quad 1.11$$

$$\sum_{i=1}^n C_{v_i}^s \varepsilon_s^{v_i} = -1 \quad 1.12$$

1.3 Supply-demand Analysis

In this section the theoretical background on supply-demand analysis (SDA), as well as an example of its experimental application for analysis of a metabolic network, will be addressed.

In its simplest form metabolism can be described as a molecular economy that is shaped by its demand and supply characteristics for metabolic products and cofactor cycles

(NAD^+/NADH , etc.) [9]. Metabolic supply-demand analysis allows for a quantitative description of how a pathway or system functions in terms of the sensitivity of the respective “supply and demand blocks” [9]. What makes this type of analysis so attractive is that these sensitivities may be determined experimentally [9 & 11].

1.3.1 *Theoretical background*

How metabolism is regulated to fulfill a specific physiological function is one of the key questions addressed in biochemistry. The ordered assembly of any reaction network is limited by certain thermodynamic constraints and must adhere to the laws of mass action [25 & 26]. Therefore metabolic regulation can loosely be defined as the adjustment of reaction properties so as to supplement or offset the mass-action trend within a reaction network [25 & 26]. Regulation of metabolism is achieved on both a transcriptional and translational scale by varying the absolute concentration of enzymes, as well as a post-translationally, by altering both the catalytic activities and substrate/product affinities of certain key enzymes [24 & 27]

Essential to understanding cellular metabolism, is knowledge of the hierarchal structure and organization of metabolic networks [9]. Fundamentally metabolism can be divided into three distinct sections: catabolism, biosynthesis and growth (see also Section 1.1). The catabolic block provides carbon intermediates and free energy in the form of ATP and reducing equivalents [9]. The biosynthetic block produces monomers for macromolecular synthesis and the growth block is responsible for the production and maintenance of cellular structure and machinery [9]. These distinct blocks may be linked via either one common metabolic intermediate or a group of intermediates that form a conserved moiety / or cofactor cycle, such as ATP-ADP-AMP [28]. The producing block in such metabolic network is called the supply and the consuming block, the demand [29].

At chemical equilibrium the flux through any pathway is zero, hence equilibrium is excluded as a possible attainable state for metabolism as a whole [9], however it is still an important reference point [9]. The distance of any reaction from equilibrium as determined by the disequilibrium ratio Γ/K_{eq} , is crucial for determining the behavior of a reaction network [9]. As metabolic function is by definition multi-layered in design,

enzymes are regulated to perform both low level (reaction catalysis) and high level functions [9]. These high level functions include: (i) steady-state determination [9], (ii) steady-state flux and concentration control [9], (iii) steady-state stability in response to parameter perturbations [30], (iv) length of the transition period between steady-states [31] and (v) the dynamic nature of the transitions (oscillatory or monotonic) [32 & 33].

Supply demand analysis is based on the theory of metabolic control analysis and as such rate characteristics for both the supply and demand blocks can be constructed [9]. These rate characteristics yield the respective elasticities of supply and demand which are then used for determining the flux and concentration control coefficients [9]. A combined graph of both the supply and demand rate characteristics is compiled by plotting the logarithm of the rate through the supply and demand block against the logarithm of the concentration of the linking metabolite or moiety (Fig. 1.2) [9]. As both metabolic supply and demand consist of a network of multiple reactions, the rate plotted represents the variation in the steady state flux of the individual supply and demand blocks [9].

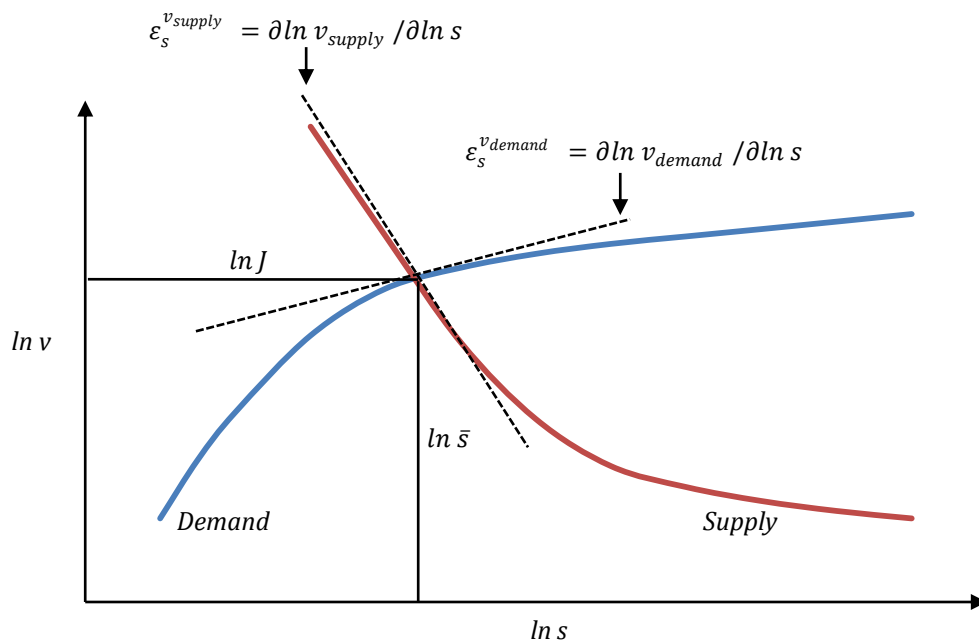


Figure 1.2: The rate characteristics of both the supply and demand blocks as plotted in double logarithmic space. v refers to the rate of supply and demand for the linking intermediate and s refers to the concentration of the linking metabolite or moiety. Figure was adapted from Hofmeyr & Cornish-Bowden [9].

The point where the supply and demand rate characteristics intersect denotes the metabolic steady state, with a specific flux J and linking metabolite concentration \bar{s} [9]. The response in the steady state variables, due to small changes in the activity of either

supply or demand is entirely determined by their respective elasticity coefficients [9]. The expression for the elasticities of supply and demand is given in Fig. 1.2. These elasticity coefficients represent the overall sensitivity of all the respective reactions making up the supply and demand blocks [9] and are calculated as the gradient of the tangent fitted through the steady state intercept, for both the supply and demand rate characteristics [9].

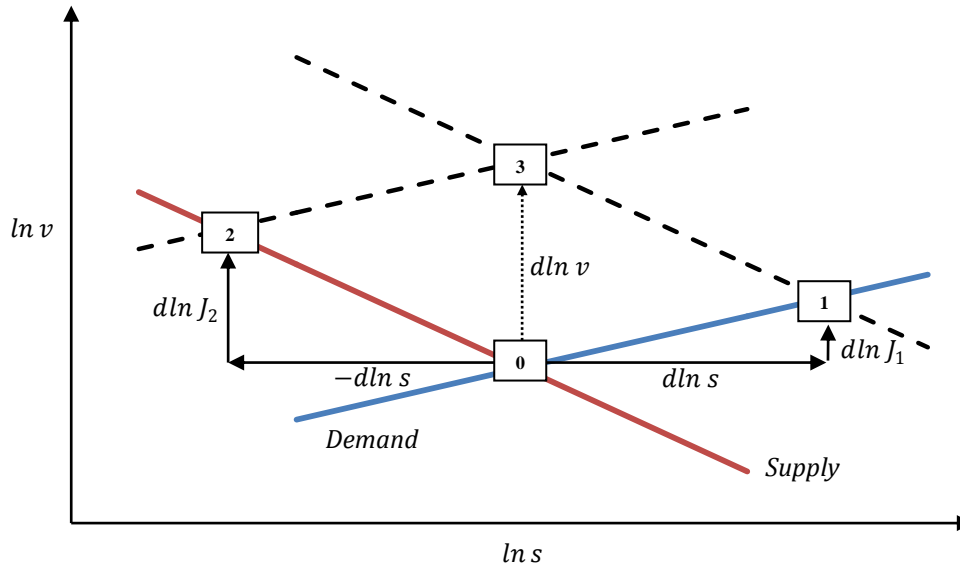


Figure 1.3: Steady state (0) response caused by perturbations in the activities of supply (1) and demand (2) or both (3). v refers to the rate of supply and demand for the linking intermediate and s refers to the concentration of the linking metabolite or moiety. Figure was adapted from Hofmeyr & Cornish-Bowden [9].

Fig. 1.3 illustrates how the flux and concentration control coefficients can be quantified [34]. By perturbing the activities of both the supply and demand individually as well as simultaneously new steady states are reached, each with its own unique set of values for J and \bar{s} [9]. The expressions for flux and concentration control coefficients follow below [9].

I. *Flux control coefficients:*

$$C_{supply}^J = \frac{d \ln J_1}{d \ln v_{supply}} \quad 1.13$$

$$C_{demand}^J = \frac{d \ln J_2}{d \ln v_{demand}} \quad 1.14$$

II. *Concentration control coefficients:*

$$C_{supply}^s = \frac{dln s}{dln v_{supply}} \quad 1.15$$

$$C_{demand}^s = \frac{-dln s}{dln v_{demand}} \quad 1.16$$

With reference to Fig. 1.3, steady state three is reached when both the supply and demand block are increased equally by $dln v$ [9]. At this new revised steady state (3), $dln J_3 = dln J_2 + dln J_1 = dln v$, while there is no change in the steady state concentration of, s $dln s_3 = 0$ [9]. Using the definitions for the control coefficients (Equations 1.13 through 1.16) the summation theorems can be expressed as follows [4].

I. Flux summation theorem:

$$C_{supply}^J + C_{demand}^J = 1 \quad 1.17$$

II. Concentration control summation theorem:

$$C_{supply}^s + C_{demand}^s = 0 \quad 1.18$$

By combining the expression for the elasticities of supply and demand (Fig. 1.2) with the summation theorems (Equation 1.17 and 1.18), the following two connectivity theorems can be obtained [4].

I. Connectivity theorems of flux control:

$$C_{supply}^J \varepsilon_s^{v_{supply}} + C_{demand}^J \varepsilon_s^{v_{demand}} = 0 \quad 1.19$$

II. Connectivity theorem of concentration control:

$$C_{supply}^s \varepsilon_s^{v_{supply}} + C_{demand}^s \varepsilon_s^{v_{demand}} = -1 \quad 1.20$$

Through substitution of the summation theorems into Equations 1.19 and 1.20, it is possible to express the flux and concentration control coefficients for supply and demand, in terms of their elasticities [9].

I. Flux control coefficients:

$$C_{supply}^J = \frac{\varepsilon_s^{v_{demand}}}{\varepsilon_s^{v_{demand}} - \varepsilon_s^{v_{supply}}} \quad 1.21$$

$$C_{demand}^J = \frac{-\varepsilon_s^{v_{supply}}}{\varepsilon_s^{v_{demand}} - \varepsilon_s^{v_{supply}}} \quad 1.22$$

II. Concentration control coefficients:

$$C_{supply}^S = -C_{demand}^S = \frac{1}{\varepsilon_s^{v_{demand}} - \varepsilon_s^{v_{supply}}} \quad 1.23$$

It is clear from Equations 1.21 and 1.22 that the ratio of the elasticities determines to what extent flux is controlled by either the supply or the demand block [9], whilst the sum of their absolute values determines the degree of concentration control (see Equation 1.23) and thus homeostasis of \bar{s} .

1.3.2 Experimental supply-demand analysis

Approaches such as top-down control analysis [8] and the double modulation method [10] exist for calculating the control coefficients for specific reaction blocks or modules within a metabolic network, without prior knowledge of block structure in terms of constituent enzymes and their explicit kinetics. The latter technique allows for determination of the elasticities (of supply and demand), by relating the responses of two independent variables (flux and steady state metabolite concentration) to separate perturbations in the activities of both the supply and demand blocks [10].

An example of the experimental implementation of the double modulation method for performing a complete supply demand analysis on yeast anaerobic free energy metabolism is provided by Kroukamp et al. [11]. Similar to the study presented here, Kroukamp et al used glycolytic flux (J_{EtOH}) as an indicator for both the supply rate of and demand for free energy (see Preface) and the [ATP]/ [ADP] ratio (linking cofactor couple) as a measure of the cellular energy state [11]. Perturbation of the demand block was achieved by titrating with the un-coupler benzoic acid, resulting in a drop in the [ATP] / [ADP] ratio and a concomitant compensatory change in J_{EtOH} [11]. These demand modulations then yielded the data used for construction of the supply rate characteristic [11]. Conversely the data generated by performing perturbations in the supply block were used for the construction of the demand rate characteristic [11].

Kroukamp et al. [11] used variations in the dilution rate (yeast culture was grown in a chemostat) as a means for perturbing the supply block.

Kroukamp et al. [11] successfully calculated the elasticities of the glycolytic supply and demand for free energy (Fig. 1.4), followed by determination of the flux and concentration control coefficients for both the supply and demand blocks (refer to Equations 1.21 – 1.23) [11]. The results obtained showed that the majority of flux control is situated in the supply and not in the demand for ATP as was originally proposed by Hofmeyr and Cornish-Bowden [9]. For a more in depth discussion, refer to Section 3.2 where a comparative and critical analysis is made between literature and the findings of this thesis.

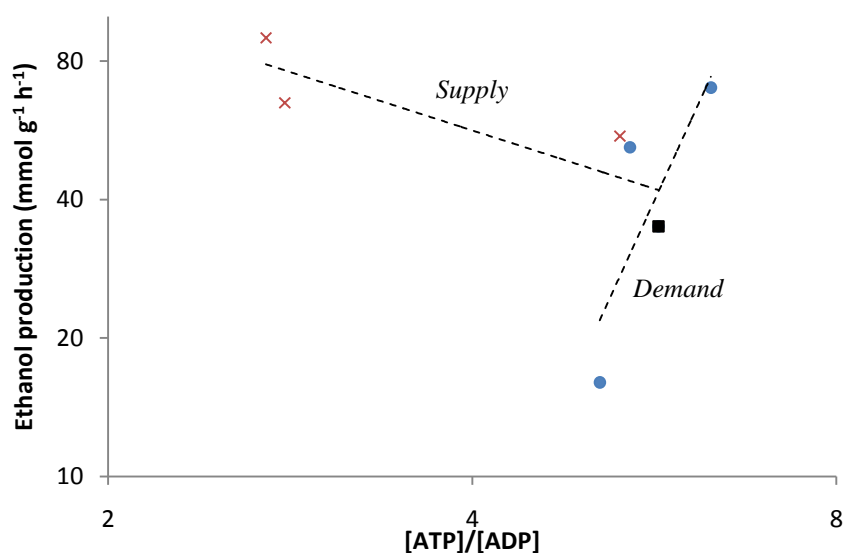


Figure 1.3: The variation in glycolytic supply and the demand for free energy (ATP) with different $[ATP] / [ADP]$ ratios in the yeast *S.cerevisiae*. Red crosses show the supply rate characteristic when the demand for ATP was modulated by the addition of the un-coupler benzoic acid. Blue circles show the demand rate characteristic when the glycolytic supply was altered through changes in the dilution rate. The Black square is taken as the reference steady state point, where no benzoic acid is added at a dilution rate of 0.2 h^{-1} . Dotted lines represent the slopes of both rate characteristics and were fitted to the data by means of linear regression. This figure was adapted from Kroukamp et al. [11].

1.4 Kinetic modeling

Cellular metabolism is complex and dynamic in nature and as such can give rise to a wide array of biochemical phenomena ranging from multiple steady states to metabolite oscillations [35]. To ultimately predict metabolic behavior is a key driving force in the

post genomic era [36, 37, 38, 39 & 40], for this reason much emphasis has been placed on the development of detailed kinetic models describing metabolic networks of interest [41 & 42]. Mathematical models are extremely useful as biochemical tools in modern day science. Models can be viewed as a “virtual laboratory” where a large amount of information regarding pathway behavior and metabolic function may be obtained [43, 44 & 45]. Models also have industrial applications where in conjunction with the theory of metabolic control analysis the feasibility of certain biotechnological questions or optimizations may be probed before up-scaling to more costly experimental manipulations [46].

A kinetic model uses only the explicit kinetics of the pathway enzymes as well as certain relevant metabolic constraints to mathematically describe system behavior [47]. Such classical kinetic models are based on a set of ordinary differential equations and are often referred to as deterministic in nature, as they allow for relevant simulations regarding metabolite concentrations and metabolic fluxes [47]. To model more transient and random metabolic events stochastic approaches are applied [48].

In the following section a detailed kinetic model for yeast glycolysis, developed by Teusink et al. [13] will be described. Emphasis is also placed on the importance of detailed kinetic models, for describing and broadening our understanding of metabolic regulation and control.

1.4.1 The kinetic model for yeast glycolysis as developed by Teusink et al.

This detailed kinetic model of yeast glycolysis and its side branches (Fig. 1.4) was developed by Teusink et al. [13] in the Westerhoff group at the University of Amsterdam. This model differs fundamentally from other kinetic models in the sense that kinetic parameters were not optimized or manipulated to produce a desired output matching experimental observations [13]. Instead the purpose of this model was to ascertain to what extent *in vitro* determined parameters could succeed in describing system behavior *in vivo*, in terms of metabolic fluxes and steady state metabolite concentrations [13].

One of the prerequisites for construction of such a model was that all the kinetic parameters needed to be determined from the same yeast source, under the same assay conditions and to abstain from refining these parameter values [13]. Similarly the experimental data concerning metabolic fluxes and intermediate concentrations were collected from the same yeast source, to ensure model compatibility [13]. It is for this reason that this model is presently one of the most comprehensive and kinetically complete glycolytic models found in literature [13].

What ensued was the development of two separate models of yeast glycolysis. The first was the un-branched model starting with glucose transport into the yeast cell, running through glycolysis and ending up with production of ethanol and CO₂ [13]. The second was a far more thorough model comprised of the main pathway as in the first, but also including the glycolytic side branches for succinate, glycerol, trehalose, and glycogen production (Fig. 1.4) [13].

The results showed that the un-branched model failed to reach a steady state, with a steady accumulation of the glycolytic intermediates; F1, 6 BP, GAP and DHAP being observed [13]. The flux through the top half of glycolysis (Glc to GAP) was found to be in excess of the flux through the lower half (GAP to EtOH), explaining the consequent accumulation of these intermediates [13]. This phenomenon is similar to that which is observed in trehalose-6-phosphate synthetase yeast mutants and is termed the turbo-effect [49, 50 & 51]. However, increasing the maximum activity of pyruvate decarboxylase by six fold allowed the system to attain a steady state [13]. The inclusion of side branches did lead to a qualitative improvement, as the model was now able to attain a steady state using the original set of kinetic parameters. However the branched model did not produce a better correspondence with experimental results than the modified form of the un-branched model [13].

Although kinetic modeling was not attempted during our investigation, the yeast glycolytic model developed by Teusink et al. [13], may serve as an excellent reference point for future comparison to the experimental findings of this thesis, in terms of steady state fluxes and metabolite concentrations. For a further discussion on the findings of this model concerning the turbo effect, refer to Sections 2.2 and 3.3.

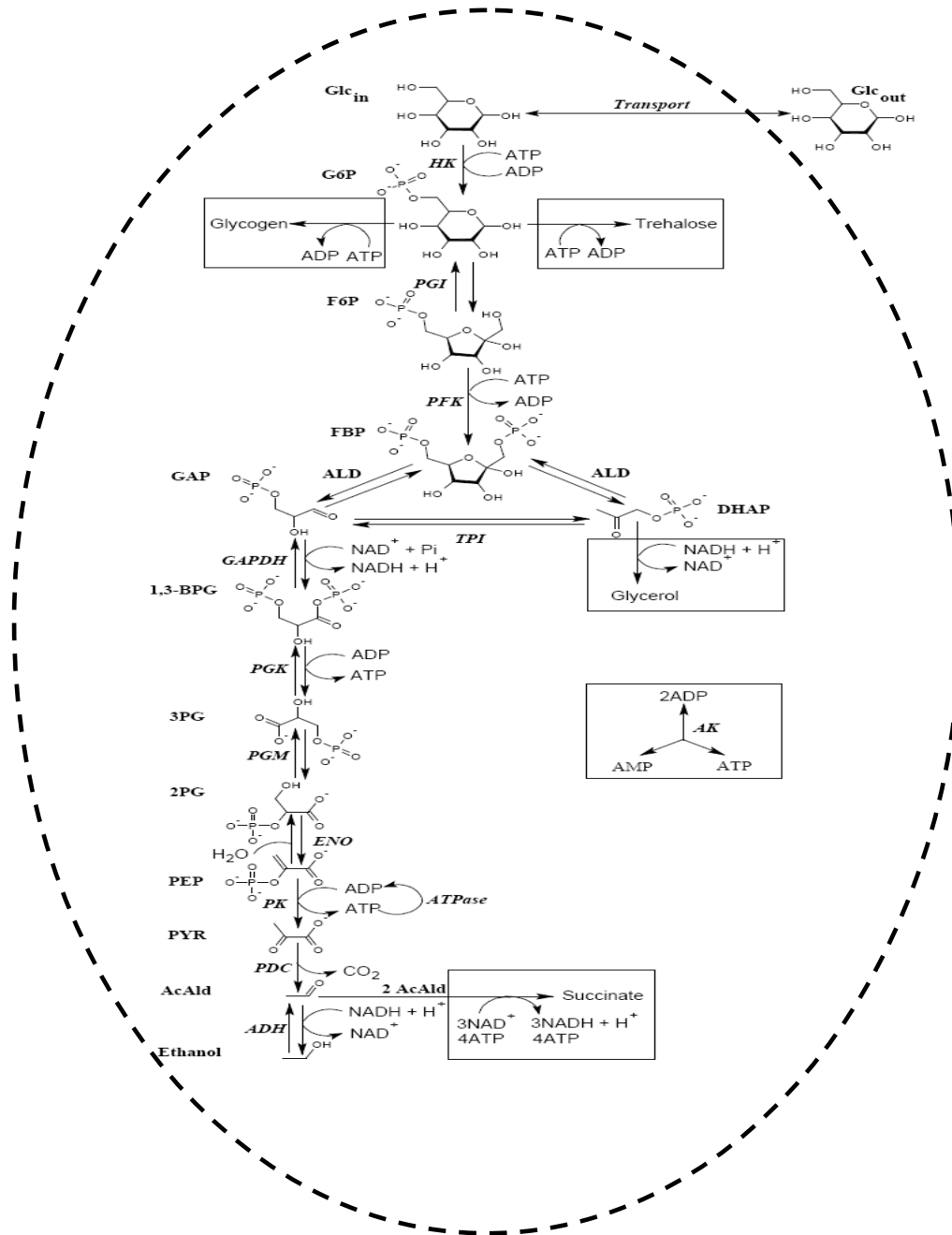


Figure 1.4: Outline of yeast alcoholic fermentation as modeled by Teusink et al. [13]. Rectangle boxes indicate the side branches included in the second extended model for yeast glycolysis. Abbreviations are defined on page vi and vii.

1.5 Chemical differences between the test-tube and the cytoplasm

This section refers to the contrast between the physicochemical environment encountered *in vivo* in comparison to the *in vitro* setting, and the implications thereof for accurately determining kinetic parameters relevant to its cellular location. In spite of fundamental differences, most of what we know in terms of enzyme mechanisms and kinetics has been obtained through the study of these enzymes in isolation and *in vitro*. However biochemists are not limited by technology as they once were, with advances in fields such as high-field NMR spectroscopy (Section 1.6 and 2.1) making it now possible to probe metabolism *in vivo*.

1.5.1 Chemical differences and similarities

The cytoplasm in comparison to the dilute aqueous environments encountered in test tube chemistry, differs most fundamentally in terms of its behavior as a fluid [52]. The cytoplasm's properties as a non-newtonian fluid have been extensively studied in the past; however the physical source for its non-newtonian conduct seems to have eluded scientists [53 -64]. As a result of the cytoplasm behavior as a non-ideal fluid, particle diffusion is affected in a size dependent manner, with large molecules ($> 260\text{\AA}$) suspected to be almost completely non-diffusible within the confines of the cell [52]. These physical constraints lend credence to the hypothesized immobility of cell organelles and large multi-enzyme complexes as a result of their sheer size [52].

The cytoplasm is a non-homogenous suspension, with certain sections or regions having their own unique micro-environment in terms of the degree of macromolecular crowding and the type background molecules encountered [65]. In addition cytoplasmic content cannot be generalized as it differs between various cell types depending on the degree of biochemical specialization, e.g. the erythrocyte densely packed with hemoglobin in comparison to adipocytes and their fatty deposits [65].

The manner in which the unique intracellular architecture and the degree of macromolecular crowdedness influence reaction kinetics and thermodynamics can be understood in terms of the interactions between reactants and parts of the neighboring environment [65]. Three types of interactions may be distinguished:

I. Macromolecular Crowding

The cellular milieu is densely packed with macromolecules (such as proteins and RNA complexes) at a concentration up to 40 times higher than would be encountered *in vitro* [58]. As large macromolecules cannot interpenetrate or permeate one another the volume available for the stacking of large molecules is much less in comparison to the total volume accessible to small molecules [66]. Therefore the free energy of interaction between any molecule and its surroundings is inversely proportional to the probability of placement of that molecule at a random position within the cytoplasm [67]. In layman's terms more energy is required to transfer a larger molecule in a crowded medium in comparison to the transfer of a smaller molecule in a less crowded medium [67]. The amount of energy required as a result of the steric hindrance encountered, depends on the size of the molecule being transferred and the size and shape of the background species [68].

II. Macromolecular Confinement

By and large the fluid phase of the cytoplasm is contained within the spongy networks of intracellular membranes [69]. These so called interstitial fluid filled spaces are analogous to porous channels [66]. The repulsive forces experienced by a macromolecule at the pores' edge, reduce the volume available to it [66]. Thus free energy is required to transfer a macromolecule from an unbound solution to a pore of equal size and volume [70]. Similar to the crowding affect, the amount of energy required for a successful transfer depends on the dimensions of both the molecule and pore [70 & 71].

III. Macromolecular Adsorption

If the macromolecule in question has a net charge opposite to that of a nearby membrane or filament it may be reversibly adsorbed as a result of ionic interactions with the surface [72, 73 & 74]. Post-translationally modified proteins that have a linked hydrophobic lipid side chain may similarly be nonspecifically adsorbed to lipid bi-layers [75]. When the surface adsorption of macromolecules is spontaneous, the free energy change involved is of course negative. The magnitude of the free energy change depends on entropic factors that are related to the size and shape of the molecule being adsorbed [76].

1.5.2 Implications for cellular thermodynamics and reaction kinetics

The validity of the law of mass action to describe biochemical reactions has been called into question in light of the chemical diversity and uniqueness of the intracellular milieu [77, 78 & 79]. As the intracellular environment is highly crowded, it impacts on cellular thermodynamics as well as the rates of molecular diffusion [80, 81 & 82]. As described above, reaction thermodynamics is vulnerable to the effects of volume exclusion, which plays a determining role on the mobility of large molecules. In addition the cytoplasm may undergo phase separation due to variations in the locality and the degree of macromolecular crowding [83, 84 & 85]. The effects of macromolecular crowding may enhance protein associations for the formation of multi enzyme or protein complexes as well as the self association of monomers [86 & 87], improve the rate of protein folding and refolding [88 & 89] whilst simultaneously increasing the stability of proteins by lowering the entropy associated with protein denaturation [90].

When considering the following reaction; $A + B \leftrightarrow C$ in terms of the law of mass action the equilibrium constant can be described as follows: $K_{eq} = \frac{\gamma_C[C]}{\gamma_A[A]\gamma_B[B]}$, where γ_i represent the activity coefficients of the respective substrates and products. In the ideal world of test tube chemistry these activity coefficients are assumed to approach unity [91]. As mentioned above, the intracellular conditions are far removed from the homogenous nature of dilute solutions. *In vivo* these activity coefficients take on a more complicated form ($\gamma_i \neq 1$), arising from the cytoplasm's non ideal behavior due to nonspecific background interactions [92]. The apparent equilibrium constant can then be defined as; $K' = K_{eq} \cdot \tau$, where K_{eq} is the equilibrium constant as measured under ideal conditions and τ is a non ideal correction factor defined in terms of the activity coefficients for the respective reactants [93].

When considering the effect of macromolecular crowding on classical kinetics as described by Michaelis-Menten, the Michaelis constant (K_M) takes on a different form (similar to the equilibrium constant) as a result of varying activity coefficients [81 & 94]. Experimentally it has been shown that the so called apparent Michaelis and inhibition constants ($K'_M = K_M \cdot \tau$; $K'_i = K_i \cdot \tau$) decrease upon the addition of macromolecular crowding agents for mono and bi-substrate reactions [94].

Other more complicated theories such as the power law approximation, [95 & 96] and fractal like kinetics [79 & 97] have evolved as more generic theories for describing both test-tube and *in vivo* enzyme kinetics [91].

Many of the differences discussed above pertain to enzymes that catalyze reactions with macromolecular substrates or products; it is however unclear to what extent, or at all, small molecule kinetics (not diffusion limited) are affected. It is evident that the study of enzymes and metabolism in their natural environment is required to ultimately lay this debate of *in vitro* versus *in vivo* obtained parameters to rest. This emphasizes the importance of applying non-invasive techniques such as NMR spectroscopy (Section 1.6) for performing biochemical analyses in intact cell suspensions (Section 2.1).

1.6 Nuclear Magnetic Resonance Spectroscopy

This section is devoted to NMR spectroscopy, the main analytical method of choice employed during this study. Some of the more theoretical aspects of this technique and the terminology used will be discussed first, followed by an historical and present day overview of NMR spectroscopy's application in the field of biochemistry and more specifically metabolism.

1.6.1 *Theoretical background*

NMR is unique in the sense that excitations are performed on atomic nuclei rather than electrons as encountered in most other spectroscopic techniques. The concepts of nuclear quantum spin and magnetic dipole moments are essential to understand the theoretical complexity surrounding the analytical application of NMR spectroscopy.

I. Nuclear Quantum spin

All sub-atomic particles such as neutrons and protons continually spin along their axes; these spinning masses essentially pair up (proton with proton and neutron with neutron) so that the overall spin of a pair is zero [98]. In certain nuclei, there are unpaired neutrons or protons and the nuclei are set to have an overall quantum spin number. Nuclei with an even number of protons and neutrons have zero quantum spin, nuclei with a odd total of protons plus neutrons have half integer quantum spin numbers and

lastly nuclei with odd numbers of both the subatomic particles have full integer quantum spin numbers [98]. It is only these nuclei with an overall non-zero quantum spin number that can be detected by NMR spectroscopy.

II. Energy states in an externally applied magnetic field

The overall quantum spin number I , is important as it determines the number of possible orientations the nucleus will have in an externally applied magnetic field according to the formula $2I + 1$ [98]. The nuclei of both ^{13}C and ^{31}P have $I = 1/2$ and hence have two possible orientations. When such nuclei are placed in a magnetic field the two spin orientations are of different energy, the low energy α state and the high energy β state [99 & 98]. The population demographics regarding the number of nuclei in either the α or β state is determined by the Boltzman distribution [98]. Initially upon exposure to an external magnetic field there is a slight excess of nuclei in the α state. The nuclei in the low energy spin orientation can be boosted to the high energy β state by means of the absorption of electromagnetic radiation (EMR) [98]. The frequency of EMR required is related to the energy difference between the two states and is characterized as

follows: $\Delta E = \frac{\gamma h B}{2\pi}$ where γ is the magnetogyric ratio and is a nuclear constant, h is Planck's constant and B is the magnetic field strength experienced by the nucleus [98 & 99]. It is important to note that once the populations of nuclei belonging to either state are equal, there will be no net absorption of electromagnetic radiation and the system is said to be saturated [98].

III. Nuclear relaxation

Nuclear relaxation refers to the mechanism by which the nuclei in the high energy orientation revert back to the lower energy state. There are two forms of nuclear relaxation: spin lattice relaxation-where the excited nuclei interact with the nuclei of the sample tube or matrix, and spin-spin relaxation-where the nuclei in the sample relax with the corresponding excitation of other sample nuclei [98]. During spin-spin relaxation, the overall nuclear population demographic does not change although the half life for nuclei in the excited state decreases with time [98]. The time it takes for nuclei to relax back to their low energy state is an important constant called $T1$ [98 & 99]. It is essential to know what the $T1$ relaxation time of the nucleus under study is, so

as to formulate an appropriate excitation – relaxation sequence and evade the problems associated with nuclear saturation.

IV. *The phenomenon of chemical shift*

The magnetic field encountered by each nucleus differs from the applied magnetic field (however slightly) due to nuclear shielding caused by electrons located in close proximity to the nucleus [98 & 99]. Electrons are themselves spinning charges and therefore they also produce their own magnetic fields [98 & 99]. *s*-Orbital electrons generate opposing magnetic fields and are said to shield the nucleus from the external magnetic field, thus an increased magnetic field strength is required to allow the nuclei affected to resonate at their respective transitional frequencies [98]. *p*-Orbital electrons have no spherical symmetry and produce relatively large magnetic fields and are said to de-shield the nucleus, as a lower applied magnetic field is required for nuclear resonance [98]. Chemical shift can be defined as the ratio of nuclear shielding over the applied magnetic field strength ($shift = shielding/B$), and is dependent on the chemical environment of the nuclei being radiated [98]. Chemical shift is calibrated in parts per million (ppm) and is used as an arbitrary scale on which the resonance position of nuclei can be displayed. The scale is said to be arbitrary as the chemical shift of any compound or nucleus is measured relative to an internal standard. The most widely used internal standard is tetramethylsilane (TMS) for both ^{13}C and ^1H NMR [98 & 99]. TMS produces only one signal for all four of its carbon atoms (^{13}C NMR spectra) and all twelve of its hydrogen atoms (^1H NMR spectra), due to the exact chemical similarity between these nuclei.

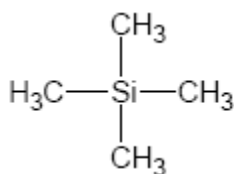


Figure 1.5: Chemical structure of tetramethylsilane.

The application of NMR spectroscopy as an analytical tool for the study of biochemistry and metabolism requires a good understanding of nuclear physics and structural chemistry. For a more comprehensive review refer to literature where cited.

1.6.2 Quantitative applications

In most spectroscopic techniques, including NMR spectroscopy, the stronger the detected signal the greater the abundance of the molecule producing the signal. The signal response (I_x), is directly proportional to the number of nuclei (N_x), producing the resonance signal; $I_x = k_s \cdot N_x$ where k_s is a spectrometer constant [100]. The signals generated by the relaxing nuclei are subjected to a Fourier transformation, which converts these time domain signals to peaks in a frequency domain (Fig. 1.6) [99].

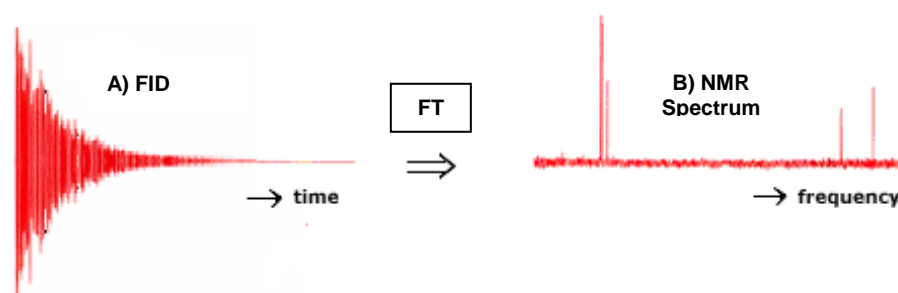


Figure 1.6.: Fourier transformation (FT) of signals in a time domain to signals in a frequency domain. In NMR spectroscopy the signal time domain is called an free induction decay (FID) and is converted via FT to peaks on a frequency axis called a spectrum.

The area underneath the peak is calculated through integration of the signal, either via the classical Newtonian approach or through a deconvolution routine. Through superimposing an ideal reference peak onto the spectrum, the deconvolution algorithm removes any spectral convolution and distortion artifacts caused by magnetic field inhomogeneity and ultimately yields pure Lorentzian peak shapes [101 & 102], thus making this approach well suited for analyzing severely crowded and entangled biological spectra [100 & 102].

An internal standard is required to relate the numerical values obtained through reference deconvolution, to actual concentrations. Quantifiable internal standards in terms of biological NMR should adhere to three important criteria:

1. Should not be pH sensitive (no shift)
2. Should not overlap with biologically important signals
3. Should not interfere with the metabolic behavior of the system under study

In our analyses, tri-ethylphosphate was used as internal standard for ^{31}P spectra, while PIPES buffer was used as the standard for ^{13}C spectra (see Chapters 2 and 4).

1.6.3 NMR spectroscopy in metabolic profiling and biology

Nuclear magnetic resonance spectroscopy is primarily an analytical method and has been used in this regard since its inception in the field of structural chemistry; however since the late 1970's NMR spectroscopy started emerging as a quantitative tool used for probing microbial metabolism. This is largely attributed to technological improvements made in high field spectroscopy in terms of increased sensitivity, which paved the way for the pioneering work done by Shulman et al. [103].

I. *In vivo* NMR

Studying *in vivo* systems is mostly limited to ^{13}C and ^{31}P NMR which covers most of the important metabolic pathways in microbial organisms. With the ^{31}P isotope being 100% naturally abundant, phosphorous NMR allows for the tracking and profiling of cellular phospho-metabolites including the more abundant sugar-phosphates and phospho-nucleotides like ATP. As a result of poor spectral resolution, quantification still proves tricky for the lesser metabolites, especially as signals are broadened in the presence of paramagnetic ions such as Mg^{2+} [103]. As the natural abundance of the ^{13}C isotope is only a meager 1.1%, labeled compounds or extremely high concentrations of substrate are required for performing ^{13}C NMR assays *in vivo*. Whole cell ^{13}C NMR spectra are however generally better resolved and yield greater signal to ratios than their ^{31}P counterparts [104]. Three factors contribute to the improved resolution of carbon spectra; 1) ^{13}C signals have reduced peak widths at half peak height in comparison to ^{31}P [104], 2) ^{13}C (~100 ppm) has much wider chemical shift range than ^{31}P (~20 ppm) [104], and finally 3) due to the low natural abundance of the ^{13}C isotope spin-spin coupling interactions are minimized resulting in less cluttered spectra.

The advantages of using a non invasive technique such as NMR to perform experiments *in vivo* include the following [103]: 1) NMR allows for online or real time acquisition of spectra, 2) metabolite time courses regarding substrates, intermediates and end products can be obtained from the same sample and 3) samples may be probed multiple times which allows for the monitoring of parameters that may be unobservable *in situ* or *in vitro*.

Various systems have been devised for studying cells *in vivo*; these include non-perfused systems (Fig 1.7), essentially consisting of a glass NMR tube with a sealed capillary containing the internal standard in the center. By contrast, perfused systems (Fig. 1.8) are similar to bioreactors fitted with both a fresh medium inlet and excess medium outlet valves, permitting continuous circulation of the system [103].

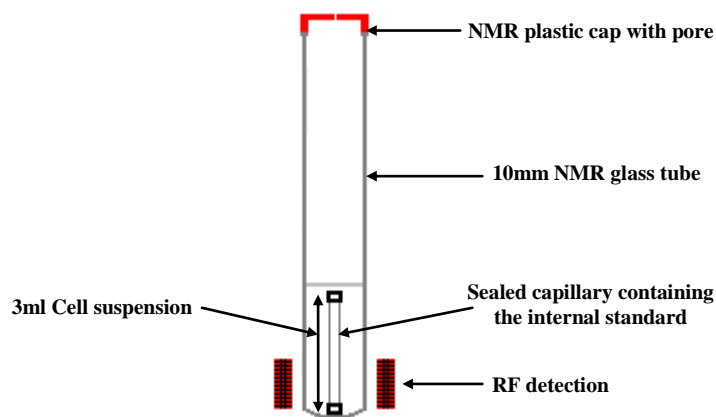


Figure 1.7: Example of a non-perfused system setup, for *in vivo* NMR. This is similar to the system used in the work presented in this study. Cells may also be kept under a carbon dioxide atmosphere to ensure anaerobic fermentation. Figure was adapted and modified from Grivert & Delort [103].

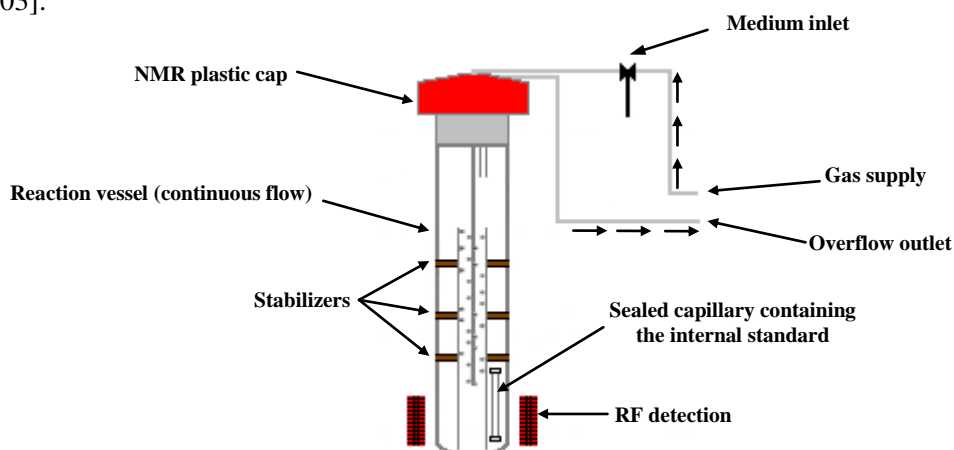


Figure 1.8: Example of perfused system for *in vivo* NMR. Gas enters through the capillary tubing creating circulation through the vessel; fresh medium is pumped in through the rubber seal and an overflow tube is fitted to prevent leakage of excess medium in the spectrometer. Figure was adapted and modified from Malvin & Shanks [105].

II. Bioenergetics with ^{31}P NMR

High resolution ^{31}P NMR has been used to probe metabolic processes in various cells [106], tissue types [107 & 108] and even in intact mammalian organs [109 & 110]. ^{31}P NMR may be applied for the quantification of various cellular contained phospho-metabolites and for measuring the internal pH of both intact cells and organelles [111].

In addition to the current work presented here, ^{31}P NMR spectroscopy has proved useful for tracking important molecules such as ATP *in vivo* [111].

ATP's α , β and γ phosphates (Fig. 1.9) give rise to three distinctive resonance signals (Fig. 1.10). Unfortunately the α and β phosphate resonances of ADP overlap with those of α and γ ATP, when measured *in vivo* [103]. Resolution may however be increased through optimization of experimental conditions and acquisition parameters used during the assay or by reverting to the use of purified cell extracts for quantification of these and other nucleotides [103].

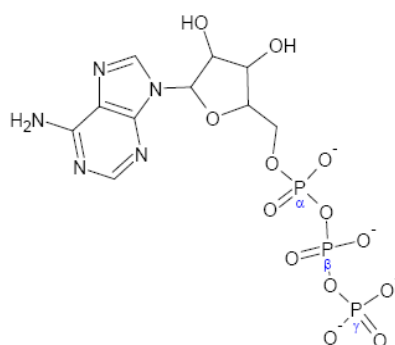


Figure 1.9: Chemical structure of ATP.

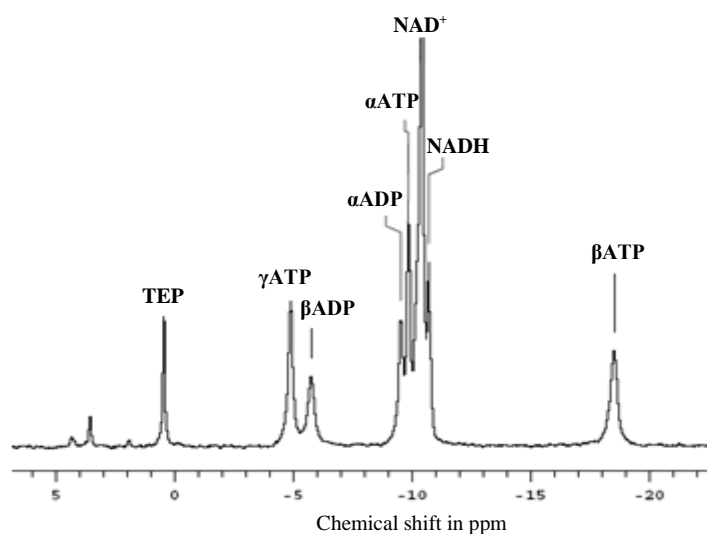


Figure 1.10: ^{31}P Spectrum showing the resonance positions for the following metabolite standards (pure components were used): 5mMATP, 2.5mMADP, 2.5mM TEP, 5mM NAD^+ and 2.5 mM NADH. Samples were prepared in 100mM PIPES buffer pH 6.1. Refer to Chapter 4, for standard acquisition parameters.

Measuring internal pH with NMR is based on the proton exchange between the various ionic forms of inorganic phosphate [103]. This proton exchange is extremely fast leading to the observation of only a single peak for inorganic phosphate, with its resonance position dependent on the ratio of the protonated vs. de-protonated species

and hence pH [103]. Phosphate resonance can therefore be correlated to pH by constructing a P_i chemical shift versus pH calibration curve.

^{31}P NMR can prove useful for the study of microbial energetics as both transmembrane pH gradients and nucleotide triphosphates may be assessed [103]. Many *in vivo* ^{31}P NMR studies have focused exclusively on *S. cerevisiae* metabolism, these include the measurement of steady state fluxes between inorganic phosphate and ATP [112], intracellular pH comparisons under various conditions and general metabolic assessments between wild type and mutant yeasts [113 & 114].

III. Flux measurements with ^{13}C NMR

Understanding biochemical systems in terms of the identity of metabolic intermediates, substrates, end-products and network topology provides us merely with a stationary view of metabolism [103]. Measuring metabolic fluxes yields both qualitative (which pathways) and quantitative information (reaction rates) regarding pathway activity under varying physiological conditions, and as such helps paint a more dynamic picture of metabolism [103]. The application of NMR spectroscopy for measurement of metabolic flux has several advantages over the more laborious methods of the past: 1) it allows for the simultaneous assay of chemically distinct compounds, 2) the unraveling of complex labeling patterns, 3) the analysis of isotopomer distribution and 4) it negates the problems associated with the use of radioactive compounds [103].

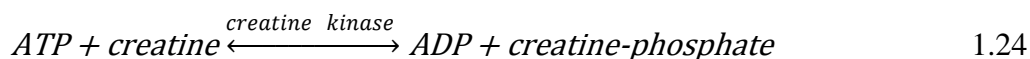
The use of NMR spectroscopy for quantifying metabolic flux started in the 1980s when Walsh and Koshland measured the reaction rates of the TCA cycle and glyoxylate shunt enzymes [115]; this was shortly followed by the extensive series of publications by Shulman's group on metabolic fluxes in yeast [116]. Presently NMR spectroscopy has become an established method for metabolic flux determinations and has further evolved and matured with new techniques such as 2D fluxomics, and linked NMR-GC-MS assays [103, 117, 118 & 119].

To follow up on this review of NMR spectroscopy, the phospho-creatine system will be discussed next in terms of its free energy buffering capability and use for estimating intracellular ATP and ADP.

1.7 Creatine kinase as an artificial free energy buffering system in yeast

This section describes the ability of creatine phosphate to function as a cellular free energy stockpile, along with some of the thermodynamic constraints of the reaction catalyzed by creatine kinase, which makes this phenomenon possible. This review serves as general background regarding the phospho-creatine system, its application and relevance for the purpose of performing a SDA will however be discussed in Chapter 2.

In metabolic terms ATP functions as a free energy transmitter, able to release the chemical energy contained in its phospho-ester bonds almost instantaneously [1]. However, at any given moment, the amount of ATP in a cell can sustain its demand for free energy for only a limited period of time [1]. Therefore the cell requires a means for the continuous regeneration of ATP, a sort of buffering system so as to prevent ATP from dropping to dangerously low concentrations [1]. In muscle tissue which has an extremely high rate of ATP turnover, a free energy reservoir is maintained for the purpose of rapidly regenerating ATP [1]. The phospho-creatine system is most often used in this regard. Creatine kinase rapidly and reversibly catalyzes the phosphate transfer from ATP to creatine forming the high energy compound creatine phosphate.



Under standard conditions this reaction operates endergonically [120], however in muscle tissue this reaction manages to maintain near equilibrium between all its respective reactants [120, 121 & 122]. During rest when ATP demand is low the equilibrium lies in the direction of creatine-phosphate (CrP); conversely during strenuous exercise or times of increased free energy demand the equilibrium shifts towards the production of ATP [120]. Therefore the CrP pool functions analogously to a buffer system in terms of keeping ATP (more specifically the [ATP] / [ADP] ratio) constant in cells or tissues that express creatine kinase [1]. Due to this equilibrative nature, the equilibrium constant of the creatine kinase reaction has extensively been applied for determining cytosolic concentrations of ATP and ADP in muscle and other cell types [123, 124, 125 & 122].

1.7.1 Apparent equilibrium constant of the creatine kinase reaction

The equilibrium constant as measured for a biochemical reaction actually refers to the apparent equilibrium constant (K_{app} or K') and not to the chemical equilibrium constant (K_{eq} or K). The concentration terms in the expression for K' (Equation 1.26) refer to the sum of all the ionic forms (including metal complexes) of the particular reactant present (Equations 1.27 – 1.29), and in many instances this expression is not balanced in terms of charge and mass as is the case for a chemical equilibrium constant at specified pressure, temperature and ionic strength (Equation 1.26). Therefore in biochemistry appropriate readjustment of any reactions K' to the parameters pH and the concentration of free metal ions are of utmost importance if relevant estimations regarding the reactant concentrations are to be made from the biochemical equilibrium expression [126]. The reaction catalyzed by creatine kinase is by no means different, with the value for K' shown to vary accordingly with changes in pH and the free concentration of Mg^{2+} [126, 121 & 120].

$$K_{\text{creatine kinase}} = \frac{[ATP^{4-}] \cdot [Cr]}{[ADP^{3-}] \cdot [CrP^{2-}] \cdot [H^+]} \quad 1.25$$

$$K'_{\text{creatine kinase}} = \frac{[ATP] \cdot [Cr]}{[ADP] \cdot [CrP]} \quad 1.26$$

$$[ATP] = [ATP^{4-}] + [HATP^{3-}] + [MgATP^{2-}] + [MgHATP^{1-}] \quad 1.27$$

$$[ADP] = [ADP^{3-}] + [HADP^{2-}] + [MgADP^{1-}] + [MgHADP] \quad 1.28$$

$$[CrP] = [CrP^{2-}] + [HCrP^{1-}] + [MgCrP] \quad 1.29$$

Obtaining comparable values from literature for $K'_{\text{creatine kinase}}$, even when determined under identical physical circumstances through the same analytical method proves to be difficult, with values ranging between 100-200 under physiologically relevant conditions [121 & 127]. Ultimately resorting to a combination of $K'_{\text{creatine kinase}}$ values obtained from literature and those determined during this study seems the most satisfactory route for implementing the phosho-creatine system in permeabilized yeast (see Chapters 2 and 4).

With all the required background information as well as some of the more theoretical aspects being discussed up to this point, the results obtained upon performing an experimental supply demand analysis on yeast fermentative free energy metabolism will

be presented next. For a discussion concerning the exact means of implementation of the techniques used during this study refer to materials and experimental procedures presented in Chapter 4.

Chapter 2

Experimental supply demand analysis of anaerobic yeast glycolysis

The results chapter is divided into four main sections; *in vivo* NMR spectroscopy (2.1), the study of glycolysis *in situ* (2.2), application of creatine kinase as a free energy buffer in permeabilized yeast (2.3), and whole cell experimental SDA on yeast fermentative metabolism (2.4). In each section preliminary data (appropriate controls and checks) are presented first followed by the definitive results and data interpretation.

2.1 In vivo NMR spectroscopy

In order to perform an SDA analysis on yeast fermentative free energy metabolism, both steady state [ATP] / [ADP] ratios and glycolytic flux measurements are required (refer to Section 1.3 & 3.3). As NMR spectroscopy is a non-invasive technique that can be applied to the study of microbial metabolism in intact cell suspensions (Section 1.6), it was hoped that this method would afford us with the ability to accurately quantify both glycolytic flux and the [ATP] / [ADP] ratio in order to perform a supply demand analysis *in vivo*. This section is therefore concerned with the application of NMR spectroscopy for probing yeast fermentative metabolism *in vivo*, both in terms of steady state fluxes (^{13}C NMR) and intermediate concentrations (^{31}P NMR).

The preliminary results include characterization of yeast cell growth, metabolic profiling through NMR resonance assignments, intracellular pH determination with ^{31}P NMR and the calibration of ^{13}C spectra for the effects of saturation. The main results comprise *in vivo* steady state [ATP] / [ADP] time course data and glycolytic flux measurements.

2.1.1 Characterization of Saccharomyces cerevisiae cell growth

The *Saccharomyces cerevisiae* strain CEN.PK-113.7D was grown in batch culture on normal YPD medium (Chapter 4). Growth was assayed by following the culture optical density ($\ln \text{OD}_{600}$) over time. Data were analyzed via linear regression and yielded an

excellent R^2 fit of 0.999, reflecting the constant rate of growth maintained by these yeasts during the exponential phase. The maximal specific growth rate was calculated at $\mu_{max} = 0.537 h^{-1}$ and is in good agreement with previous determinations in our laboratory ($\mu_{max} = 0.540 h^{-1}$) [128].

2.1.2 ^{31}P NMR resonance assignments

The main purpose of these ^{31}P *in vivo* NMR assays was to determine the $[ATP] / [ADP]$ ratio for correlation with glycolytic flux measurements. As the analyte is not preselected during NMR spectroscopic assays, a whole host of phospho-metabolites can be observed during spectral analysis. The ^{31}P NMR spectra obtained from intact yeast cells, hence contain a lot of additional information regarding metabolite concentrations and the relative composition of the phospho-metabolite pool. Identification of the resonance signals observed *in vivo* is a complicated task owing to the unique chemical environment that predominates intracellularly (Section 1.5). Sample spiking can yield ambiguous results concerning the exact resonance positions of protonatable metabolites *in vivo* [129], as the enhanced signals stem from spiked metabolites that are located outside the cell at a different pH to that encountered intracellularly. By comparing the relative chemical shifts of glycolytic standards to peaks in the spectrum along with reports from literature, resonance assignments were made.

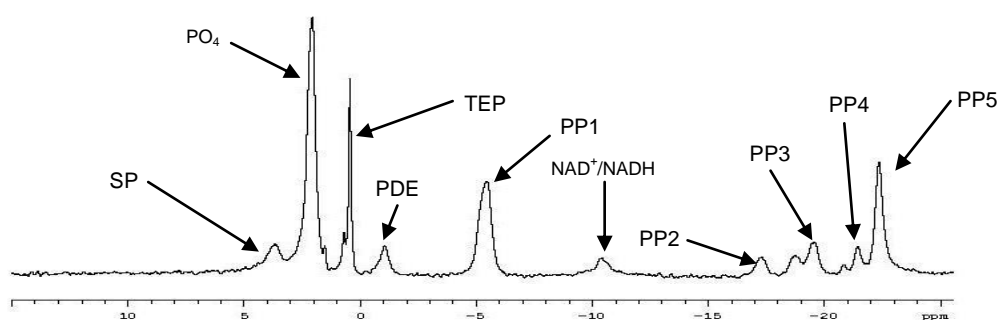


Figure 2.1: A typical ^{31}P *in vivo* background spectrum. This figure is representative of an $OD_{600} = 500$ cell suspension prepared in 100mM PIPES buffer pH 6.1. SP; sugar phosphates, PO_4 ; inorganic phosphate, TEP; Triethyl-phosphate, PDE; phospho-diester, PP1-PP5; polyphosphates 1 to 5.

The spectrum shown in Fig. 2.1 depicts the phospho-metabolites present in resting yeast cells prior to the addition of glucose. The major components identified were inorganic

phosphate (PO_4), and four separate resonance signals corresponding to the terminal (PP1), penultimate (PP2-PP3) and inner (PP4-PP5) phosphates of storage polyphosphates [130 & 131]. Less abundant signals corresponded to: PDE-which coincides with the resonances for phosphodiesteres such as mRNA and tRNA [132 & 133]; SP- which includes the glycolytic sugar phosphates (mostly FBP) and an overlapping resonance for NAD^+ and NADH [130 & 131] was also observed.

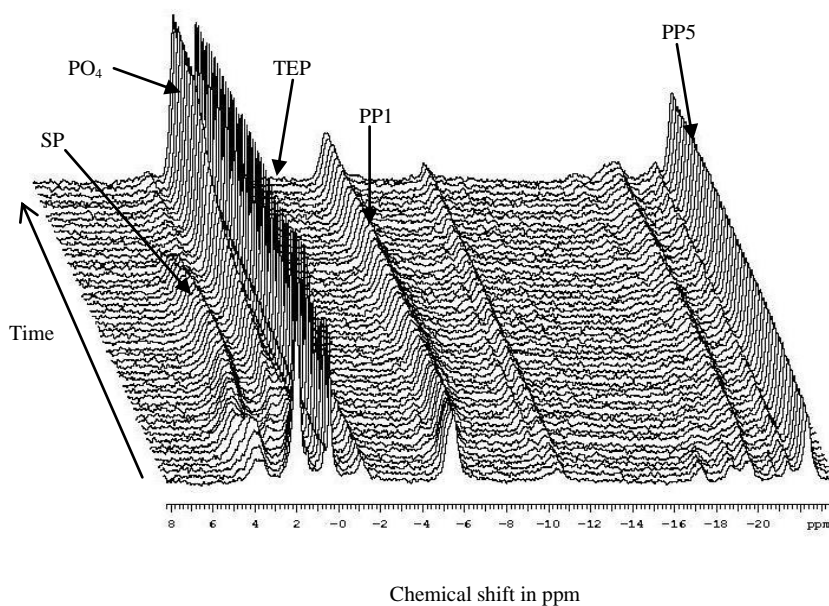


Figure 2.2: A typical *in vivo* ^{31}P NMR stack plot obtained during anaerobic fermentation in yeast. This figure is representative of an $\text{OD}_{600} = 500$ yeast cell suspension fed with 100mM glucose at time zero. Successive spectra are separated by 1 minute time intervals; refer to Chapter 4 for standard acquisition parameters.

With the onset of fermentation, dynamic metabolic changes occur (Fig 2.2).

Polyphosphate metabolism seems to be undisturbed with no significant changes in signal intensity observed over time. The sugar phosphate (SP) peak reflects the intermediary behavior of yeast glycolysis, increasing at first it reaches a quasi steady level and then slowly declining until depletion. The pH dependent shift of both the SP and inorganic phosphate signals, points towards a general acidification of the cytoplasm during the initial stages of fermentation (up-field shift).

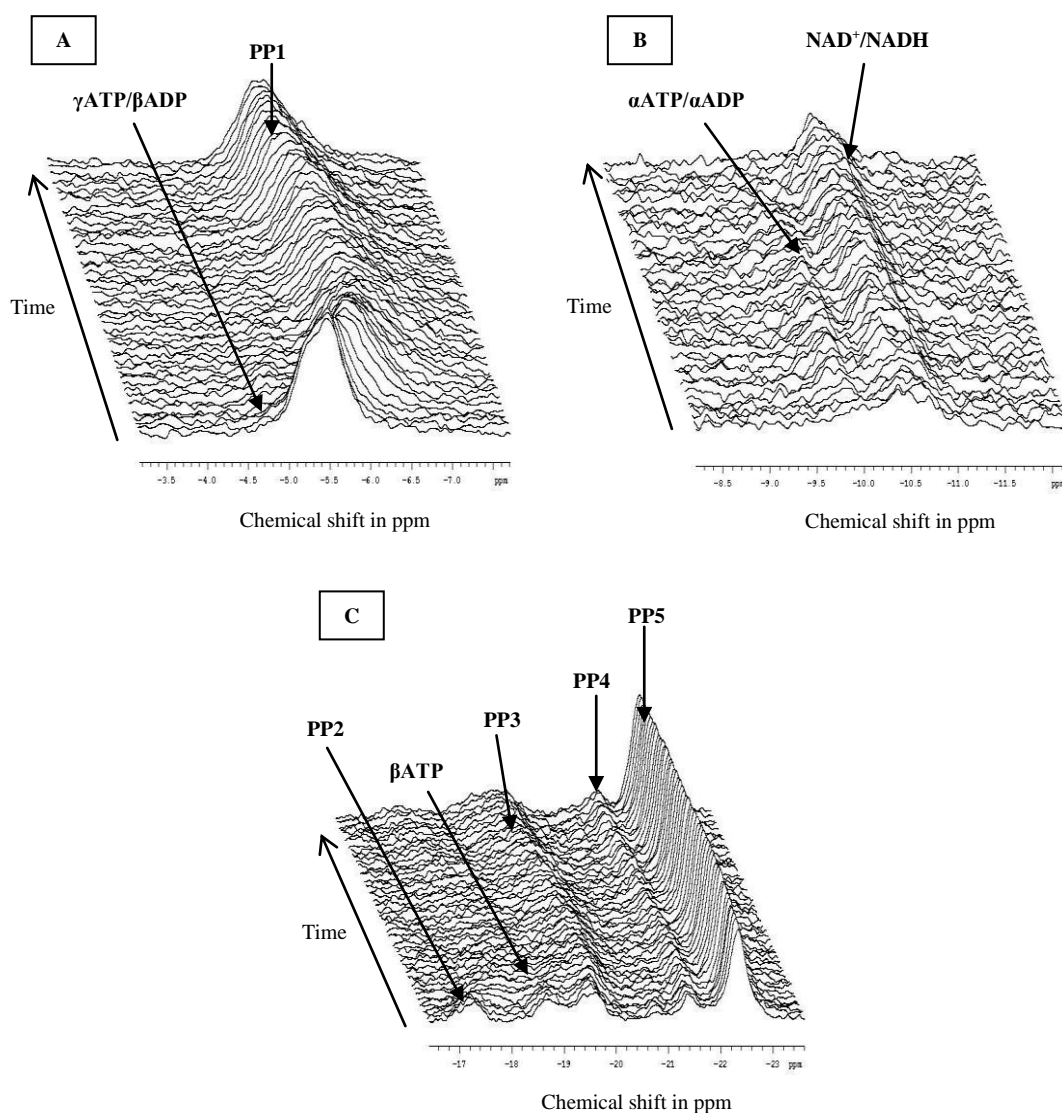


Figure 2.3: Close up of the stack plot shown in Fig. 2.2 in the regions of: A) -3.5 to -7ppm; B) -8 to 12ppm and C) -17 to -23ppm.

The unresolved resonances for $\gamma\text{ATP}/\beta\text{ADP}$ and $\alpha\text{ATP}/\alpha\text{ADP}$ as well as their close proximity to the larger signals belonging to PP1 and NAD^+/NADH can be seen in Fig. 2.3 A and B, with the solitary position for βATP located between PP2 and PP3 shown in Fig. 2.3 C.

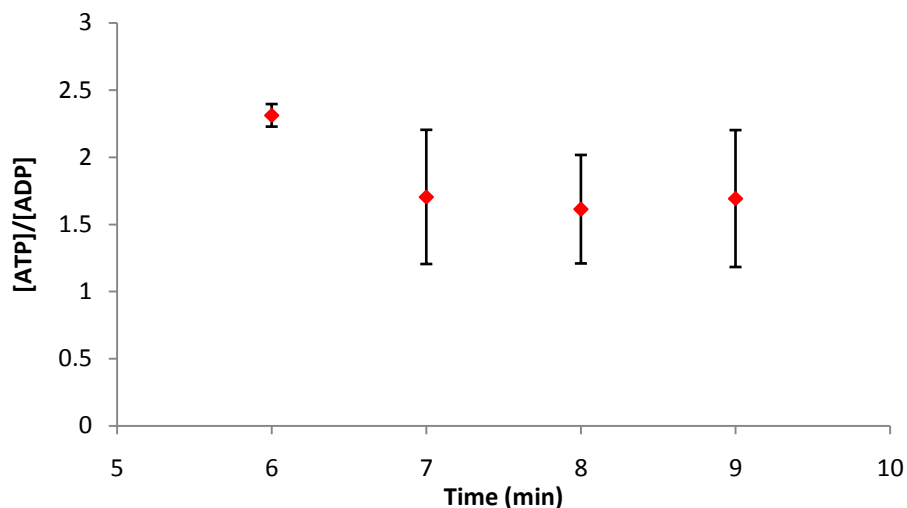


Figure 2.4: *In vivo* time course for the steady state [ATP] / [ADP] ratio in fermenting yeast. Data represent the averaged values as assessed across three separate fermentations. In all three experiments 100mM glucose was added as substrate, at time zero. Y-error bars reflect the standard error of the mean. For discussion on how ATP and ADP were calculated refer to main text below.

Steady state [ATP] / [ADP] ratios were tentatively calculated (1.83 ± 0.64) from *in vivo* ^{31}P NMR spectra (Fig. 2.4). Only the β ATP (Fig. 2.3 C) signal was directly quantified by means of deconvolution, ADP was calculated through subtraction of the β ATP signal from the α ATP / α ADP (Fig. 2.3 B) overlap at -10ppm. Unfortunately, inadequate resolution combined with low signal intensities lead to the large errors associated with these measurements. These ^{31}P assays were therefore not deemed sufficient for an accurate and robust analysis of the ATP-ADP moiety *in vivo*. Similar problems concerning the direct measurement of specifically ADP using *in vivo* NMR have also previously been reported [134]. This does, however, not exclude the potential for the successful application of *in vivo* NMR to quantify the [ATP] / [ADP] ratio in organisms other than yeast, which are not hindered by large polyphosphate peaks that obscure the view of any closely related metabolite of lower abundance [135].

2.1.3 Determination of intracellular pH with ^{31}P NMR spectroscopy

^{31}P NMR allows for the measurement of intracellular pH as a result of the pH dependent chemical shift of the inorganic phosphate signal [103]. The chemical energy contained within transmembrane pH gradients is often used for the active transport of various molecules, hence changes in cytoplasmic pH may disrupt these gradients and thereby affect cellular energy charge and the physiological state of the cell [103]. With distinct

signals being identified for intracellular and vacuolar P_i pools (Fig. 2.5), the opportunity presented itself for quantifying both intracellular pH and the up-field shift observed in spectra obtained during glycolysis. By setting up an appropriate pH vs. P_i chemical shift calibration curve (Fig. 2.6) intracellular pH could be determined.

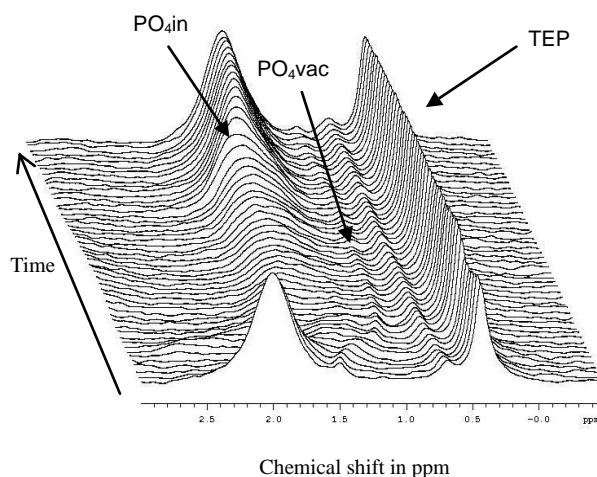


Figure 2.5: Expansion of the down field region of Fig. 2.3, displaying the pH dependent shift observed for both cytoplasmic and vacuolar phosphate signals. Resonance assignments were made according to Shulman et al. (1981, 1985) [130 & 131]. PO_4in - intracellular P_i ; PO_4vac - vacuolar P_i .

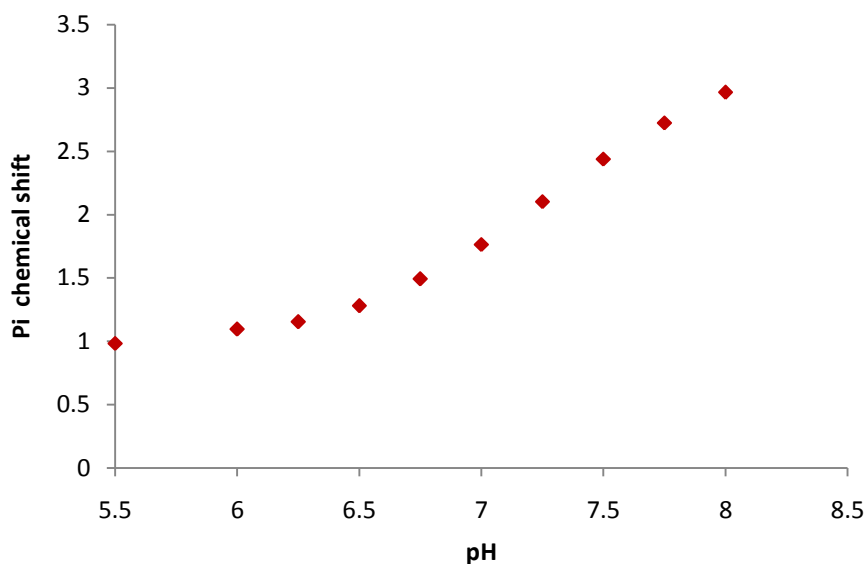


Figure 2.6: Chemical shift of P_i versus pH calibration curve. Titrations were performed in 100mM PIPES buffer, containing 5mM KH_2PO_4 , 5mM $MgCl_2$ and 5mM EDTA.

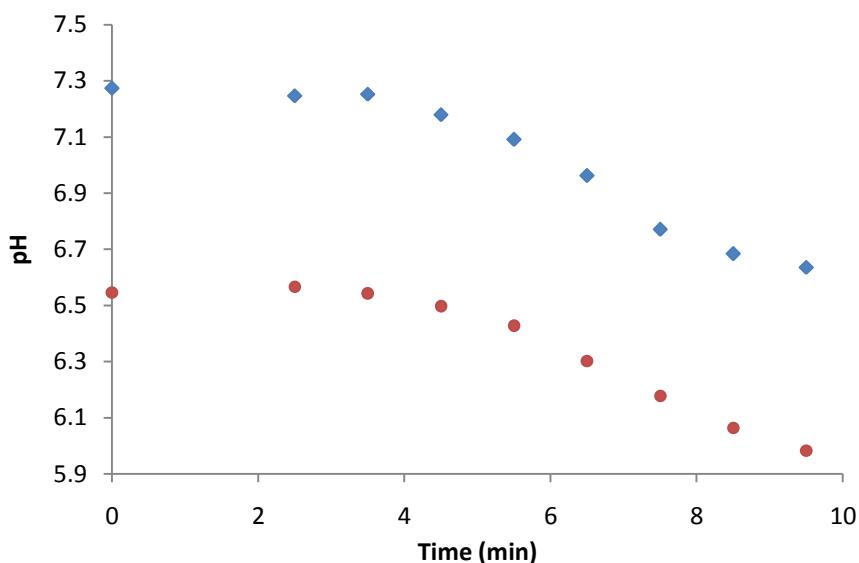


Figure 2.7: Cellular acidification during the onset of yeast glycolysis. Representative of an $OD_{600} = 500$ cell suspension fed with 100mM glucose at time point zero. Blue diamonds = cytoplasmic pH; Red circles = vacuolar pH

The value for yeast intracellular pH as calculated under resting conditions (nitrogen, carbon and energy limited) was 7.27, and is somewhat more basic than the pH range (5.7-6.9) reported in starved yeast by Salhany et al. (1975) [132]. It is evident from Fig. 2.7 that both the cytoplasm and the vacuole acidify within the first eight minutes after the addition of glucose and start of fermentation. Unfortunately the diminished signal intensity observed for inorganic phosphate during the middle parts of the spectrum (see Fig. 2.5) hampered resolution and prevented a more detailed analysis of these intracellular pH changes. However cytoplasmic pH did recover somewhat after the initial drop, stabilizing at pH~ 6.75 during the later stages of fermentation. The transvacuolar pH gradient remained relatively constant at ~0.65 in spite of the large pH changes encountered intracellularly.

In a related study performed by Shulman et al. [131] a similar trend concerning the acidification of the cytoplasm following the onset of glycolysis in yeast was found, however a temporary pH increase was also observed immediately after glucose addition (± 2 min) prior to the general pH drop (pH < 7.0). The long dead times (time elapsed between the addition of substrate and acquisition of the first spectrum) associated with the *in vivo* NMR assays performed in this study, makes the observation of transient behavior directly following the glucose pulse (± 2 min) impossible and may clarify the absence of the proposed pH spike (see Fig. 2.7). In the absence of any vessel circulation (no gas perfusion), Shulman et al. [131] identified the buildup of CO_2 as carbonic acid

as the most likely cause for the observed cytoplasmic acidification. This proposed explanation may be extended to the present situation, as no gas bubbling was employed during our assays.

2.1.4 Determination of glycolytic flux with ^{13}C NMR spectroscopy

Glycolytic flux can be quantified in terms of the absolute rate of substrate (glucose) utilization or the rate of end product (ethanol) formation. The natural abundance of ^{13}C is a mere 1.1%; therefore in order to measure fluxes accurately using NMR spectroscopy, ^{13}C labeled substrate (glucose) is required. During glycolysis, the C6 and C1 carbon atoms of glucose end up at the C2 position of ethanol, and the glucose ring carbons C2 and C5 are incorporated at the C1 position [104]. The central glucose ring carbons; C3 and C4 are lost as CO_2 through decarboxylation [104]. Therefore in order to measure the ethanol production rate, ^{13}C enriched glucose at positions C1 or C6 was used as substrate. Depending on the purpose of the experiment either pure label or a combination of labeled and unlabeled glucose may be used. All fluxes measured were normalized to total protein by means of a Bradford protein determination assay [139].

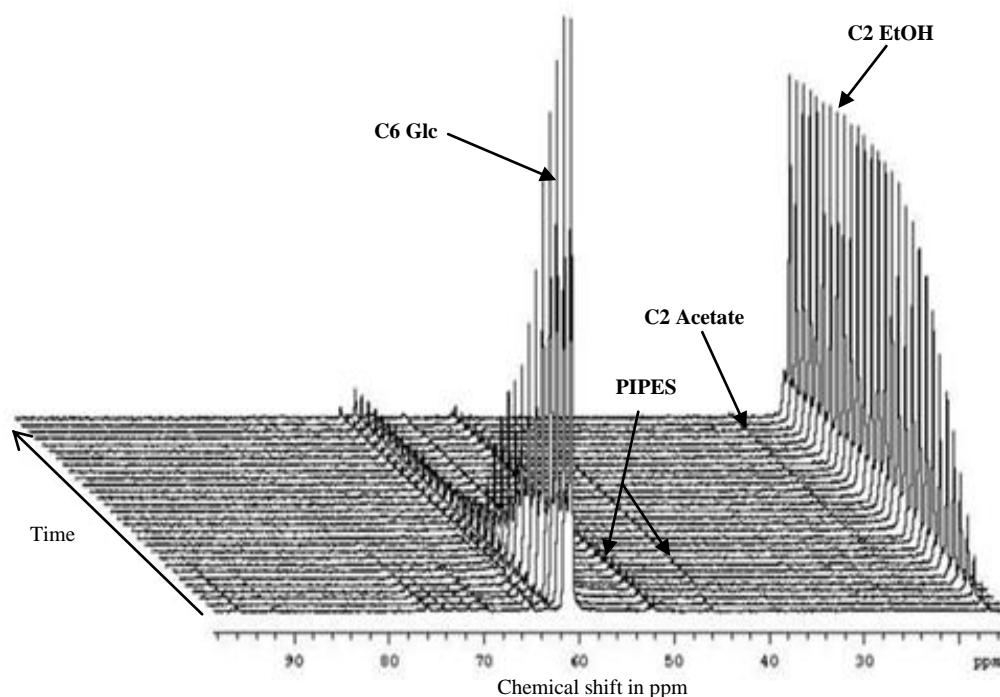


Figure 2.8: A typical *in vivo* ^{13}C NMR stack plot obtained during anaerobic fermentation in yeast. This figure is representative of an $\text{OD}_{600} = 500$ yeast cell suspension fed with 100mM $^{13}\text{C}_6$ pure labeled glucose at time zero. Successive spectra are separated by 1 minute time intervals; refer to Chapter 4 for standard acquisition parameters.

With reference to Fig. 2.8, the addition of $^{13}\text{C}_6$ labeled glucose yielded only a solitary peak for the substrate (compare with Fig. 2.14) with the other major resonance corresponding to the C2 carbon of ethanol. The three small resonance signals in the middle of the spectrum stem from the natural abundance of ^{13}C in the PIPES buffer. A weak signal for the C2 carbon of the fermentation by product acetate was also observed in the up-field region of the spectrum [140 & 104].

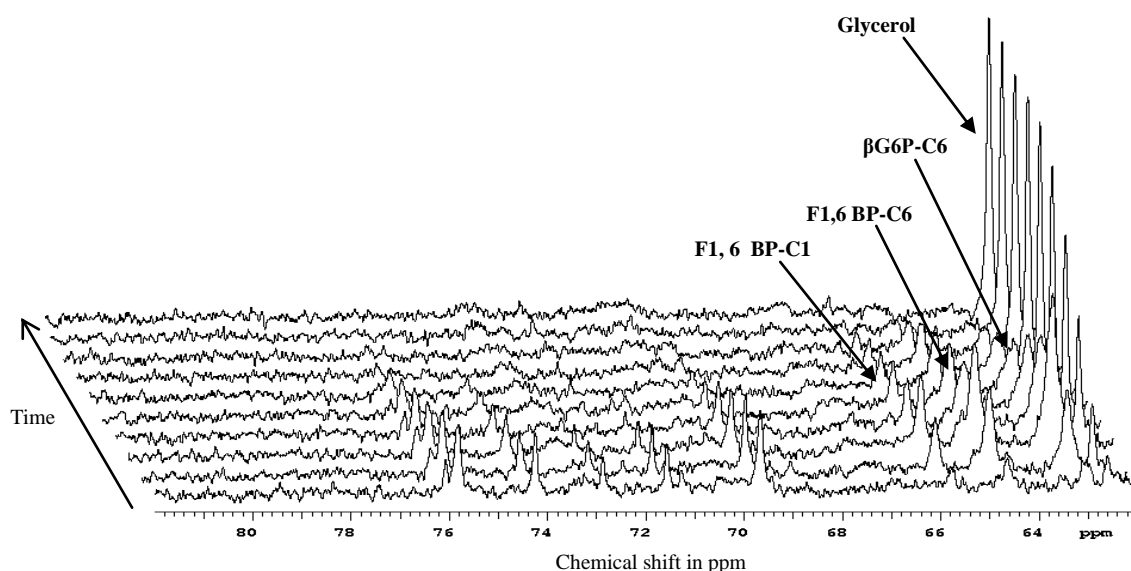


Figure 2.9: Expansion in the midfield region of the typical *in vivo* ^{13}C NMR stack plot displayed in Fig. 2.8. This figure is representative of an $\text{OD}_{600} = 500$ yeast cell suspension fed with $100\text{mM } ^{13}\text{C}_6$ labeled glucose at time zero. Successive spectra are separated by 1 minute time intervals; refer to Chapter 4 for standard acquisition parameters.

The close-up view in Fig. 2.9 illustrates the high degree of resolution obtained with ^{13}C NMR, with FBP, G6P and glycerol being separated in the narrow band from 63 to 66 ppm. The unmarked resonances in the middle of the spectrum arise from impurities ($\pm 1\%$) contained in the labeled substrate.

The presence of both $^{13}\text{C}_1$ and $^{13}\text{C}_6$ -FBP in the sample was a result of label shuffling occurring at the level of TPI which is responsible for scrambling of the ^{13}C signal between the C6 atom and C1 atom of F6P [104]. All resonance assignments were made in accordance with Shulman et al. [130, 140 & 104].

Consecutive excitations of quantum-spin nuclei are achieved through rapid pulse spectrometry, these assays are characterized by pulse sequences with short acquisition and delay times (refer to Chapter 4). During rapid pulsing some of the nuclei will become partially saturated (not fully relaxed) upon sequential exposure to the resonating

RF field and will produce signals of diminished intensity (see Section 1.6). Through experimental analysis it was shown that with the employed pulse sequence both the $^{13}\text{C}_2$ carbon of ethanol and the $^{13}\text{C}_3$ carbon of glycerol were affected. Appropriate calibration curves were set up to quantify the extent of nuclear-saturation on the estimated concentration of these metabolites.

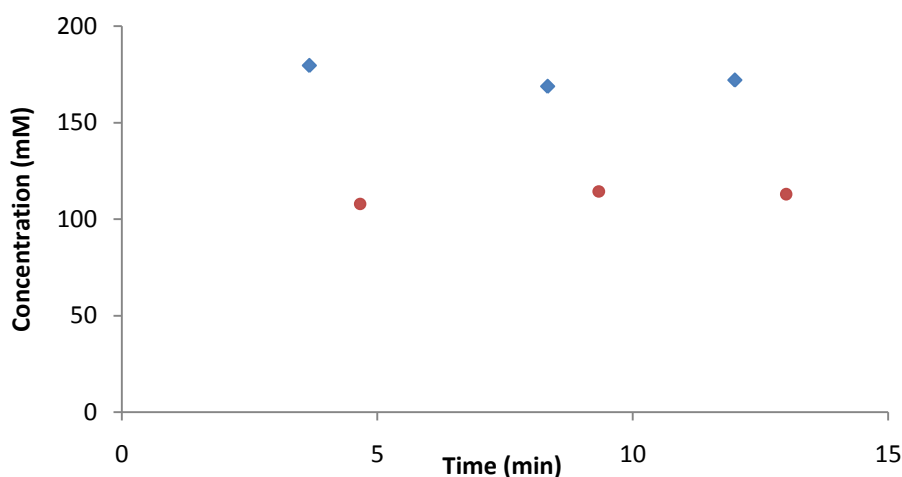


Figure 2.10: Saturation calibration curve for ethanol labeled with ^{13}C at its C2 position. Concentrations were determined through normalization of ^{13}C peak heights to those measured for the internal standard (100mM PIPES buffer). Refer to Chapter 4, for acquisition parameters; Red circles = rapid pulsed; Blue diamonds = fully relaxed.

The errors associated with saturation may be quite large such as in the case for ethanol shown in Fig. 2.10, and should not be ignored when a true quantitative assessment is needed. Saturation correction factors were calculated for the C2 carbon of ethanol (1.67) and the C3 carbon of glycerol (2.92) and were used throughout for estimating the concentrations of these metabolites from ^{13}C spectra. A similar calibration was set up for both the C1 and C6 carbons of glucose, but saturation was found to be negligible.

The time course displayed below in Fig. 2.11 shows the conversion of glucose to the major fermentation end products, ethanol and glycerol. Data were analyzed by means of linear regression (time points 2 through 10) and yielded good R^2 values > 0.94 . Steady state fluxes were calculated from the regression lines.

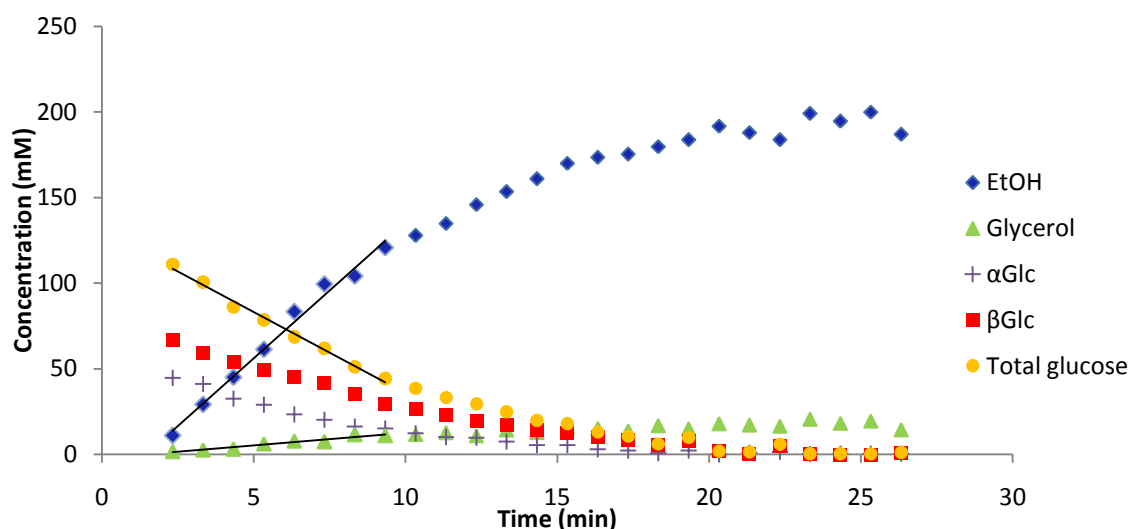


Figure 2.11: Fermentation time course for the external metabolites ethanol, glucose and glycerol. This figure is representative of an $OD_{600} = 300$ yeast cell suspension fed with 133mM glucose (10% ^{13}C -labeled) at time zero. α Glc and β Glc refer to the α and β anomers of D-glucose labeled at its C1 position. Linear regression lines were fitted for EtOH, Glc and glycerol and are indicated in black. All concentrations were determined from ^{13}C NMR spectra.

Table 2.1: Basal glycolytic flux

Metabolite	Normalized flux ($\mu\text{mol}/\text{min}/\text{mg}$ protein)	% Of glycolytic flux directed towards metabolite	% Total of carbon recovered
Glc	1.69 ± 0.01	-	96.6
EtOH	2.81 ± 0.02	83.2	
Glycerol	0.45 ± 0.01	13.3	

The results in Table 2.1 represent the averaged rates of change for ethanol, glucose and glycerol as assessed across three separate fermentations. The reproducibility of these data is reflected by the minimal standard error in the measurement. 96.6 % of the total carbon was recovered through the synthesis of ethanol (~83% of flux) and glycerol (~13% of flux) the two major fermentation end products. The minimal amounts of acetate (Fig. 2.8) and glycogen (generally a broad resonance obscured by C1 glucose at 102ppm) observed during fermentation can potentially account for the unrecovered label (~3%), although quantitative verification is still required. In a similar study by Shulman et al. [140] substantial losses in the ^{13}C label were reported during fermentation with only a mere 60% of the total glucose consumed recovered in the production of ethanol

(55%) and glycerol (5%). In this regard the data presented here compares exceptionally well, however differences in assay protocols and spectrometer sensitivity may partly account for these discrepancies [140].

In this section we have shown that whole cell glycolytic flux can accurately be quantified with the use of ^{13}C NMR. Unfortunately measuring the internal [ATP]/[ADP] ratio with ^{31}P NMR proved problematic. Next we attempted to quantify fluxes and nucleotide ratios in permeabilized yeast (*in situ*) as an alternative to the *in vivo* work. With such an *in situ* study we hoped to stay close to the intracellular environment whilst obtaining a higher degree of spectral resolution for NMR measurements.

2.2 In situ metabolic analysis

In the light of the inaccuracies associated with the *in vivo* measurement of the [ATP] / [ADP] ratio (Section 2.1.2), cell permeabilization was pursued as a means for producing cleaner highly resolved ^{31}P NMR spectra, from which these nucleotides could be accurately quantified for performing an *in situ* supply demand analysis. The permeabilized state, designated *in situ*, closely resembles that of the *in vivo* environment as it is similar in terms of protein concentration and macromolecular composition [141 & 142]. As these permeabilized yeasts essentially have porous cell membranes, the diffusion of metabolites and small biological molecules across the lipid bi-layer cannot be prevented [141], so that effectively metabolic intermediates will become diluted in the larger reaction volume (cell volume + extracellular medium). During the permeabilization procedure most of the paramagnetic ions and almost all metabolites are thus washed off in the extraction buffer, this increases the signal to noise ratio and enhances the resolution of *in situ* ^{31}P NMR spectra.

In this section preliminary results in the form of *in situ* enzyme assays are presented first, followed by the main bulk of results consisting of ^{13}C glycolytic flux determinations, nucleotide quantification with ^{31}P NMR spectroscopy, experimental modulations of the *in situ* steady state [ATP] / [ADP] ratio and an *in situ* rate characteristic displaying the relationship between glycolytic flux and the [ATP] / [ADP] ratio.

2.2.1 *In situ* enzyme activity determination

To optimize the yeast permeabilization protocol for performing *in situ* NMR, the first step was to check for glycolytic enzyme activity after exposure to the permeabilizing agent, toluene. Enzyme assays were performed in a linked fashion by relating enzyme activity to the intrinsic ability of glycolysis to oxidize NADH (ADH) and reduce NAD⁺ (GAPDH). The purpose of these experiments was to identify and circumvent potential bottlenecks associated with *in situ* glycolysis and to optimize flux through the addition of cofactors and glycolytic regulators.

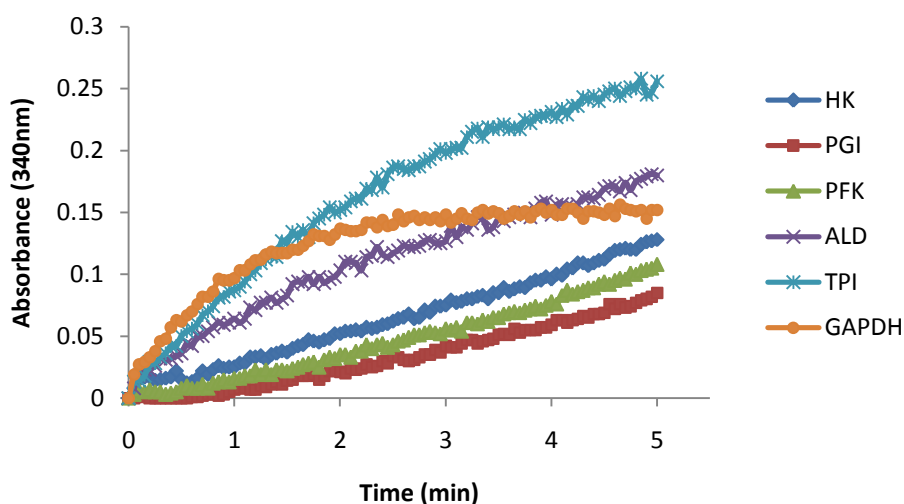


Figure 2.12: *In situ* enzyme kinetic data for the first six reactions of glycolysis. Absorbance was followed spectrophotometrically at 340nm at 25°C. Graphs are representative of an OD₆₀₀ = 60 yeast cell suspension. Substrate addition was taken as time zero; refer to Chapter 4 for assay parameters. Abbreviations are defined on page vi.

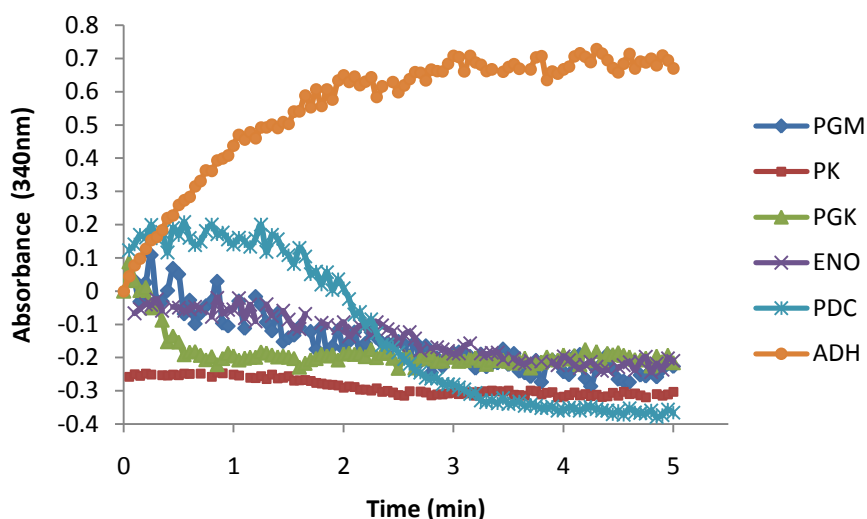


Figure 2.13: *In situ* enzyme kinetic data for the bottom six reactions of glycolysis. Absorbance was followed spectrophotometrically at 340nm at 25°C. Graphs are representative of an OD₆₀₀ = 60 yeast cell suspension. Substrate addition was taken as time zero; refer to Chapter 4 for assay parameters. Both ADH and PGK were assayed in the reverse direction. Abbreviations are defined on page vi.

All twelve glycolytic enzymes (Fig 2.12 and 2.13) were shown to be active *in situ*, however the bottom half, specifically PK, showed extremely slow rates of catalysis. In addition to the more common cofactors; ATP, ADP, NAD⁺ and NADH, supplementation of F1,6 BP was required for the activation of PK [13 & 21], the glycolytic regulator 2,3BPG was vital as it forms part of PGM's reaction mechanism [13 & 143] and the cofactor TPP was essential for the activity of PDC [13].

2.2.2 *In situ* glycolytic flux determination with ¹³C NMR spectroscopy

Using the information obtained from the activity assays, the next step was to generate and measure fluxes *in situ*. In a similar fashion to the *in vivo* data presented in Section 2.1, ¹³C NMR spectroscopy was used for quantifying glycolytic flux.

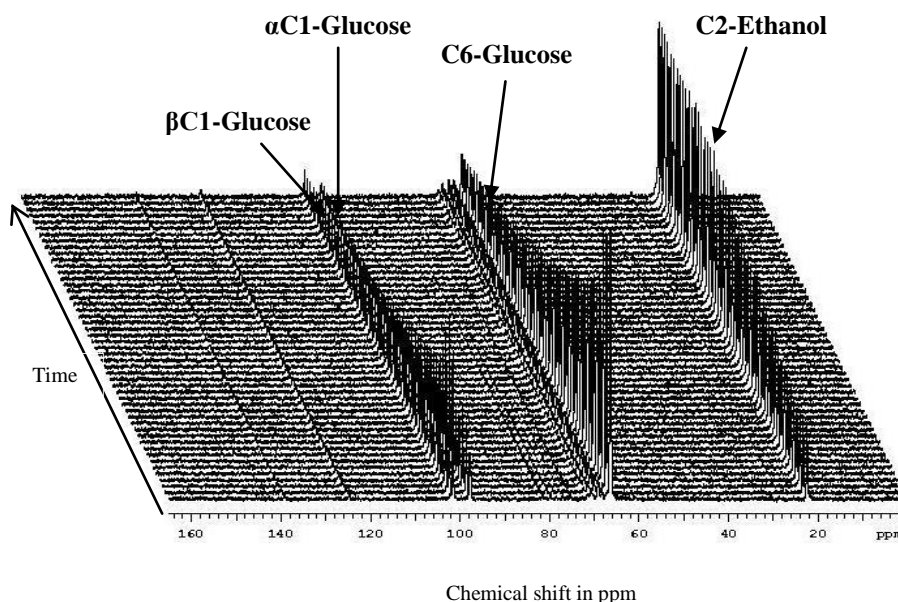


Figure 2.14: A typical *in situ* ¹³C NMR spectrum displayed as a stack plot, obtained during alcoholic fermentation in yeast. This figure represents an OD₆₀₀ = 60 cell suspension fed with 20mM ¹³C_{1, 6} labeled glucose at time zero. Successive spectra are separated by 1 minute time intervals. ATP and ADP were initialized in 1:1 ratio at 2.5mM each, all other glycolytic cofactors were added at standard concentrations as described in Chapter 4.

A full ¹³C spectrum obtained during alcoholic fermentation in permeabilized yeasts is displayed in Fig 2.14. With the addition of ¹³C_{1, 6} labeled glucose as substrate three distinct signals for glucose were observed with the other major resonance corresponding to C2 carbon of ethanol, which provides further evidence for intact glycolytic function *in situ*. No resonances corresponding to glycerol or acetate were observed during fermentation.

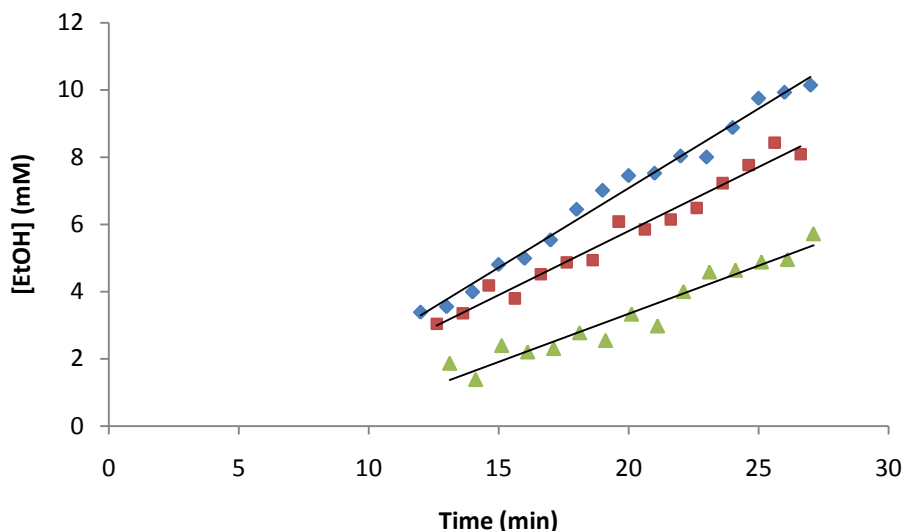


Figure 2.15: Permeabilized yeast fermentation time courses at different initiator concentrations of ATP and ADP. This figure is representative of an $OD_{600} = 30$ cell suspension fed with 50 mM $^{13}C1$ labeled glucose at time zero. All glycolytic cofactors (excluding ATP and ADP) were added at standard concentrations as described in Chapter 4. Initialized cofactor concentration: Blue diamonds = 5mM ATP, 0 ADP; Red squares = 5mM ATP, 2.5mM ADP; Green triangles = 2.5mM ATP, 2.5mM ADP. All concentrations were determined from ^{13}C NMR spectra.

In Fig. 2.15 the rate of ethanol production for three separate *in situ* fermentations is displayed. The data was subjected to a linear regression and yielded good R^2 fits ($\blacksquare = 0.97$, $\blacklozenge = 0.99$ and $\blacktriangle = 0.93$). Glycolytic flux was calculated as the rate of change of these regression lines. The glucose consumption rate did not remain linear throughout fermentation and was omitted from the data plot (for a further discussion, refer to Section 2.2.4).

Table 2.2: *In situ* glycolytic flux

	Metabolite	Normalized flux (μ mol/min/mg protein)
<i>In situ</i>	EtOH	1.91 (± 0.10)
<i>In vivo</i>	EtOH	2.81 (± 0.01)

The glycolytic flux (J_{EtOH}) as measured in permeabilized yeast was substantially lower (33%) in comparison to that measured in intact cell suspensions (Table 2.2). This difference may be ascribed to a loss in enzyme activity, indirectly caused through cell permeabilization [144]. As toluene disrupts vacuoles which contain an abundance of cellular proteases [145], unabated proteolytic degradation of glycolytic enzymes may occur affecting the overall flux through glycolysis [144]. However a more direct effect

seems unlikely as enzyme activity data obtained from cell free extracts and permeabilized yeast suspensions are comparable [141].

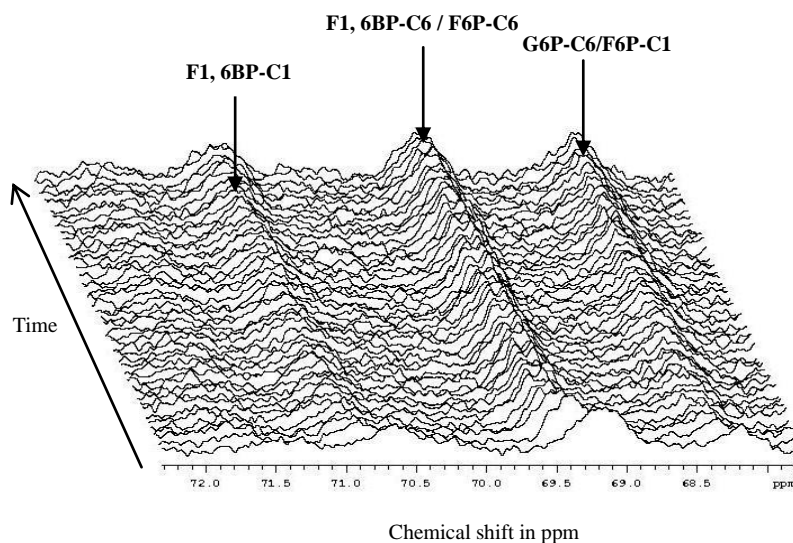


Figure 2.16: Expansion in the midfield region of the *in situ* ^{13}C NMR stack plot displayed in Fig. 2.14.

In Fig. 2.16 the behavior of the glycolytic sugar-phosphates during permeabilized yeast fermentation is displayed. In spite of the enhanced spectral resolution on offer *in situ*, overlap occurred between F6P and F1, 6 BP labeled at their respective C6 positions, with interference from G6P obscuring the signal from F6P-C1 [130]. Peak assignments were made according to Shulman et al. [130]. *In situ* ^{13}C NMR spectra were not quantitatively assessed in terms of intermediate concentrations, however the trend observed points to the persistence of elevated sugar phosphates throughout fermentation (refer to Fig. 2.18 and 2.19).

2.2.3 *In situ* ^{31}P NMR spectroscopy

After the successful reconstitution of intact glycolysis in permeabilized yeast, we focused on *in situ* ^{31}P NMR spectroscopy assays for quantification of the [ATP] / [ADP] ratio.

Cell permeabilization was deemed to be successful in light of the increased resolution displayed in ^{31}P NMR spectra obtained *in situ* (Fig. 2.17). In comparing Fig. 2.17 with Fig. 2.2 (^{31}P *in vivo* stack plot), the major difference was the absence of the polyphosphate peaks *in situ*. This allowed for the detection of resonances assigned to γATP , βATP and βADP . Peak separation in the -9 to -12 ppm region still proved

problematic as this is by default a cluttered part of the spectrum, owing to the proximity of the chemical shift for α ADP, α ATP, NAD^+/NADH and the cofactor TPP (see also Fig. 1.10).

Both ATP and ADP seemed to continually decrease from their initialized values throughout fermentation, almost disappearing in the latter parts of the spectrum. The observation of an increased signal intensity in the up field region (0 – 6ppm), corresponding to the accumulation of sugar phosphates was another recognizable feature of *in situ* alcoholic fermentation.

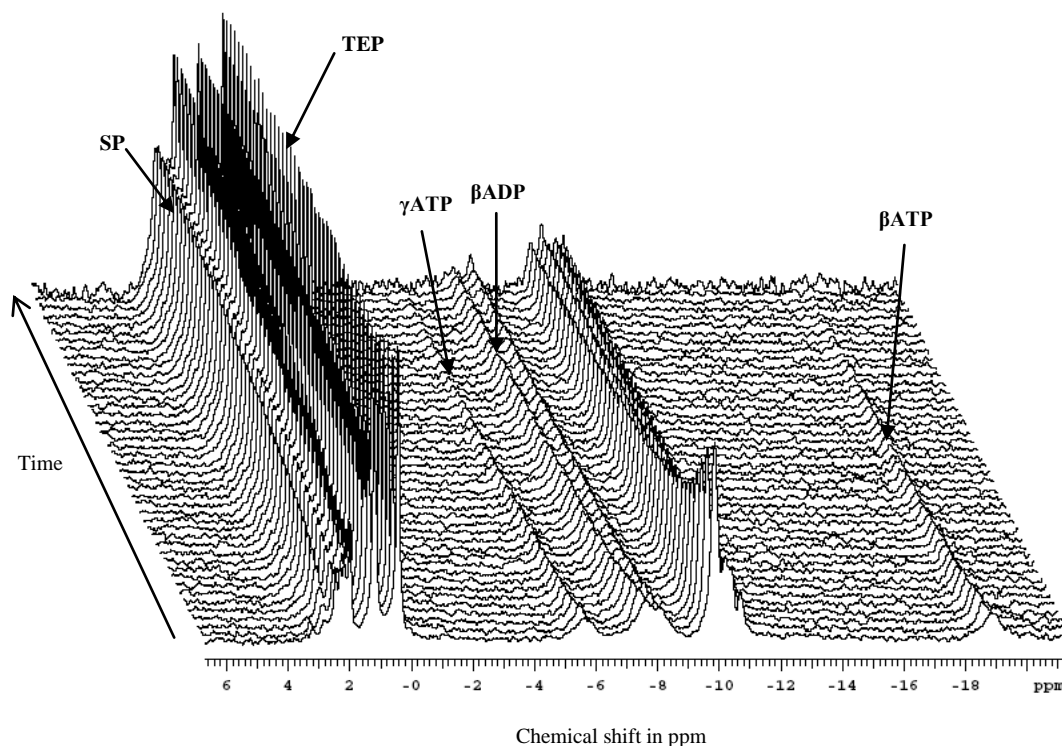


Figure 2.17: Typical *in situ* ^{31}P NMR spectrum, displayed as a stack plot obtained during alcoholic fermentation in yeast. Representative of an $\text{OD}_{600} = 30$ permeabilized cell suspension fed with 50mM Glc. Successive spectra are separated by 1 minute time intervals. ATP and ADP were initialized in 1:1 ratio at 2.5mM each, the rest of the glycolytic cofactors were added at standard concentrations as described in Chapter 4.

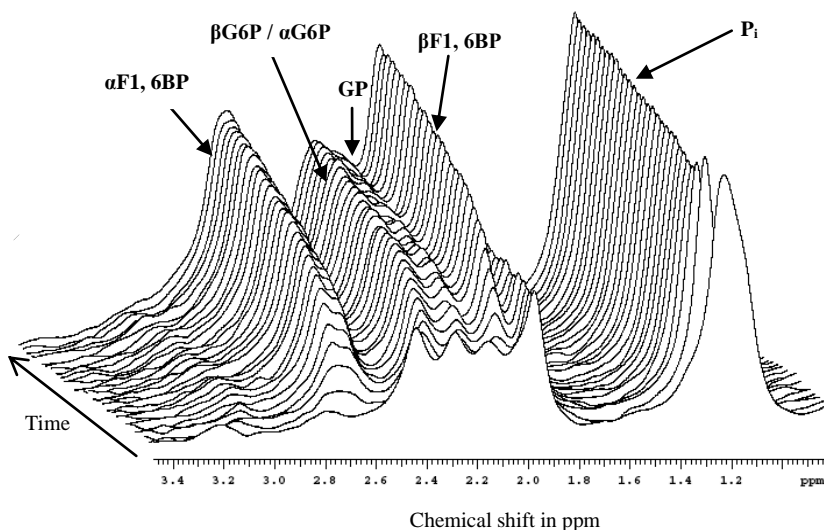


Figure 2.18: Expansion in the up-field region of the *in situ* ^{31}P NMR stack plot displayed in Fig. 2.17.

With reference to Fig. 2.18, both the anomeric forms of F1, 6BP were resolved, in contrast to the overlap observed for α and β G6P. The peak labeled GP (glycero phosphates) corresponds to the coinciding resonances for GAP and DHAP. F6P could not be resolved due to interference of the much larger F1, 6BP peak. Peak assignments were made according to the chemical shifts of metabolites in isolation or through their addition to the sample mixture, and are in good agreement with Shulman et al. [130 & 131].

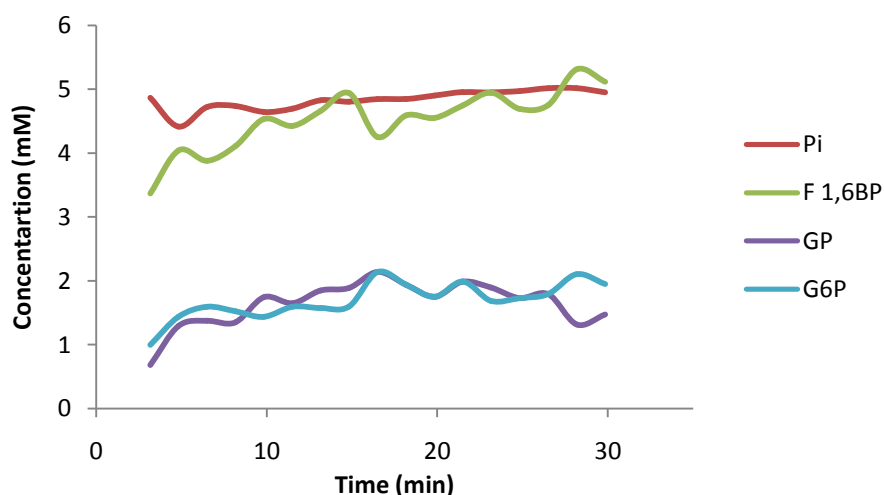


Figure 2.19: Time course for yeast glycolytic intermediates obtained during alcoholic fermentation in permeabilized yeast. Representative of an $\text{OD}_{600} = 30$ cell suspension fed with 50mM Glucose at time zero. ATP and ADP were initialized in a 1:1 ratio at 2.5mM each. All other glycolytic cofactors were added at standard concentrations as described in Chapter 4. Concentrations were determined from ^{31}P NMR spectra.

As a result of the enhanced spectral resolution gained through cell permeabilization, intermediates could be quantified accurately through application of the deconvolution routine (Chapter 4), which allowed for the construction of the time course displayed in Fig. 2.19. F1,6 BP was shown to accumulate and remained high throughout fermentation; reaching a similar concentration to that measured *in vivo* ($\pm 5\text{mM}$). G6P and the glycerol phosphates were also shown to increase during the initial stages of glycolysis and remained elevated at a concentration of $\pm 2\text{mM}$ during the latter parts of the time course. In light of the metabolic behavior observed (decreasing ATP and elevated sugar phosphates) the question arose whether a true “*steady state*” was indeed attained *in situ*, in spite of the constant rate of ethanol production.

The *in situ* metabolic behavior is similar to that which is observed in yeast mutants containing deletions in the *TPS1* gene, coding for the enzyme trehalose 6 phosphate synthetase [50, 146, 147 & 148]. These mutants are characterized by the buildup of sugar-phosphates, specifically F1,6 BP, and the resultant rapid consumption of ATP and sequestration of phosphate [146, 149, 150, 151, 152 & 153]. No intermediary steady state is obtained, with glucose utilization continuing at a steady pace until the ATP pool is depleted [51]. It would seem as if the rate maintained by the top, ATP consuming half of glycolysis exceeded that of the lower ATP producing half [50]. This can be explained in the light of the now considered important regulatory role of trehalose 6 phosphate, in restricting the flow of glucose into glycolysis in wild type yeasts [50]. In the case of the permeabilized yeasts, the branch of glycolysis directed towards trehalose synthesis was not selectively activated through specific cofactor addition (see Section 3.2) and thus may be functioning at an extremely slow rate or not at all, potentially explaining the similarity to the $\Delta TPS1$ phenotype.

In this section we showed that yeast glycolysis could be reconstituted *in situ* and still yield reproducible fluxes; and that cell permeabilization increased the degree of resolution attained during ^{31}P NMR spectroscopy assays, thus allowing for accurate detection of both ADP and ATP. With both these systemic variables quantifiable *in situ*, a putative analysis regarding the sensitivity of glycolytic flux in response to changes in the $[\text{ATP}] / [\text{ADP}]$ ratio was possible (refer to Sections 1.2 and 1.3). The method by which the $[\text{ATP}] / [\text{ADP}]$ ratio was varied and the results obtained will be presented next in terms of the *in situ* rate characteristic.

2.2.4 Perturbing the [ATP] / [ADP] ratio *in situ*

Perturbing the [ATP] / [ADP] ratio in intact cell suspensions can be achieved by either modulating the supply or demand for ATP, usually through addition of compounds which rely on membrane transport steps to exert their respective effects (see Section 2.4.2 and 2.4.3). The loss of membrane selectivity in permeabilized yeast negates the use for membrane transporters as molecules traverse the membrane via simple diffusion, therefore a different means for modulating the [ATP] / [ADP] ratio is required in order to measure the sensitivity of glycolysis *in situ*.

By varying the initial concentration of ATP and ADP added to the permeabilized yeast suspensions, different [ATP] / [ADP] ratios could be obtained during fermentation. With highly resolved ^{31}P NMR spectra generated *in situ*, the peaks for β and γ ATP along with β ADP were marked for integration and used for producing metabolite time courses. These experiments were then duplicated for ^{13}C NMR flux analysis.

With reference to Fig. 2.20, the metabolic behavior displayed was indeed dependent on the initial concentrations of ATP and ADP used, however the [ATP] / [ADP] ratio always remained relatively stable during the second half of the time course (time points 8 through 15). The overall concentration for both ATP and ADP was shown to decrease from its original value, with ATP being the most affected. The observed build up of sugar and triose phosphates can potentially account for these losses in ATP and ADP [50 & 51]. Unfortunately we were unable to directly measure AMP *in situ*; as the AMP signal was obscured due to extensive overlap with the strong signals produced by the accumulating hexose phosphates in the up-field region of the *in situ* ^{31}P NMR spectrum (see Figs. 2.17 and 2.18). However, by assuming that the adenylate moiety ([ATP] + [ADP] + [AMP]) remained conserved throughout fermentation, AMP was calculated by subtracting the measured concentrations of [ATP] + [ADP] from the total nucleotide pool ($[\text{ATP}]_{\text{initial}} + [\text{ADP}]_{\text{initial}}$) supplied at the start of fermentation.

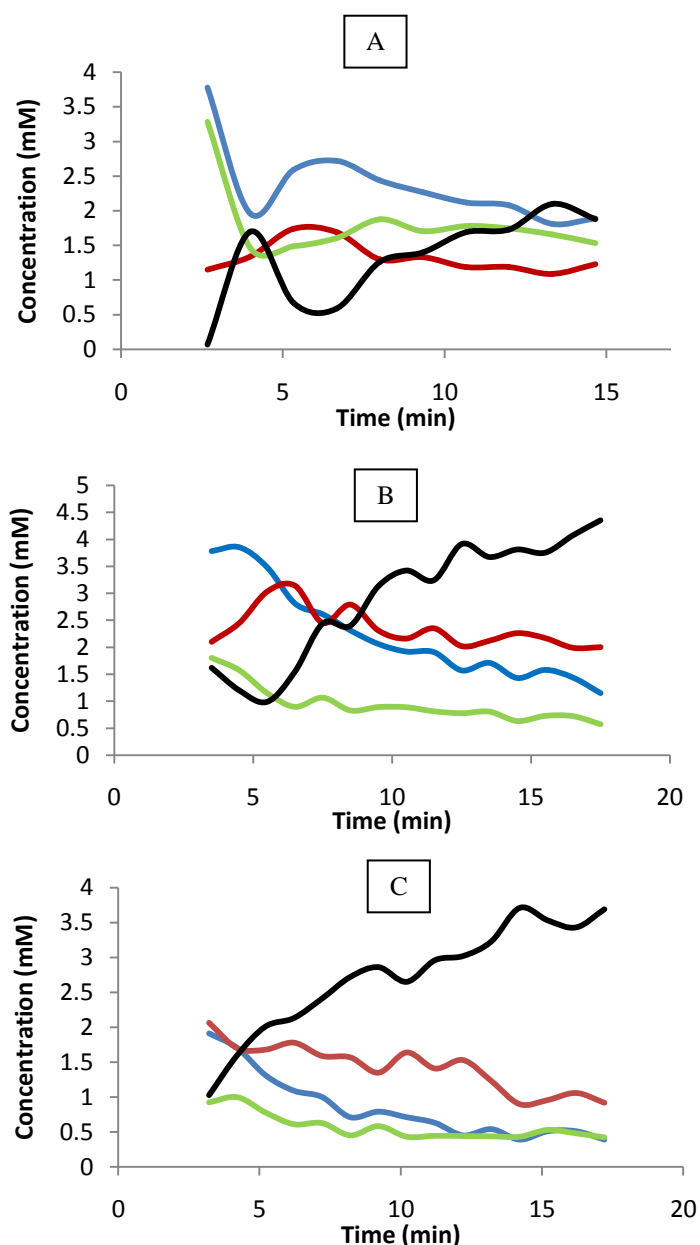


Figure 2.20: *In situ* adenylate nucleotide levels. Representative of an $OD_{600} = 30$ cell suspension fed with 50mM glucose at time zero. The initialized values for ATP and ADP were: A) ATP = 5mM, ADP = 0; B) ATP = 5mM, ADP = 2.5mM & C) ATP = 2.5mM, ADP = 2.5mM. All other glycolytic cofactors were added at standard concentrations as described in Chapter 4. ATP = blue, ADP = red, AMP = black and $[ATP] / [ADP]$ = green. Concentrations were determined from ^{31}P NMR spectra.

Table 2.3 displays the overall glycolytic flux and intermediate data as measured in permeabilized yeast. These nucleotide ratios were significantly lower than those calculated from the perchloric acid cell extracts (see Section 2.4.1) and showed a positive correlation with the initial $[ATP] / [ADP]$ ratio, whilst the ethanol production rate tended to drop off with a decreased $[ATP] / [ADP]$ ratio. Nucleotide ratios represent the averaged value as measured across time points 8 through 15 (see Fig. 2.20). With

[AMP] calculated as described above, cellular energy potential could also be expressed in terms of the charged-to-uncharged nucleotide ratio (c/u), where $c/u = ([ATP] + 0.5[ADP]) / ([AMP] + 0.5[ADP])$ [168]. As was the case for the $[ATP] / [ADP]$ ratio, the ethanol production rate also increased with increasing c/u .

Table 2.3 Changes in glycolytic flux in response to varying $[ATP] / [ADP]$ ratios and the charged-to-uncharged ratio as measured in permeabilized yeast.

Initialized ATP:ADP	Ethanol production rate ($\mu\text{mol}/\text{min}/\text{mg}$ protein)	Settled $[ATP] / [ADP]$ ratio	c/u
∞	1.91	1.77 ± 0.03	1.34 ± 0.1
1	1.35	0.81 ± 0.02	0.68 ± 0.06
2	0.88	0.46 ± 0.02	0.33 ± 0.03

The data shown in Table 2.3 was used for plotting the *in situ* rate characteristic presented in Fig. 2.21. The overall changes observed in the glycolytic flux are a direct result of experimental manipulations in the $[ATP] / [ADP]$ ratio and do not reflect compensatory changes in response to independent perturbations in the free energy demand. Therefore the rate characteristic can essentially be viewed as a global response curve (Section 1.2.2) that depicts the sensitivity of glycolytic flux to varying $[ATP] / [ADP]$ [4].

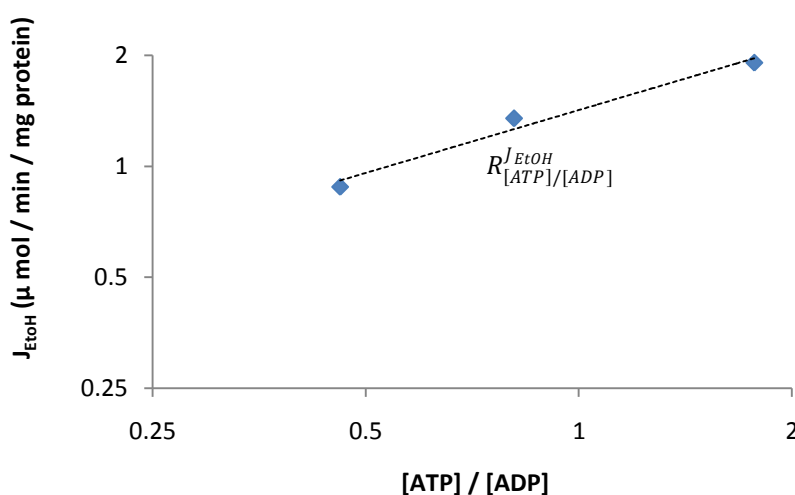


Figure 2.21: Variations in the *in situ* glycolytic flux (expressed as the ethanol production rate) as a function of varying $[ATP] / [ADP]$ ratios. Perturbations were performed by directly modulating the initial concentrations of ATP and ADP added to the cell suspension, prior to the start of fermentation. Graph represents a re-plot of the data displayed in Table 2.3.

The data in Fig. 2.21 were analyzed by means of linear regression (dotted line) and yielded a good R^2 value of 0.96, emphasizing the linear relationship between $\log_2([ATP]/[ADP])$ and $\log_2[J_{EtOH}]$. The gradient of the regression line was calculated as the response coefficient $R_{[ATP]/[ADP]}^{J_{EtOH}} = 0.74$ (Section 1.2.2). By plotting the response of the *in situ* glycolytic flux to the charged/uncharged ratio (Fig. 2.22), an even better correlation ($R^2 = 0.98$) and a more pronounced response ($R_{c/u}^{J_{EtOH}} = 0.99$) was observed.

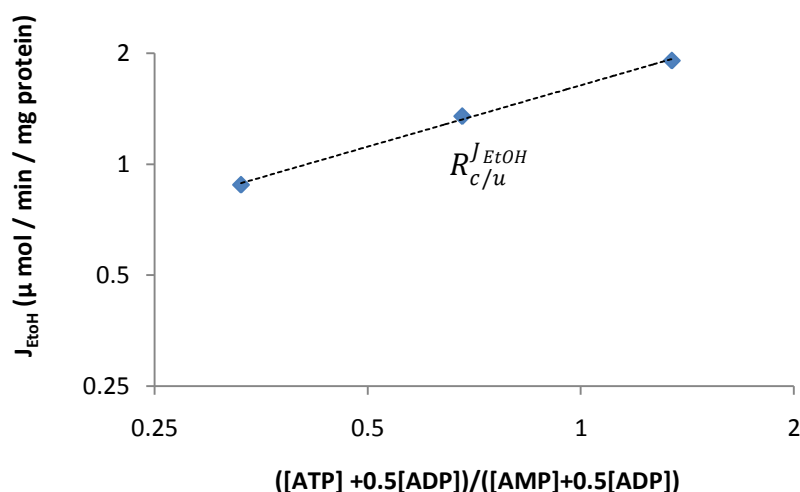


Fig. 2.22: Variations in the *in situ* glycolytic flux (expressed as the ethanol production rate) as a function of varying adenylate charged to uncharged ratio. Perturbations were performed by directly modulating the initial concentrations of ATP and ADP added to the cell suspension, prior to the start of fermentation. Graph represents a re-plot of the data displayed in Table 2.3.

The positive correlation displayed between glycolytic flux and the $[ATP] / [ADP]$ or c/u ratios (Fig. 2.21 & Fig.2.22) seems almost counterintuitive, as high concentrations of ATP and ADP are thought to respectively inhibit and activate glycolysis (Refer to Section 1.1). This paradoxical type of behavior brings the legitimacy of the *in situ* steady state assumption into question. In the search of an attempted explanation, it becomes evident that the “turbo effect” [51] plays a role that can no longer be ignored. The diminished nucleotide pool, low “steady state” $[ATP] / [ADP]$ ratio and accumulating sugar and triose-phosphates are all characteristic of the metabolic conduct displayed in the $\Delta TPSI$ phenotype [146, 149, 150, 151, 152 & 153]. As this system is not truly at steady state, the overall global elasticity measured in Fig. 2.21 and Fig.2.2, takes into account the response for both the top and lower half of glycolysis to varying $[ATP] / [ADP]$ and c/u ratios. The experimental observation of inconsistencies in the glucose consumption rate and disparity between J_{EtOH} and J_{Glc} can further attest to the

unsynchronized nature of *in situ* yeast glycolysis (see Section 2.2.2). The top ATP consuming half of glycolysis, already maintaining a high rate as a result of the unregulated flow of glucose into the pathway, would be further activated by high [ATP] and low [ADP] through the laws of mass action as both ATP and ADP are respective substrates and products of HK and PFK [138] (refer to Fig. 2.22). Even though high [ATP] is known to allosterically inhibit PFK, ATP dropped rapidly after the start of fermentation *in situ* and remained well below its estimated K_i value of 3mM [20] (see Fig.2.20) therefore this regulatory effect can be ignored. The lower, ATP producing half of glycolysis would be slowed down by increasing [ATP] / [ADP] ratios as a result of mass action, however the elevated levels of GAP (substrate for GAPDH) and F1,6 BP (activator of PYK) associated with the turbo effect and further aggravated by high initial [ATP] / [ADP], might help overcome this mass action trend (refer to Fig. 2.23) and can potentially account for the positive correlation displayed between the [ATP] / [ADP] ratio and glycolytic flux in permeabilized yeast (Fig. 2.21)

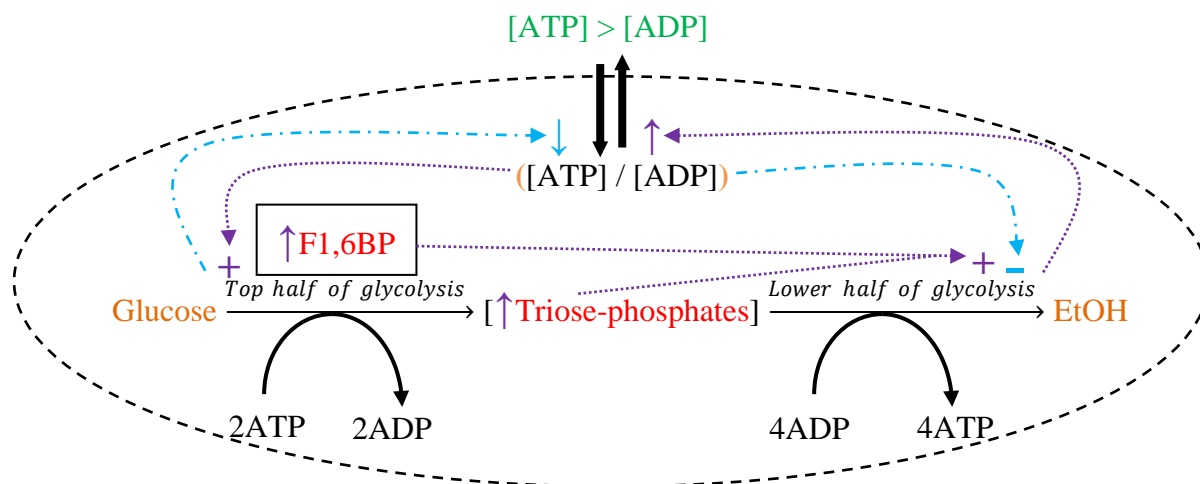


Figure 2.23: The mechanism through which varying $[ATP] / [ADP]$ ratios affect the glycolytic flux *in situ*. Metabolites in black have attained a pseudo steady state, metabolites in red represent elevated glycolytic intermediates, metabolites in green are experimentally controlled and metabolites in orange represent glycolytic substrates and end products. ↓ Decreasing metabolite or moiety; ↑ increasing metabolite or moiety; + positive effect on pathway flux and – negative effect on pathway flux.

The application of the phospho creatine system as a potential tool for counteracting the resultant changes caused by the turbo effect concerning the “*steady state*” $[ATP] / [ADP]$ ratio and total nucleotide pool will be presented next.

2.3 Creatine kinase as an artificial means for clamping the $[ATP] / [ADP]$ ratio in permeabilized yeast

Because the phospho-creatine system functions so efficiently in mammalian muscle tissue, it was hypothesized that the addition of creatine kinase in conjunction with creatine and creatine-phosphate to permeabilized yeast cultures would permit the same degree of ATP buffering, and allow us to artificially clamp a specified $[ATP] / [ADP]$ ratio. In this section this hypothesis will be experimentally addressed, preliminary results include quantification of $K'_{\text{creatine kinase}}$ with the main results presented as a metabolic time course for ATP and ADP “clamped” at a predetermined ratio.

The near equilibrium nature of the creatine kinase reaction in muscle tissue, allows this system to function so rapidly and effectively as a free energy store [1]. Creatine kinase has successfully been co-expressed in yeasts and used for determining minute quantities of cytosolic ADP through algebraic substitution of the quantifiable variables; ATP, Cr and CrP into its equilibrium expression [134]. The novelty in our approach lies in the

attempt to clamp the $[ATP] / [ADP]$ ratio over a wide range of values for correlation to *in situ* glycolytic flux.

2.3.1 Determination of the apparent equilibrium constant for the reaction catalyzed by creatine kinase by means of ^{31}P NMR spectroscopy

The difficulties associated with finding some degree of consistency among the published values for $K'_{\text{creatine kinase}}$, have already been highlighted in Section 1.7. For this reason the apparent equilibrium constant was determined under similar physical conditions to what would be experienced during *in situ* fermentations.

Table 2.4: The apparent equilibrium constant (K') for the creatine kinase reaction as determined by ^{31}P NMR spectroscopy

pH	Mg ²⁺ (mM)	Temp (°C)	K'
7.5	5	25	240 ± 7.5
6.5	5	25	41 ± 1.4

Refer to Chapter 4 for discussion on standard assay parameters and protocol.

The data in Table 2.4 represents the averaged value for $K'_{\text{creatine kinase}}$ (\pm standard error) as determined across four experiments assayed in both the forward and reverse direction. The apparent equilibrium constant was defined in the forward direction towards the net production of ATP. $K'_{\text{creatine kinase}} = [ATP]_{eq} \cdot [Cr]_{eq} / [ADP]_{eq} \cdot [CrP]_{eq}$. The large difference between the K' determined at pH 6.5 and 7.5 highlights the effect of pH change on the thermodynamics of this reaction.

2.3.2 Clamping the $[ATP] / [ADP]$ ratio *in situ*

The purpose of these experiments was to enforce a predetermined $[ATP] / [ADP]$ ratio *in situ*, and to counteract the rapid loss in ATP observed during fermentation. By applying the buffering capabilities of the phospho creatine system, it was hoped that $[ATP]$ and $[ADP]$ would remain constant (within a $\pm 10\%$ limit), long enough so as to correlate the imparted ratio to a glycolytic flux.

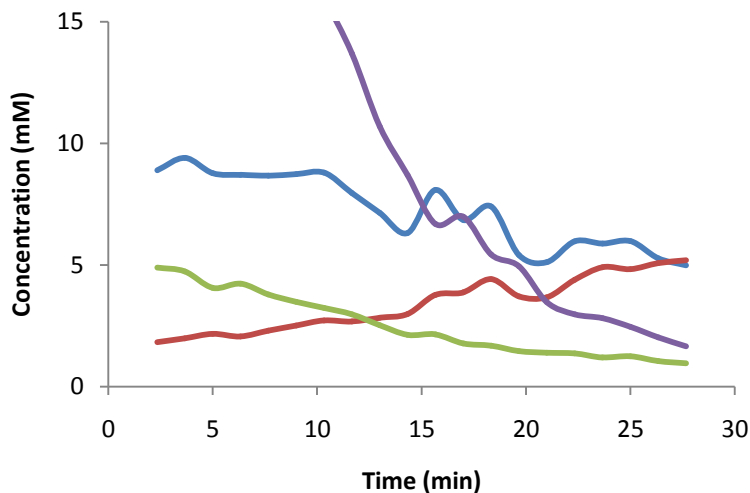


Figure 2.24: *In situ* time course for the creatine kinase buffered [ATP] / [ADP] ratio. Representative of an $OD_{600} = 30$ cell suspension pH 6.5, fed with 50mM Glc at time zero. ATP and ADP were added in a 10:1 ratio, along with equilibrium concentrations of creatine (30mM) and creatine phosphate (120mM). All other cofactors and regulators were added at standard concentrations as described in Chapter 4. ATP = blue, ADP = red, [ATP] / [ADP] = green and CrP = purple. All concentrations were determined from ^{31}P NMR Spectra.

With reference to Fig. 2.24, ATP followed a general decrease displaying somewhat erratic behavior during the middle parts of the time course, with a concomitant steady increase observed for ADP. The [ATP] / [ADP] ratio decreased throughout, showing no enhanced signs of stabilizing (compare with Fig. 2.20). CrP was included in the time course for verification of creatine kinase activity, CrP dropped rapidly from its initial value of 30mM, and was almost undetectable by the end of fermentation.

In comparison with the *in situ* behavior shown in Fig. 2.20, the addition of creatine kinase did not seem to have any beneficial effect on the homeostatic maintenance of the [ATP] / [ADP] ratio, although significant losses in the overall added nucleotide pool ([ATP] + [ADP]) were circumvented. It appears as if the phospho-creatine system was unable to keep up with the large drain of ATP associated with *in situ* glycolysis, as the system itself became depleted (rapid loss of CrP).

Uncertainty surrounding the accuracy of the determined value for $K'_{\text{creatinase}}$ and practical limitations concerning creatine solubility, combined with the complicated metabolic behavior displayed *in situ*, were all identified as key contributing factors responsible for the inability of the phospho-creatine system to act effectively as a free energy buffer. Changes in the physico-chemical environment in terms of pH and

composition brought on by metabolic activity can severely affect the thermodynamics of a reaction. In muscle cells changes in the $K'_{\text{creatine kinase}}$ by almost a factor of 10, caused by a lowering of cytoplasmic pH during strenuous exercise, have been reported [154]. Such changes in the $K'_{\text{creatine kinase}}$ can potentially explain the limited buffering capabilities of the phospho creatine system when applied to the artificial *in situ* environment. Owing to the hydrophobic nature of creatine, solubility presented a problem with the highest workable concentration attained, being about 80mM. To function as a free energy buffer considerable pools of creatine and CrP are needed: combined with the large values for $K'_{\text{creatine kinase}}$, addition of creatine in excess of 100mM was required, ultimately leading to errors in the estimation of the apparent equilibrium constant. Finally the problems associated with the “turbo effect” and the pseudo steady-state like behavior observed *in situ* have already been discussed in Section 2.2.4, trying to predict or produce a desired [ATP] / [ADP] ratio by the addition of even more variables seemed to further complicate the matter.

Rather more questions than answers arose during the *in situ* study presented here, specifically concerning the metabolic behavior (pseudo steady state) of permeabilized yeast and the potential role for the turbo effect in explaining these observations. These topics will again be addressed in some depth in the concluding discussion in Chapter 3. In the next section we combine the approach of whole cell ^{13}C NMR used for determining glycolytic flux (see Section 2.1.4) with an *in vitro* determination of the [ATP] / [ADP] ratio, and attempt to perform an experimental supply demand analysis on yeast fermentative free energy metabolism.

2.4 Whole cell experimental supply demand analysis

Supply demand analysis of yeast free energy metabolism allows the control of glycolytic flux to be understood in terms of the supply and demand for free energy in the form of ATP [9]. Yeast anaerobic free energy metabolism can be viewed as a supply-demand system centered around the linking metabolite ATP and the ADP moiety. The supply block consists of yeast glycolysis responsible for ATP production whilst the demand block refers to all cellular processes which require the net use of ATP (cell maintenance) [9 & 11] (refer to Preface and Section 1.3).

The viability of this analysis rests on our ability to accurately measure both glycolytic flux and the steady state [ATP] / [ADP] ratio. In Section 2.1.4 we have shown that fluxes can be measured with relative ease in whole cells using ^{13}C NMR spectroscopy; refer to example spectrum (Fig. 2.8) and fermentation data plot (Fig. 2.11). As a result of complications concerning the determination of the [ATP] / [ADP] ratio *in vivo* (see Section 2.1.2) and uncertainties surrounding the *in situ* steady state (see Section 2.2.4), we attempted to quantify the [ATP] / [ADP] ratio in perchloric acid yeast cell extracts as a final alternative.

2.4.1 ^{31}P NMR determination of the steady state [ATP] / [ADP] ratio in yeast perchloric acid cell extracts

During the cell extraction procedure (refer to Chapter 4) samples were freeze dried and concentrated by a factor of three, hence signal strengths were increased and thereby negating the problems associated with the low signal intensities experienced *in vivo*. Furthermore cell extracts were suspended in EDTA, which serves as a chelating agent removing free paramagnetic ions from the solution and thus helps decrease peak broadening [136]. Finally as these samples were not metabolically active, an increased number of transients and additional acquisition and delay times could be incorporated into the pulse sequence which increased the signal to noise ratio and enhanced spectral resolution.

Upon performing cell extractions, the spectra obtained through ^{31}P NMR (Fig. 2.25), were of sufficient resolution allowing for quantitative analysis of both αATP and αADP (compare to Fig. 2.3B). The multiplicity of the peaks assigned in Fig. 2.25 is a result of spin-spin coupling interactions and does not represent the individual signals of other closely related molecules [130, 131 & 137]. The peaks labeled αATP and αADP in actual fact represent a composite overlay of all the NTPs and NDPs present in yeast, however as the concentration of ATP and ADP are deemed to be far in excess over these less abundant nucleotides their contribution to the overall signal were neglected [130 & 131]. All metabolites were assigned according to Shulman et al. [130, 131 & 133]. The steady state [ATP] / [ADP] ratio as calculated from yeast cell extracts was 5.29 ± 0.30 and is substantially higher than the *in vivo* measurement of 1.83 ± 0.64 (see Section

2.1.2). The PCA extract data compared well with published values for $[ATP] / [ADP]$ [11 & 138].

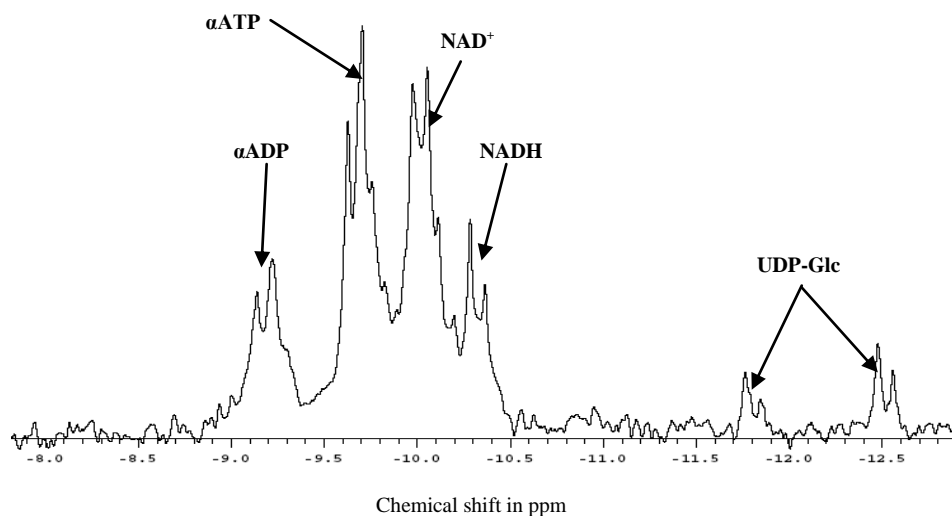


Figure 2.25: ^{31}P NMR spectrum of a perchloric acid yeast cell extract as obtained during anaerobic fermentation. Extraction was performed six minutes after the addition of 133mM glucose to an $\text{OD}_{600} = 300$ yeast cell suspension at time zero. The cell extract was then concentrated via one round of freeze drying, followed by resuspension in 30mM EDTA pH 8.2. Refer to Chapter 4 for standard acquisition parameters.

With both glycolytic flux (*in vivo* ^{13}C NMR) and the NTPs (^{31}P NMR cell extracts) being readily determinable, an experimental SDA of yeast fermentative free energy metabolism was now possible.

By implementing the double modulation method, as originally described by Kacser and Burns [10] (see Section 1.3), both the demand and supply blocks can be separately be perturbed through the addition of benzoic acid (Section 2.4.2) and the glucose transport inhibitor maltose (Section 2.4.3), respectively. The effect of these modulations can then be quantified in terms of changes in the steady state $[ATP] / [ADP]$ ratio and the resultant change in glycolytic flux (see Section 2.4.2 and 2.4.3). Rate characteristics may then be constructed using the flux and intermediate data for elucidating the sensitivity of supply and demand (Section 2.4.4). These elasticity coefficients can in turn be used to calculate both the concentration and flux control coefficients of supply and demand (see Section 2.4.4) [9].

2.4.2 Demand perturbations by the addition of the un-coupler benzoic acid

Benzoic acid is a weak organic acid that facilitates metabolic uncoupling and is often applied in this regard to prevent microbial growth [155]. The protonated form of benzoic acid enters the cell via simple diffusion, once inside the cytoplasm the weak acid dissociates (cytoplasmic pH > pKa of 5.5) thereby dissipating the trans-membrane proton gradient [155]. Cells remove excess benzoate from their interior by means of an ATP dependent transporter [156]. Therefore titrating intact yeast cell suspensions with increasing concentrations of benzoic acid should add to the demand for free energy in the form of ATP [11]. Perturbing the demand for ATP causes changes in the [ATP] / [ADP] ratio, which in turn leads to a compensatory response in the supply of ATP (glycolytic flux) and the establishment of a new steady state with unique values for $J_{Glycolysis}$ and [ATP] / [ADP] [9].

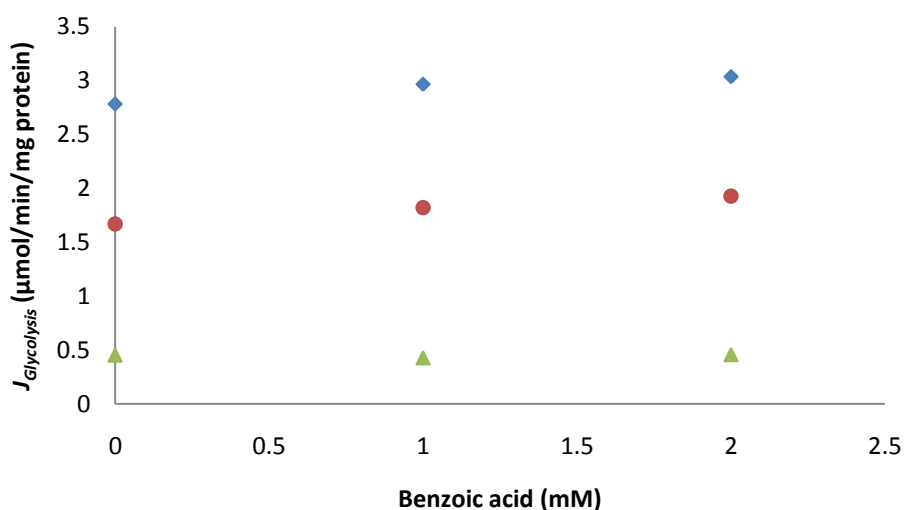


Figure 2.26: Changes in yeast glycolytic flux at increasing concentrations of benzoic acid. Rates were normalized to total protein and quantified by means of ^{13}C NMR spectroscopy. Blue diamonds = ethanol production rate; Red circles = absolute rate of glucose consumption; Green triangles = glycerol production rate.

The graph in Fig. 2.26 depicts the positive effect benzoic acid addition had on yeast glycolytic flux. Steady state rates were plotted for glucose, ethanol and glycerol. Both J_{EtOH} and $|J_{Glc}|$ were shown to increase with rising concentrations of benzoic acid, whilst glycerol production remained largely unaffected. The percentage of glycolytic flux directed towards ethanol synthesis decreased slightly (-4.5%) upon titration with benzoic acid (Table 2.5). Due to practical constraints concerning the availability of spectrometer time, this experiment was not duplicated.

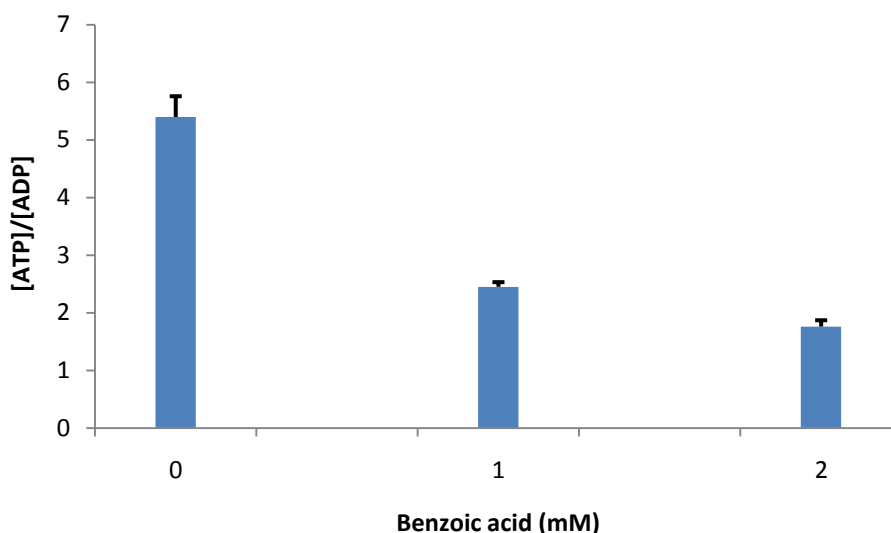


Figure 2.27: Changes in the steady state [ATP] / [ADP] ratio at increasing concentrations of benzoic acid. Nucleotide ratios were quantified by performing ^{31}P NMR spectroscopy on perchloric acid yeast cell extracts. Data represent the averaged value across three steady state time points taken at; 4, 6 and 8 min after the addition of glucose at time zero. Y error bars reflect the standard error of the mean.

Substantial decreases in the steady state [ATP] / [ADP] ratio were observed at increasing concentrations of benzoic acid (Fig. 2.27), with the ratio dropping by 51 and 65% for the first and second titration points with respect to that of the unperturbed steady state (Table 2.5). This decrease in the steady state [ATP] / [ADP] ratio should effectively cause an increase in the supply rate of ATP (glycolysis), and this is exactly what was observed (see Fig. 2.26). The changes observed in both the steady state variables following the addition of benzoic acid, justified the use of this compound for modulating cellular free energy demand.

Table 2.5: Overall glycolytic flux and steady state metabolite data for benzoic acid induced demand perturbations.

Benzoic acid (mM)	J_{EtOH} ($\mu\text{ mol/ min/ mg protein}$)	J_{Glc} ($\mu\text{ mol/ min/ mg protein}$)	J_{Glycerol} ($\mu\text{ mol/ min/ mg protein}$)	Steady state [ATP] / [ADP]	Flux stoichiometry EtOH:Glc	% Of glycolytic flux directed towards ethanol production	% Total of carbon recovered
0	2.78	1.67	0.45	5.39 ± 0.36	1.67	83.3	96.9
1	2.97	1.82	0.43	2.45 ± 0.08	1.57	81.5	93.3
2	3.04	1.93	0.46	1.76 ± 0.11	1.49	78.8	90.7

2.4.3 Perturbing glycolytic supply by addition of maltose a competitive inhibitor of glucose uptake

Maltose has been shown to bind to the extracellular face of glucose transporters located in the yeast cell membrane and effectively blocks or prevents these carriers from binding to and transporting glucose [157]. Therefore in the presence of glucose, maltose acts as a competitive inhibitor of glucose transport [157]. Titrating cell suspensions with increasing concentrations of maltose can therefore be viewed as a supply perturbation as the glucose uptake rate becomes limiting, which will affect the rest of downstream glycolysis. Such supply perturbations should lower the steady state $[ATP] / [ADP]$ ratio and cause a compensatory change in the demand flux until a new steady state is established [9].

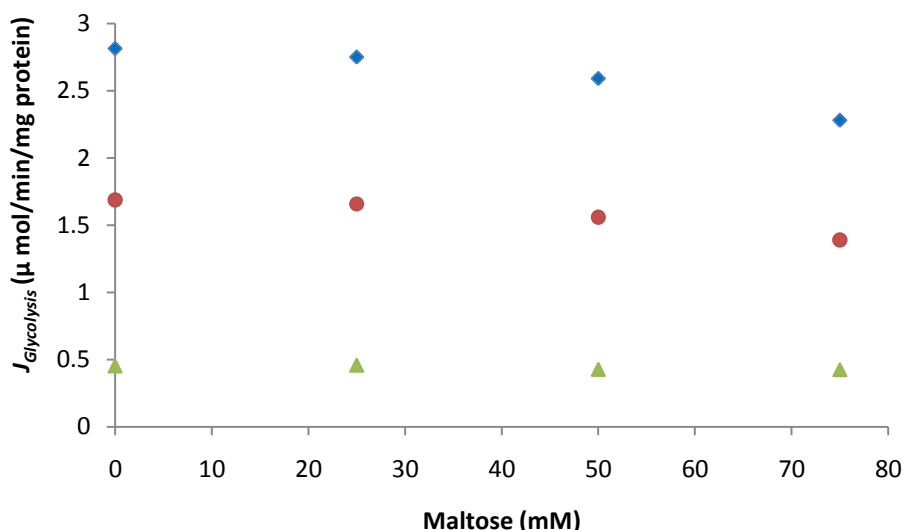


Figure 2.28: Changes in glycolytic flux at increasing concentrations of the glucose transport inhibitor, maltose. All rates were measured using ^{13}C NMR spectroscopy and normalized to total protein. Blue diamonds = ethanol production rate; Red circles = absolute rate of glucose consumption and Green triangles = glycerol production rate.

Fig. 2.28 displays the inhibitory effect of maltose on glycolytic flux. The first titration point of 25mM (estimated K_i for maltose [157]) did not cause any significant reductions in glycolytic flux, probably as glucose still greatly exceeds maltose at this point (133mM Glc). The subsequent 25mM incremental titration points led to a decrease in the glycolytic flux both in terms of J_{EtOH} and $|J_{Glc}|$, whilst glycerol production remained largely unaffected (Table 2.6). Due to practical constraints concerning the availability of spectrometer time, this experiment was not duplicated.

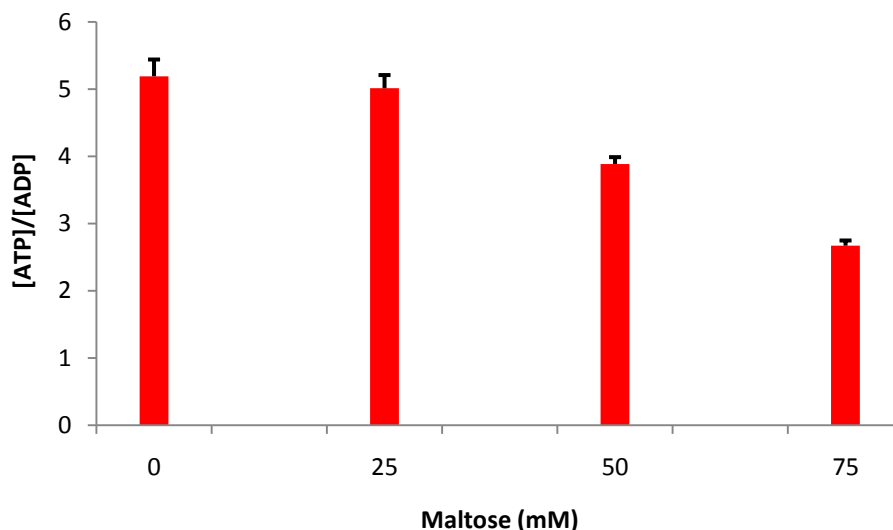


Figure 2.29: Changes in the steady state [ATP] / [ADP] ratio at increasing concentrations of the glucose transport inhibitor maltose. Nucleotide ratios were quantified by performing ^{31}P NMR spectroscopy on perchloric acid yeast cell extracts. Data represents the averaged value across three steady state time points taken at; 4, 6 and 8 min after the addition of glucose at time zero. Y error bars reflect the standard error of the mean.

Fig. 2.29 shows the decrease in the steady state [ATP] / [ADP] ratio at increasing concentrations of the glucose transport inhibitor maltose. Similar to the flux assays (Fig. 2.28) the first titration point did not have a marked effect on the steady state [ATP] / [ADP] ratio, however for the last two inhibition points, a respective 22 and 47% drop in the steady state [ATP] / [ADP] ratio was calculated (Table 2.6).

Maltose inhibition produced the expected effect (decreasing steady state [ATP] / [ADP] ratio and glycolytic flux), validating the use of this compound for modulating the glycolytic supply.

Table 2.6: Overall glycolytic flux and steady state metabolite data for maltose induced supply perturbations.

Maltose (mM)	J_{EtOH} ($\mu\text{mol}/\text{min}/\text{mg}$ protein)	J_{Glc} ($\mu\text{mol}/\text{min}/\text{mg}$ protein)	J_{Glycerol} ($\mu\text{mol}/\text{min}/\text{mg}$ protein)	Steady state [ATP]/[ADP]	Flux stoichiometry EtOH:Glc	% Of glycolytic flux directed towards ethanol production	% Total of carbon recovered
0	2.81	1.69	0.45	5.19 ± 0.25	1.66	83.1	96.7
25	2.75	1.66	0.46	5.01 ± 0.20	1.66	83.8	96.7
50	2.59	1.56	0.43	3.89 ± 0.10	1.66	82.9	96.7
75	2.28	1.39	0.42	2.67 ± 0.08	1.64	82.1	96.7

2.4.4 Rate characteristics of supply and demand

Rate characteristics of supply and demand graphically display the behavior of both the respective blocks (measured as changes in glycolytic flux) in response to variations in the linking metabolite ($[ATP] / [ADP]$), and are usually plotted in log-log space so as to represent percentage changes (refer to Preface and Sections 1.2 and 1.3) [9]. The intercept of the supply-demand rate characteristics denotes the metabolic steady state [9 & 8]. The sensitivity (defined elasticity coefficient) of supply and demand is quantified as the gradient of the tangents drawn to their respective rate characteristics [9].

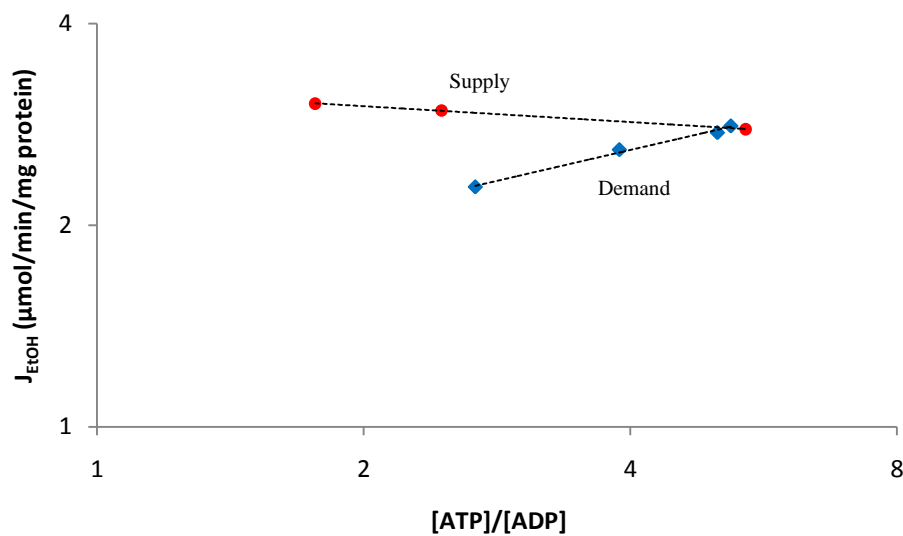


Figure 2.30: Variations in the glycolytic supply and demand for ATP (expressed as the ethanol production rate) as a function of the steady state $[ATP] / [ADP]$ ratio. Red circles represent the supply rate characteristic when ATP demand is perturbed through benzoic acid addition. Blue diamonds depict the demand rate characteristic when the glycolytic supply of ATP is modulated through maltose inhibition of glucose transport. The intercept of the supply and demand rate characteristic is taken as the reference point and indicates the non perturbed steady state.

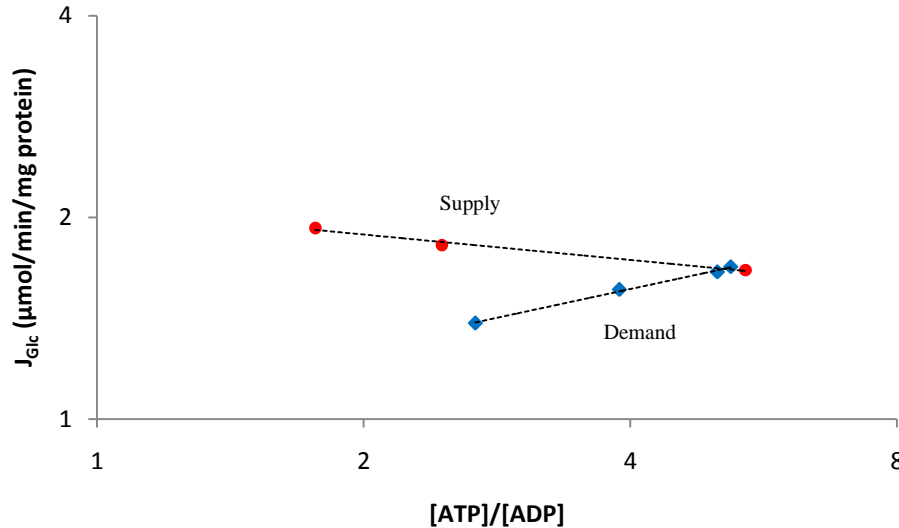


Figure 2.31: Variations in the glycolytic supply and demand for ATP (expressed as the glucose consumption rate) as a function of the steady state $[ATP] / [ADP]$ ratio. Red circles represent the supply rate characteristic when ATP demand is perturbed through benzoic acid addition. Blue diamonds depict the demand rate characteristic when the glycolytic supply of ATP is modulated through maltose inhibition of glucose transport. The intercept of the supply and demand rate characteristic is taken as the reference point and indicates the non perturbed steady state.

The overall flux and steady state metabolite data (Table 2.5 and 2.6) were used for plotting of the rate characteristics shown in Fig. 2.30 and 2.31. Regressions lines (dotted lines) were fitted through both the supply and demand data points yielding good R^2 values ($Sup_{EtOH} = 0.99, Sup_{Glc} = 0.94, Dem_{EtOH} = 0.98$ and $Dem_{Glc} = 0.99$) in all four cases, indicating the linear relationship between $\log_2([ATP] / [ADP])$ and \log_2 [glycolytic flux]. The gradients of these regression lines were used to calculate the elasticities of supply and demand. These elasticities were substituted into equations 1.21 and 1.22 for determining the flux and concentration control coefficients (Table 2.7).

Table 2.7: Elasticities and control coefficients of supply and demand

	$J = dEtOH/dt$	$J = dGlc/dt $
$\epsilon_{ATP/ADP}^{supply}$	-0.07	-0.07
$\epsilon_{ATP/ADP}^{demand}$	0.20	0.11
C_{supply}^J	0.75	0.64
C_{demand}^J	0.25	0.36
$C_{supply}^{ATP/ADP}$	3.73	5.59
$C_{demand}^{ATP/ADP}$	-3.73	-5.59

When either ethanol production or glucose consumption was used as the indicator of glycolytic flux, the demand elasticity exceeded that of the supply, pointing to the heightened sensitivity of the demand block towards the steady state $[ATP] / [ADP]$ ratio. This leaves the majority of flux control to the less receptive supply block, as confirmed by the control coefficients presented in Table 2.7. The slight discrepancy between the two sets of data (J_{EtOH} versus J_{Glc}) can be explained in light of the heterofermentative nature of these yeasts. As the absolute rate of change for glucose is essentially equivalent to the sum of the rates of change for all fermentation end products, the constructed rate characteristic will reflect a net or overall sensitivity comprised of individual pathway elasticities to variations in the steady state $[ATP] / [ADP]$ ratio, which may affect the overall shape of the rate characteristic. Furthermore quantifying supply and demand flux in terms of the absolute value of J_{Glc} can be viewed as being in violation of SDA, as the supply and demand blocks no longer communicate solely via the ATP-ADP moiety, as carbon is also shunted to the redox biased production of the fermentation side products glycerol and acetate [9]. It is most likely for these reasons that J_{EtOH} is most often used as an indicator of glycolytic flux when performing a supply demand analysis.

The experimental findings of this study will be discussed in the next chapter, where the data will be critically assessed and compared to previous publications.

Chapter 3

General discussion

Supply demand analysis and the more general theory of metabolic control analysis have developed into powerful tools for describing and quantifying the control and regulatory structure of metabolic pathways and other biological systems. The theory of MCA has helped biochemists replace the dogmatic belief of the rate limiting step as the sole dictator of pathway flux [4, 5 & 9]. Using high field NMR spectroscopy, these theories can now be tested on a whole cell level. The work presented in this thesis attests to this fact and in its entirety yields valuable information regarding the control of flux through glycolysis, the most researched biochemical pathway.

3.1 Synopsis

The experimental results were presented in Chapter 2 and can be divided into two main sections, *whole cell* experimental supply demand analysis of yeast fermentative free energy metabolism and *in situ* glycolysis.

Starting off with the whole cell experiments, the analytical power and sensitivity of NMR spectroscopy was applied to perform *in vivo* phosphorous assays on intact yeast cell suspensions. Signals for a host of phospho metabolites were identified, including inorganic phosphate, a multi-component peak consisting of the glycolytic sugar phosphates, polyphosphates (1 through 5), NAD^+/NADH and overlapping resonances for ATP and ADP [130 & 131] (see Fig. 2.2). On closer examination of the P_i peak, two signals corresponding to intra and vacuolar phosphate pools were identified [130, 131, 150 & 158] (see Fig. 2.5). Through calibration of the pH dependent P_i chemical shift [103 & 132], cytoplasmic pH was monitored during fermentation. Cytoplasmic pH was close to neutral under resting conditions ($\text{pH} = 7.27$), and was shown to acidify following the onset of glycolysis (see Fig. 2.7). Unfortunately the spectral resolution obtained *in vivo* was insufficient for accurate quantification of the adenine nucleotides. Low metabolite concentrations (specifically ADP), proximity to the far larger polyphosphate peaks and a less than adequate signal to noise ratio (see Fig.2.3), were

identified as the major causes of the diminished resolution. As an alternative, ^{31}P NMR assays were performed on perchloric acid yeast cell extracts (see Fig. 2.24), and yielded a comparative steady state $[\text{ATP}] / [\text{ADP}]$ ratio of 5.29 ± 0.31 [11 & 138] (see Table 2.5 and Table 2.6).

Glycolytic flux was quantified both in terms of the glucose consumption and ethanol production rate using ^{13}C NMR spectroscopy (see Fig. 2.11). Over 80% of the total glucose consumed was converted to ethanol, with roughly 13% shunted towards the production of glycerol (see Table 2.1). As glycerol formation requires the net use of NADH, these yeasts must produce some product more oxidized than glycerol if redox homeostasis is to be ensured during fermentation. From the ^{13}C spectra only an extremely faint signal assigned to the C2 carbon of acetate was observed, however it is doubtful that enough redox equivalents would be produced via this route to sustain glycerol synthesis. It has been hypothesized that the high rates of glycerol production observed during predominantly alcoholic fermentation in yeast may function as a redox valve re-oxidizing excess NADH formed during the assimilation of glucose to biomass [159]. It is probable that the ^{13}C signal arising from these assimilated polymers is obscured by the far larger glucose peaks during spectral acquisition. During fermentation more than 90% of the ^{13}C label was recovered through ethanol and glycerol formation; the minute amounts of acetate formed were neglected and hence alcoholic fermentation was effectively viewed as the only supply of ATP. The major glycolytic intermediates; G6P and F1, 6BP were identified *in vivo*. Label scrambling and inadequate resolution prevented a more detailed description of these and other glycolytic intermediates.

The double modulation method as originally described by Kacser and Burns [8] was employed for performing the supply demand analysis on yeast fermentative free energy metabolism. Benzoic acid titrations were carried out for modulating ATP demand (thus quantifying the effect of changes in cellular free-energy state on the glycolytic supply) [8], while maltose inhibition of glucose transport [157] was used to perturb the free-energy supply (yielding the demand response curve towards $[\text{ATP}]/[\text{ADP}]$) [8 & 11]. The resultant effect of these perturbations on glycolytic flux were determined using ^{13}C NMR. The addition of benzoic acid, led to an increase in the glycolytic flux (see Fig 2.26), whilst maltose supplementation caused a reduction in the glycolytic rate (see Fig.

2.28). The corresponding changes in the $[ATP] / [ADP]$ ratio were determined by performing ^{31}P NMR on yeast perchloric acid cell extracts. Decreased steady state $[ATP] / [ADP]$ ratios were observed both in the case of maltose ($\downarrow 47\%$) and benzoic acid ($\downarrow 65\%$) addition (see Fig. 2.27 and 2.29). Rate characteristics were constructed (see Fig. 2.30 and 2.31) and elasticities were calculated (see Table 2.7); $\varepsilon_{[ATP]/[ADP]}^{Sup} = -0.07$ and $\varepsilon_{[ATP]/[ADP]}^{Dem} = 0.20$. The larger demand elasticity points to the increased sensitivity of the ATP consuming demand towards the $[ATP] / [ADP]$ ratio, leaving the bulk of the flux control to the supply block [9]. The flux control coefficients as calculated from the respective elasticities were $C_{Sup}^{JEtOH} = 0.75$ and $C_{Dem}^{JEtOH} = 0.25$. However when the glycolytic flux was expressed as the glucose consumption rate, flux control was distributed in a more equal fashion; $C_{Sup}^{JGlc} = 0.64$ and $C_{Dem}^{JGlc} = 0.36$. These discrepancies were attributed to the hetero-fermentative nature of these yeasts, specifically concerning the ATP and NADH consuming production of glycerol, which would impact on the shape of both the rate characteristics when incorporated into the overall glycolytic flux.

In Section 2.2 permeabilized yeast glycolysis was presented. Yeast cell membranes were successfully disrupted through toluene induced permeabilization. Fluxes were successfully generated *in situ*, and were analyzed using ^{13}C NMR spectroscopy (see Fig. 2.14). *In situ* fluxes were shown to be lower in comparison to whole cell assays (see Table 2.2) and these differences were explained in light of a potential loss in glycolytic enzyme activity. The greater signal to noise ratios and enhanced spectral resolution gained through cell permeabilization was the motivation behind the use of this technique as an alternative to *in vivo* NMR. Effectively this technique was viewed a success as it allowed for the detection of both ATP and ADP *in situ* by means of phosphorous NMR (see Fig. 2.17).

The $[ATP] / [ADP]$ ratio was modulated *in situ* by varying the initial amount of ATP and ADP supplied to the system, which allowed these nucleotides to settle at different pseudo-steady-state ratios during fermentation (see Fig. 2.20). Changes in the steady state $[ATP] / [ADP]$ ratio as well in the charged/uncharged ratio were correlated to glycolytic flux and used for plotting an *in situ* rate characteristic (see Fig. 2.21 & Fig. 2.22). As the $[ATP] / [ADP]$ ratio was directly altered, effectively the *in situ* rate

characteristic represents the global response in glycolytic flux to varying $[ATP] / [ADP]$ or c/u [4 & 8]. The response coefficients ($R_{[ATP]/[ADP]}^{J_{EtOH}}$, $R_{c/u}^{J_{EtOH}}$) were calculated as 0.74 and 0.99 respectively. The origin of this contradictory response, although speculative, was attributed to the “turbo like” behavior observed *in situ* which essentially results in the uncoupling between the top and lower half of glycolysis (see Section 3.2). These permeabilized yeast displayed characteristic profiles in terms of sugar-phosphate accumulation and low $[ATP]$, symptomatic of that observed in *TPS1* yeast mutants and is termed the turbo effect [50, 146, 147 & 148].

The application of creatine kinase and the free-energy buffering capabilities it imparts for circumventing the rapid loss of ATP associated with the “turbo effect”, proved to be unsuccessful (see Fig. 2.24). Problems associated with creatine solubility, uncertainty surrounding the validity of the calculated apparent equilibrium constant, and the metabolic behavior of the *in situ* system itself (i.e. rapid consumption of ATP) were highlighted as potential shortcomings adversely affecting the buffering capability of this system.

3.2 Critique and discussion

In a similar study performed on fermenting yeast by Kroukamp et al. [11], glycolytic flux control was also found to reside predominantly in the supply block ($\varepsilon_{[ATP]/[ADP]}^{Sup} = -0.03$ & $\varepsilon_{[ATP]/[ADP]}^{Dem} = 0.28$; $C_{Sup}^J = 0.90$ & $C_{Dem}^J = 0.10$). The slight dissimilarity between the flux control coefficients as determined in these two studies can be attributed to differences in assay conditions. Our assays were performed under non growing conditions in the presence of high glucose (batch fermentation) compared to the energy limited chemostat cultures (growing conditions) used by Kroukamp et al. [a (11)], the greater degree of flux control by the demand presented here can be explained in terms of these differences. At saturating concentrations of glucose the supply of ATP is only limited by the intrinsic ability of glycolysis to metabolize its substrate (increased $\varepsilon_{[ATP]/[ADP]}^{Sup}$), therefore under non growing conditions (low free energy requirements) it is expected that some or more of the control will be transferred to the demand block so as to prevent accumulation of ATP. Low [glucose] coupled with high cellular free energy requirements (growing cells), may cause glycolysis to become

substrate limited and as such so will the supply of ATP (decreased $\epsilon_{[ATP]/[ADP]}^{Sup}$), therefore the demand will have zero or little control over the glycolytic flux. The large concentration control coefficients reported in this study ($C_{Sup\ or\ Dem}^{[ATP]/[ADP]} = \pm 3.8$), points to a weakened homeostatic maintenance of the [ATP] / [ADP] ratio and is in strong contrast to the narrow buffering range ($C_{Sup\ or\ Dem}^{[ATP]/[ADP]} = \pm 0.12$) reported by Kroukamp et al. [11].

In a previous report by Schaaff et al. [12], it was shown that the independent and simultaneous over expression of key glycolytic enzymes in yeast did not lead to significant increases in pathway flux. Hofmeyr [30] interpreted these results as pointing to extrinsic flux control residing in the demand for ATP. Though these findings are in disagreement with the results presented here, the failure of Schaaff et al [12] to incorporate the importance of the glucose transport step during their analysis may explain these discrepancies as was originally proposed by Kroukamp et al. (2002) [11]. Glucose transport has been shown to exert a high degree of control over glycolytic flux in yeast under many conditions, with both kinetic models and experimental reports predicting a flux control coefficient close to unity [13, 160, 161 & 162]. Such a key control point within the confines of the glycolytic pathway itself may indeed transfer the majority of flux control in yeast to the supply block, even when energy is freely available.

Upon closer investigation of the metabolic trends observed *in situ*, certain abnormalities were identified. During fermentation, the sugar phosphates, specifically F1,6BP, seemed to accumulate with ATP being consumed at a rapid rate, stabilizing only at extremely low concentrations. This type of conduct is characteristic of yeast mutants deficient in the gene *TPS1*, coding for the enzyme trehalose 6 phosphate synthetase [50, 146, 147 & 148]. These yeast are unable to grow on high concentrations of glucose due to the unregulated activity of the ATP consuming reactions of glycolysis, and the phenomenon is termed the “turbo effect” [51]. The product of trehalose-6-phosphate synthetase, Tre-6P, has been shown to inhibit hexokinase activity *in vitro*, although the exact molecular mechanisms are still unclear [50]. It is now believed that the function of *TPS1* is to act as a gate to glycolysis, by restricting the flow of glucose into the pathway [50]. It was therefore suggested that the trehalose synthesis pathway might not be active *in*

situ, thus explaining the observed phenomenon. The inability of the pathway to function properly *in situ* is most likely due to the absence of the essential cofactors GTP and UDP [50] which would have been removed during cell permeabilization (Chapter 4), however toluene-induced disruption of the signaling cascades responsible for switching on this pathway cannot be ruled out at present. The albeit low but settled [ATP] / [ADP] and *c/u* ratios observed *in situ*, may be explained in spite of the accumulating hexose phosphates as follows: for ATP to remain constant its rate of consumption must equal its rate of production,

$$V_{consumption} (V_{HK} + V_{PFK} + V_{ATP\ dem}) = V_{production} (2 \cdot V_{lower\ half\ of\ glycolysis})$$

[51]. Although this relationship allows for constant fluxes and stable [ATP] / [ADP] ratios, it does not imply that $V_{HK} = V_{PFK}$ and therefore cannot be viewed as being at steady state (hexose phosphates do not remain stable) [51]. Only if the following criteria are met: $V_{top\ half\ of\ glycolysis} = \frac{1}{2} V_{lower\ half\ of\ glycolysis} = \frac{1}{2} V_{ATP\ dem}$ will glycolysis (including all intermediates and the [ATP] / [ADP] ratio) be at steady state [51].

3.3 Future Work

Concerning experiments performed on intact cell suspensions, future work would include a more comprehensive SDA on yeast fermentative free energy metabolism. By making use of various yeast strains that overexpress key glycolytic enzymes (including the glucose transporter) and yeast mutants with decreased biosynthetic activity, both the supply and demand flux may respectively be perturbed in a positive and negative direction. Although perchloric acid cell extractions were applied successfully during the course of this study for quantifying the [ATP] / [ADP] ratio with ^{31}P NMR, there are errors inherent to such metabolic extraction procedures. These include the partial cessation of metabolism during quenching and the loss of volatile metabolites [163]. Furthermore, as this method leads to the complete extraction of the total metabolite pool, it may contain both the enzyme bound and soluble fractions of ATP-ADP and thus may not accurately reflect the free cytosolic ratio. Hence in the future these nucleotide ratios should ideally be measured *in vivo*. The application of ^{13}C NMR spectroscopy for tracking glycolytic intermediates *in vivo* has previously been addressed in this thesis (Section 2.1.4), with some positive results having been obtained (Fig 2.10), a more detailed analysis of intermediate concentration profiles (*in situ* and *in vivo*) should be

attempted in the future. Such metabolite profiles combined with readily determinable ^{13}C NMR flux measurements will serve as a comprehensive data set from which kinetic models, such as that developed by Teusink et al. [13] (refer to Section 1.4), may be experimentally validated.

With reference to work on permeabilized cells, future studies should include a detailed investigation into the exact cause of the turbo effect observed *in situ*, with specific emphasis placed on circumventing the problems associated with this type of behavior and establishing an *in situ* steady state. Furthermore, the permeabilized state affords us with the ability to selectively activate specific enzymes whilst keeping downstream reactions inactive (refer to Section 2.2.1). As this situation lends itself to the study of enzyme kinetics in a close to natural environment, the derivation of kinetic parameters obtained *in situ* is a promising avenue.

3.4 Conclusion and Perspective

In conclusion, our results report that under energy excess (high [glucose], non growing conditions) the majority of anaerobic glycolytic flux control is situated in the supply block. This points to the importance of steps intrinsic to the supply block such as glucose transport, in exerting a large degree of control over the steady state flux whether under energy excess or limitation [11]. In spite of this, yeast glycolytic flux control by the demand block would be better suited under the conditions assayed, specifically concerning the homeostatic control of the $[\text{ATP}] / [\text{ADP}]$ ratio. It might be that there are other hierarchal systems or factors to consider (e.g. changes in gene expression), which may dominate metabolic regulation solely by the laws of supply and demand.

This study has proven the success of combining quantitative theory with experimental analysis for elucidating the flux control distribution within yeast anaerobic glycolysis. As described in Section 3.3, these data may yet be used in combination with computational modeling for simulating glycolytic behavior in yeast. The work presented in this thesis may further serve as an example for analyzing other metabolic networks in terms of supply and demand. Presently within our research group, this analysis is being extended to the industrially important microbes *Zymomonas mobilis* and *Lactococcus*

lactis. Although other methods such as HPLC and LC-MS may be applied with equal success regarding the quantification of external metabolites, this study illustrates the advantages of probing microbial metabolism *in vivo* using a non-invasive technique such as NMR spectroscopy; as it yields both qualitative (significant trends) and quantitative information (intermediate concentrations and fluxes) regarding real time metabolic behavior.

The *in situ* work presented in this thesis has demonstrated the value of studying glycolysis in permeabilized yeast, and as such opens up the possibility for performing trial manipulations (selective enzyme activation or inhibition) and inducing complex biochemical phenomena (such as the turbo effect [51]) in a close to natural environment. The biochemical examination of microbes with non-selective membrane permeability may yet find application beyond the scope of the work presented here, in fields such as enzyme kinetics and proteomics.

Chapter 4

Materials & Experimental Procedures

This chapter details the methods and procedures used throughout this study. All reagents were obtained from *Sigma Aldrich South Africa* unless otherwise specified and were of analytical grade or higher with a purity of $\geq 98\%$. Deuterium oxide, yeast extract and bacteriological peptone were from *MERCK South Africa*. The ^{13}C enriched glucose (purity of 99%) was obtained from *Cambridge Isotope Laboratories Inc USA*.

4.1 Cell Growth

The yeast *Saccharomyces cerevisiae* strain CEN.PK 113-7D was the organism under study and was used in all experimental analyses. Cells were grown as a batch culture on YPD liquid medium composed of 1% yeast-extract, 2% bacteriological peptone and 2% glucose. Inoculated flasks were incubated at 30°C in a Gallenkamp Orbital Shaker at 180 rpm to allow for cell growth. For overnight cultures, 500ml Erlenmeyer flasks were used containing 100ml medium, with larger quantities grown in two liter Erlenmeyer flasks holding 500ml medium. Freezer stocks were produced from these batch cultures through dilution of the sample with glycerol (1:4), followed by snap freezing with liquid nitrogen in two ml cryogenic tubes and storage at -80°C for future use. Cultures were streaked out onto YPD agar plates (1.5% agar) and incubated for 48 h at 30°C to allow for colony development. Plates were then stored at 4°C for a period of up to three months and used as a future source of inoculum.

In addition to cell growth in Erlenmeyer flasks, batch fermentations were also carried out in a ten liter Bioflo 110 Bioreactor, with the same incubation parameters as mentioned above and were used as an additional source of cell material.

4.1.1 Cell growth and harvesting procedures

Cell growth was assayed over a period of eight hours by measuring the optical density (OD) of the cell suspension at 600nm on a Jenway 6100 Spectrophotometer in one ml plastic cuvettes. Measurements were taken in triplicate every hour for both the lag and

stationary phase of growth and every 30 minutes once cells entered their exponential growth phase. Growth curves were produced in triplicate.

Using the calculated specific growth rate and the measured initial OD_{600} of the yeast culture, projections concerning cell density over time were made according to relationship stated below.

$$Time (h) = (\ln[OD_{projected}] - \ln[OD_{initial}]) / \mu \quad 4.1$$

I. Cell Harvesting

Cells were harvested during mid log phase at an $OD_{600} = 4$, by means of low speed centrifugation. Cultures were centrifuged (5min at $4420 \cdot g$, temp = $4^{\circ}C$), followed by decantation of the supernatant and re-suspension in 100mM PIPES buffer pH 6.1. Centrifugation and washing steps were repeated four times with a final re-suspension of the cell pellet in 100mM PIPES buffer pH 6.1 at an $OD_{600} \geq 700$. The cell suspension was kept on ice to inhibit metabolic activity until required for NMR runs [128].

II. Cell permeabilization

Cells were harvested through one round of low speed centrifugation (same parameters as above) followed by the decantation of the supernatant and re-suspension of the cell pellet in extraction buffer (75mM Imidazole, 100mM KCl and 10mM $MgCl_2$ at pH 6.5) to an $OD_{600} = 200$ [141]. The permeabilizing agent toluene (diluted 1:4 with 100% ethanol) was then added to the cell suspension at a total concentration of 5% (volume/volume) followed by incubation at $30^{\circ}C$ for a period of ten minutes [141]. After incubation the cell suspension was washed four times with the extraction buffer by means of low speed centrifugation (see above) for the removal of excess toluene and biological cofactors small enough to pass through the leaky cell membrane [141]. Cells were then resuspended to a final $OD_{600} \geq 600$ in 100mM PIPES pH 6.1. Harvested cells were then kept on ice, in order to keep cells metabolically inactive until required for NMR runs. The permeabilization protocol was adopted and modified from Serrano et al. [141].

III. Sterilization and controlling for cell purity

All media and reagents used for the purpose of cell growth and harvesting (excluding biological buffers) were autoclaved for 15 minutes at 121°C on the wet cycle in a Han Lien UE 650 Autoclave. Inoculations from both liquid cultures and agar plates were performed under a laminar flow hood at 200 Pa. Cells were cultivated in duplicate and purity was monitored under 40X magnification on a Zeiss Axiostar microscope.

4.2 Permeabilized yeast

To check whether yeast glycolysis was indeed able to function, post membrane permeabilization, *in situ* glycolytic enzyme activities were first determined spectrophotometrically. These assays played an important role in ultimately setting up the protocol for measuring the glycolytic flux *in situ* using ^{13}C NMR spectroscopy.

4.2.1 *In situ* glycolytic enzyme activity determination

Glycolysis can essentially be divided into two parts. The top half consists of the first six enzymes whose activity can be linked to the reduction of NAD^+ to NADH by the enzyme glyceraldehyde-3-phosphate dehydrogenase (see Fig. 4.1). The bottom half consists of the last six enzymes whose activity can be linked to the intrinsic oxidation of NADH to NAD^+ catalyzed by the final enzyme in the glycolytic pathway, alcohol dehydrogenase (see Fig. 4.2).

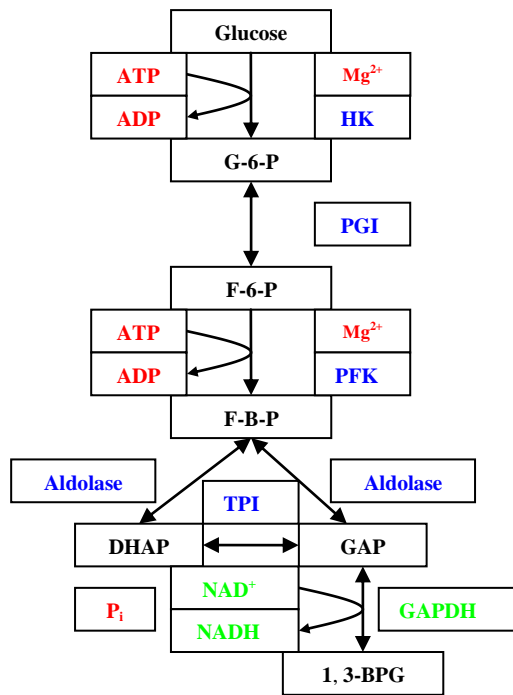


Figure 4.1 Top half of yeast glycolysis. The activity of the first six enzymes is linked to the intrinsic reduction of NAD⁺ to NADH (green) by GAPDH (green) which can be monitored spectrophotometrically at 340nm. Enzymes are in blue, reactants in black and cofactors in red. Abbreviations are defined on pp. vi and vii.

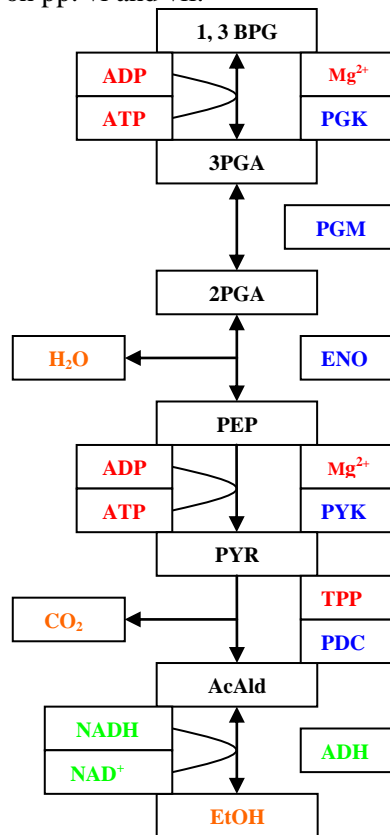


Figure 4.2: Bottom half of yeast glycolysis. The activity of the last six enzymes is linked to the intrinsic oxidation of NADH by ADH (shown in green) which can be monitored spectrophotometrically at 340nm. Enzymes are in blue, reactants in black, cofactors in red and metabolic end products in orange. Abbreviations are defined on pp. vi and vii.

For the top half, the glycolytic enzymes were sequentially activated from the bottom up. Starting with GAPDH, its substrate GAP as well as the cofactor NAD^+ and inorganic phosphate were added, activity was measured as an increase in absorbance at 340nm due to the formation of NADH. Next TPI's substrate DHAP and the cofactors of the GAPDH reaction (P_i and NAD^+) were added, increase in absorbance was again followed spectrophotometrically at 340nm which was then indicative of TPI activity. Similarly the activities of all the top half enzymes were assayed by the addition of the respective substrate and its cofactors plus the cofactors of all the downstream enzymes, hence linking it to the reduction of NAD^+ catalyzed by GAPDH.

For the bottom half, the glycolytic enzymes were sequentially activated from the bottom up. Starting with alcoholdehydrogenase (ADH), the assay was run in reverse due to the volatility of the forward substrate acetaldehyde, hence ethanol and NAD^+ were added and activity was measured as an increase in absorbance at 340nm. Next PDC was assayed and its substrate pyruvate and cofactor TPP were added along with the cofactor NADH for the ADH reaction, activity was related to a decrease in absorbance at 340nm caused through the oxidation of NADH, which was indicative of PDC activity. Similarly the activities of all the bottom half enzymes (excluding PGK) were assayed by the addition of the respective substrate and its cofactors plus the cofactors of all the downstream enzymes, linking it to the oxidation of NADH by ADH. PGK was assayed in reverse and linked to the oxidation of NADH by GAPDH.

All assays were performed in one ml plastic cuvettes placed in a thermostatted cuvette holder at 25°C. A DU-650 Beckman Spectrophotometer was used for following the absorbance at 340nm with the spectrometer software, Data capture Rev.2.3 set on receive kinetic data mode. All metabolites and reagents were added according to the concentration and pH ranges specified by Teusink et al. [13].

4.3 NMR assays

All spectra were obtained by means of pulsed Fourier transformation on a Varian Unity 600 MHz spectrometer. Continuous proton decoupling was employed during spectral acquisition for both ^{13}C and ^{31}P assays. The reaction vessel used in all *in vivo* and *in situ* assays consisted of a 10mm NMR glass tube (diameter = 10mm and length = 17.8 cm),

fitted with a plastic cap containing a small pore to prevent carbon dioxide build up during fermentation. The sample tube was allowed to spin at 15Hz for the duration of the experiment to prevent sedimentation of biological material and to keep the suspension homogeneous.

4.3.1 ^{31}P *In Vivo* NMR Assays

The total reaction volume was 3000 μl and had the following composition: 10% deuterium oxide (D_2O) which serves as a non-interfering solvent to which the magnetic field was locked, 100mM PIPES buffer pH 6.1, 5mM of the internal standard triethylphosphate (TEP) and the yeast cell suspension at a final $\text{OD}_{600\text{nm}} = 300\text{-}500$. Glucose was treated as a parameter and added at varying concentrations ranging from 100mM to 200mM. Reverse Osmosis (RO) purified water was used to fill up the reaction volume to the required 3000 μl mark.

Before the addition of glucose to the reaction mixture, the sample was inserted into the spectrometer to allow for sample tuning. Channel one was tuned to ^{31}P nuclei with channel two tuned to ^1H so as to facilitate proton decoupling. After sample tuning, shimming of the magnetic field was manually performed and locked to the D_2O signal. Background scans were taken prior to the start of fermentation to check for correct peak shapes and adequate signal to noise ratios.

The sample was then ejected from the spectrometer for the addition of substrate which was taken as time point zero followed by the reinsertion of the reaction vessel into the spectrometer and acquisition of time course data. ^{31}P Chemical shifts were recorded relative to the internal standard TEP, TEP was taken to be + 0.44 ppm (up field) from 1M phosphoric acid.

Spectra were obtained at 242.876 MHz with the following spectral parameters: spinner frequency = 15Hz, incubation temperature = 25°C, spectral width = 12135.9 MHz, pulse width = 10 μs , pulse angle = 60°, acquisition time = 0.800s and number of transients (nt) = 75.

4.3.2 ^{13}C *In Vivo* NMR assays

The total reaction volume was 3000 μl and had the following composition: 10% deuterium oxide (D_2O), 100mM PIPES buffer pH 6.1 which also served as the internal standard, and the yeast cell suspension at a final OD_{600} =300-500. As a result of the low natural abundance of ^{13}C (1.1%) the addition of labeled glucose was required so as to obtain detectable signals from the various glycolytic intermediates as well as the end product of yeast alcoholic fermentation, ethanol. Depending on the position of the labeled carbon in the glucose used as substrate, different glycolytic intermediates can be detected. The main purpose of the ^{13}C runs was glycolytic flux determination; hence in almost all experiments primarily $^{13}\text{C}6$ or $^{13}\text{C}1$ labeled glucose was used which allowed for detection of the C2 carbon of ethanol. Similarly as in the phosphorous experiments, ^{13}C labeled glucose was treated as a parameter and added at varying concentrations in the range of 100mM to 200mM, either as pure label or as a combination of labeled and unlabelled glucose (10% ^{13}C labeled, 90% cold glucose). Reverse Osmosis (RO) water was used to fill up the reaction volume to the required 3000 μl mark.

Before the addition of glucose to the reaction mixture, the sample was inserted into the spectrometer to allow for sample tuning. Channel one was tuned to ^{13}C nuclei with channel two tuned to ^1H so as to facilitate proton decoupling. After sample tuning, shimming of the magnetic field was manually performed and locked to the D_2O signal. Background scans were taken prior to the start of fermentation to check for correct peak shapes and adequate signal to noise ratios.

The sample was then ejected from the spectrometer for the addition of substrate which was taken as time point zero followed by the reinsertion of the reaction vessel into the spectrometer and acquisition of time course data. ^{13}C Chemical shifts were recorded relative to that of 1M TMS.

Spectra were obtained at 150.884 MHz with the following spectral parameters: spinner frequency = 15Hz, reaction temperature = 25 $^\circ\text{C}$, spectral width = 40000MHz, pulse width = 6 μs , pulse angle = 44 $^\circ$, acquisition time = 0.500s, delay time = 0.100s and number of transients (nt) = 100.

At the end of fermentation spectra were calibrated for the effects of saturation by intermittently exchanging rapid (above) and relaxed pulse sequences, this cycle was repeated a total of three times. For the fully relaxed acquisitions an additional delay of 1.6 seconds was added (total delay time = 1.7s), the rest of the parameters were the same as above.

4.3.3 *In Situ NMR Assays*

Similar to the *in vivo* assays, the total reaction volume was 3000ul, with the following composition: 10% deuterium oxide (D₂O), 100mM PIPES pH 6.1 (internal standard ¹³C NMR assays), 5mM of the internal standard TEP (only during ³¹P NMR assays) and the permeabilized yeast cell suspension at a final OD₆₀₀ = 30.

I. ¹³C and ³¹P NMR assays

¹³C Labeled glucose or cold glucose was used as substrate for these assays and was treated as a parameter added at varying concentrations in the range of 5mM to 50mM. As a result of the permeable cell membrane most, if not all of the glycolytic cofactors and internal metabolites are able to move via diffusion into the extra cellular medium or buffer and are washed off during the cell harvesting procedure. Therefore in order to obtain a flux through glycolysis the missing cofactors need to be replenished by their addition at physiologically relevant levels. The following glycolytic cofactors were added at their respective concentrations: 2.5mM NAD⁺, 5mM of EDTA (chelating agent), 5mM DTT (reducing agent), 5mM MgCl₂, 5mM KH₂PO₄, 1mM TPP (essential cofactor for PDC), 2.5 mM of the glycolytic regulator 2,3-diphosphoglycerate and 2.5 mM of the intermediate FBP (activator for PYK). NADH was not individually added, but as it forms part of the NADH-NAD⁺ conserved moiety, recycling occurs further downstream [9 & 28], the cofactors ATP and ADP and were added at varying concentrations ranging from zero to 5mM [13]. Assay protocol was adopted and modified from Teusink et al. [13].

Before the addition of glucose to the reaction mixture, the sample was inserted into the spectrometer to allow for sample tuning and shimming as in Sections 4.3.1 and 4.3.2.

The sample was then ejected from the spectrometer for the addition of substrate which was taken as time point zero followed by the reinsertion of the sample into the spectrometer and acquisition of time course data. The same pulse sequence and spectral parameters were used as for the respective *in vivo* ^{13}C and ^{31}P NMR assays. ^{31}P Chemical shifts were recorded relative to the internal standard TEP, TEP was taken to be + 0.44 ppm (up field) from 1M phosphoric acid. ^{13}C Chemical shifts were recorded relative to that of 1M TMS.

4.3.4 Perchloric acid cell extracts

For the production of cell extracts, bench fermentations were carried out in 15ml Greiner tubes fitted with a plastic cap containing a small pore to prevent carbon dioxide build up. The total reaction volume was 3000 μl and the sample composition was identical to that of the *in vivo* ^{31}P NMR assays (excluding the addition of D_2O).

I. Extraction procedure

Fermentation was initiated by the addition of 133mM unlabelled glucose to the cell suspension at time zero. Metabolism was then quenched by adding 300 μl of 30% ice cold perchloric acid at time points (minutes) 4, 6 and 8, followed by snap freezing of the sample in liquid nitrogen and overnight storage at -80°C . After one cycle of freeze thawing, samples were then neutralized with 100mM K_2CO_3 followed by the removal of cell debris by means of centrifugation (10min at 13148 $\cdot g$, temp = 4°C). Extracts were then diluted in 30mM EDTA pH8.2 to a final volume of ten ml, before freeze drying overnight (~12 hrs) in a Virtis Unitrap II freeze dryer. Samples were then once again thawed followed by a final resuspension in 30 mM EDTA pH8.2 to a total volume of 900 μl . Extracts were stored at -20°C until required for use in ^{31}P NMR assays. Protocol for performing cell extractions was adopted from Rogers et al. [164].

II. ^{31}P NMR assays on perchloric acid cell extracts

Assays were performed in 5mm NMR glass tubes (diameter = 5mm and length = 17.8 cm), fitted with a solid plastic cap. Total reaction volume was 1000 μl with the following composition: 10% deuterium oxide (D_2O) which serves as a non-interfering solvent to which the magnetic field was locked, 5mM of the internal standard TEP and 850 μl of the cell extract.

Sample tuning and shimming was performed manually in the same fashion as discussed previously in Section 4.3.1 and 4.3.2, excluding the steps associated with background scan measurements and substrate addition. ^{31}P Chemical shifts were recorded relative to the internal standard TEP, TEP was taken to be + 0.44 ppm (up field) from 1M phosphoric acid.

Spectra were obtained at 242.876 MHz with the following spectral parameters: spinner frequency = 15Hz, incubation temperature = 25°C, spectral width = 12135.9 MHz, pulse width = 6 μs , pulse angle = 45°, acquisition time = 0.800s, delay time = 1.2s and number of transients (nt) = 2000.

4.4 Whole cell supply and demand perturbations

4.4.1 Demand Perturbations

Cellular demand for ATP was perturbed by titrating yeast cell suspensions with benzoic acid. The effect of metabolic un-coupling was monitored as changes in the steady state [ATP] / [ADP] ratio and the glycolytic flux. The concentration range of benzoic acid assayed was 1, 2 and 10mM (lethal). The benzoic acid solution used was buffered at pH ≥ 5 , to ensure its solubility. The samples were made up with benzoic acid prior to the addition of glucose to allow for equilibration of the assay mixture.

4.4.2 Supply perturbations

The glycolytic supply of ATP was modulated by titrating yeast cell suspensions with the glucose transport inhibitor maltose. The effect of the perturbation was monitored as changes in the steady state [ATP] / [ADP] ratio and glycolytic flux. The concentration range assayed was 25, 50, and 75mM maltose. The samples were made up with maltose prior to the addition of glucose to allow for equilibration of the assay mixture.

4.5 Creatine kinase assays

4.5.1 Determination of the apparent equilibrium constant for the creatine kinase reaction

The apparent equilibrium constant for the creatine kinase reaction; $K' = \frac{[ATP] \cdot [Cr]}{[ADP] \cdot [CrP]}$ was determined with ^{31}P NMR spectroscopy. Thermodynamic equilibrium was probed in both the forward and reverse direction, with ATP, ADP, CrP and creatine varied in the range from zero to 40mM.

Assays were performed at 25°C in 100mM PIPES buffer pH 6.5 or pH 7.5 in the presence of 5mM MgCl_2 . The rest of the sample was made up in similar fashion to the permeabilized yeast assays (excluding the addition of glucose) so as to ensure the chemical similarity of assay mixture and hence the applicability of the determined K_{app} . 65 Units of creatine kinase (diluted in 75mM glycine buffer pH8.9) were added to both equilibrium and clamping experiments.

4.5.2 Clamping the $[ATP] / [ADP]$ ratio *in situ* with creatine kinase

The samples were made up in the same fashion as for the normal *in situ* runs containing the permeabilized yeast cell suspension and all the necessary cofactors and reagents. Varying $[ATP] / [ADP]$ ratios were then set before the start of fermentation. To induce the clamp, equilibrium concentrations of creatine phosphate and creatine were added as predetermined by the set $[ATP] / [ADP]$ ratio (see Table 4.1), along with the enzyme creatine kinase.

Table 4.1: Solving for the unknowns, creatine and creatine-phosphate, through use of the creatine kinase equilibrium expression and a $K' = 41$.

Clamped [ATP]/[ADP]	Added [Cr]/[CrP]
5	8.2
10	4.1
15	2.7

Samples were treated identically for both flux measurements (^{13}C NMR) and nucleotide quantification (^{31}P NMR) except for the addition of TEP in the case of the latter.

Fermentations were carried out until CrP became depleted ($\pm 30\text{min}$).

Following the addition of creatine kinase, the sample mixture was allowed to equilibrate in the spectrometer for a period of five minutes before sample tuning and shimming was manually performed. The acquisition of a background scan was then permitted followed by sample ejection and the addition of glucose at time zero and reinsertion into the spectrometer for acquisition of time course data. The same pulse sequence and acquisition parameters were used as for the respective *in situ* ^{13}C and ^{31}P NMR assays.

4.6 Experimental controls and data analysis

4.6.1 Flux normalization

All fluxes (*in vivo* and *in situ*) were normalized to total protein to allow for direct comparisons between separate sets of results. After ^{13}C NMR flux determination experiments, samples were ejected from the spectrometer and decanted into two ml cryogenic-tubes, followed by snap freezing in liquid nitrogen and storage at -80°C . After allowing samples to thaw (10min in a water bath 20°C) cell lysis was performed by means of acid washed glass bead centrifugation [13]. The supernatant was then decanted and diluted for quantification of total protein by means of Bradford protein determination assay [136]. All values were determined in duplicate across the dilution range (100 x, 10 x and 1 x) used.

Bovine Serum Albumin (BSA) was used as the protein standard (0 to 1mg/ml protein), with standard curves produced in triplicate. Absorbance was measured at 595 nm, on a Biotek Powerwave 340 plate reader using the Biotek Gen 5.105 software package. Fluxes were expressed as $\mu\text{mol}\cdot\text{min}^{-1}\cdot\text{mg protein}^{-1}$, and may be converted to $\mu\text{mol}\cdot\text{min}^{-1}\cdot\text{L cytoplasm}^{-1}$ assuming that there is 3.75ml of cell volume per gram protein [165 & 166], or $\mu\text{mol}\cdot\text{min}^{-1}\cdot\text{g dry cell weight}^{-1}$ if total protein is taken to comprise 39.5% of yeast cell biomass [167].

4.6.2 Data analysis

I. Steady state flux determination

Yeast glycolysis was viewed as being at steady state when both the rates of glucose consumption and ethanol production remained constant. In mathematical terms the second order derivative with respect to time for ethanol and glucose is equal to

zero, $\frac{d[x]}{dt} = 0$, for $x =$ ethanol or glucose. However if glycolysis is truly at a steady state, the glycolytic intermediates should remain constant over time or for the duration of the steady state. For ease of measurement however, only these external metabolites, glucose and ethanol were used as indicators of metabolic steady state in intact yeast cell suspensions.

II. Metabolite Quantification with NMR

Spectra were exclusively analyzed using the *Varian VNMR* software package. Spectra were phased automatically during data acquisition and manually post acquisition. The peaks to be analyzed were then marked and integrated by means of the deconvolution function. An exponential line broadening of 10 Hz was employed during spectral processing.

The raw files were then imported into *Microsoft Office Excel 2007* and converted to concentration profiles or time courses through relation of integral values to that of the internal standard. Peak assignments were made according to resonance positions obtained from literature (refer to Chapter 2) in addition to the spectral analysis of glycolytic standards.

References

1. Voet, D. & Voet, J.G. Biochemistry, 3rd Edition. John Wiley and sons, Inc. 2004.
2. Walsh, K. & Koshland, D.E. (1986) Characterization of rate-controlling steps in vivo by use of an adjustable expression vector. The Proceedings of the Natural Academy of Science of the United States of America. 82, 3577-3581.
3. Fell, D. (1997) Understanding the Control of Metabolism. London: Portland Press.
4. Kacser, H., Burns, J.A. & Fell, D.A. (1995) Biochemical Society Transactions. 23, 341-366.
5. Heinrich, R. & Rapoport, T.A. (1974) European Journal of Biochemistry. 42, 97-105.
6. Cascante, M., Boros, L.G., Comin-Anduix, B., de Atauri, P., Centelles, J.J. & Lee, P.W.N. (2002) Metabolic control analysis in drug discovery and disease. Nature Biotechnology. 20, 243-249
7. Hoefnagel, M.H.N., Starrenburg, M.J.C., Martens, D.E., Hugenholtz, J., Kleerebezem, M., Van Swam, I.I., Bongers, R., Westerhoff, H.V. & Snoep, J.L. (2002) Metabolic engineering of lactic acid bacteria, the combined approach: kinetic modelling, metabolic control and experimental analysis. Microbiology. 148, 1003-1013.
8. Brown, G.C., R.P. Hafner & Brand, M.D. (1990) A 'top-down' approach to the determination of control coefficients in metabolic control theory. European Journal of Biochemistry. 188:321-325.
9. Hofmeyer J.H.S., Cornish-Bowden, A. (2000) Regulating the cellular economy of supply and demand. Federation of European Biochemical societies. 476, 47-51.
10. Kacser, H. and J.A. Burns. (1979) Molecular democracy: who shares the controls? Biochemical Society Transactions. 7, 1149-1160.
11. Kroukamp, O., Rohwer, J.M., Hofmeyer, J.H.S. and Snoep, J.L. (2002) Experimental supply demand analysis of anaerobic yeast energy metabolism. Molecular Biology Reports. 29, 203-209.
12. Schaaf, I., Heinisch, J. & Zimmermann, F.K. (1989) Yeast. 5, 285-290.
13. Teusink, B., J. Passarge, K.A. Reijenga, E. Esgalhado, C.C. Van der Weijden, M. Schepper, M.C. Walsh, B.M Bakker, K. Van Dam, H.V. Westerhoff & J.L. Snoep. (2000) Can yeast glycolysis be understood in terms of in vitro kinetics of the constituent enzymes? Testing biochemistry. European Journal of Biochemistry. 267:5313-5329.
14. Cornish-Bowden, A. & Cardenas, M.L. (1993) Channelling can affect concentrations of metabolic intermediates at constant net flux: artifact or reality? European Journal of Biochemistry. 213, 87-92.
15. Mendes, P., Kill, D.B. & Welch, G.R. (1995) Metabolic channeling in organized enzyme systems: experiments and models. Advances in Molecular and Cellular Biology. 11, 1-19.
16. Lagunas, R., Dominguez, C., Busturia, A. & Saez, M.J. (1982) Mechanisms of Appearance of the Pasteur Effect in *Saccharomyces cerevisiae*: Inactivation of Sugar Transport Systems. Journal of Bacteriology. 152, 19-25.
17. Lagunas, R. (1979) Energetic irrelevance of aerobiosis for *S. cerevisiae* growing on sugars. Molecular and Cellular Biochemistry. 27:139-146.

18. Hofmyer, J.H.S. & Cornish-Bowden, A. (1991) Quantitative assessment of regulation in metabolic systems. *European Journal of Biochemistry*. 200, 223-236.
19. Goncalvez, P. & Planta, R.J. (1998) Starting up yeast glycolysis. *Trends in Microbiology*. 6, 314-319.
20. Laurentt, M. & Seydoux, F.J. (1979) Allosteric Regulation of PFK. *Journal of Biological Chemistry*. 254, 7515-720
21. Jurika, M.S., Mesecar, A., Heath, P.J. Shi, W. Nowak, T. & Stoddard, B.L. (1998) The allosteric regulation of Pyruvate Kinase by F1,6BP. *Structure*. 6, 195-210.
22. Gancedo, C. & Serrano, R. (1989) in *The Yeasts* (Vol. 3).
23. Wildermuth, M.C. (2000) Metabolic control analysis: Biological applications and insights. *Genome Biology*. 1(6) reviews 103.1-103.5.
24. Fell DA (1992): Metabolic control analysis - a survey of its theoretical and experimental development. *Biochemical Journal*. 152, 313-330.
25. Hofmeyr, J.-H.S. (1995) *Journal of Bioenergetics and Biomembranes*. 27, 479-490.
26. Reich, J.G. & Sel'kov, E.E. (1981) *Energy Metabolism of the Cell*, Academic Press, London.
27. Cornish-Bowden, A. (1995) *Fundamentals of Enzyme Kinetics*, 2nd Edition, Portland Press, London.
28. Atkinson, D.E. (1977) *Cellular Energy Metabolism and its Regulation*, Academic Press, New York.
29. Cascante, M. & Mart, E. (1997) in: *New Beer in an Old Bottle: Eduard Buchner and the Growth of Biochemical Knowledge* (Cornish-Bowden, A., Ed.), pp. 199-214. Universitat de Valencia, Valencia.
30. Hofmeyr, J.-H.S. (1997) in: *New Beer in an Old Bottle: Eduard Buchner and the Growth of Biochemical Knowledge* (Cornish-Bowden, A., Ed.), pp. 225-242. Universitat de Valencia, Valencia.
31. Llorrens, M., Nunó, J.C., Rodriguez, Y., Melendéz-Hevia, E. and Montero, F. (1999) *Biophysical Journal*. 77, 23-36.
32. Heinrich, R. and Schuster, S. (1996) *The Regulation of Cellular Systems*, Chapman and Hall, New York.
33. Goldbeter, A. (1996) *Biochemical Oscillations and Cellular Rhythms*, Cambridge University Press, Cambridge.
34. Mazat, J.P., Letellier, T. & Reder, C. (1990) *Biomedica Biochimica Acta*. 49, 801-810.
35. Steuer, R., Gross, T., Selbig, J. & Belsius B. (2006) Structural Kinetic Modeling of Metabolic Networks. *The Proceedings of the National Academy of Sciences of the United States of America* 103, 11868-11873.
36. Palsson, B. O. (2000) *Nature Biotechnology*. 18, 1147-1150.
37. Kell, D. B. (2004) *Current Opinion in Microbiology*. 7, 296-307.
38. Fernie, A. R., Trethewey, R. N., Krotzky, A. J. & Willmitzer, L. (2004) *Nature Reviews Molecular Cell Biology*. 5, 1-7.

39. Westerhoff, H. V. & Palsson, B. O. (2002) *Nature Biotechnology*. 22, 1249–1252.
40. Palsson, B. O., Joshi, A. & Ozturk, S. S. (1987) *Federation Proceedings*. 46, 2485–2489.
41. Heinrich, R. & Schuster, S. (1996) *The Regulation of Cellular Systems* (Chapman & Hall, New York).
42. Hashimoto, K., Tomita, M., Takahashi, K., Shimizu, T. S., Matsuzaki, Y., Miyoshi, F., Saito, K., Tanida, S., Yugi, K., Venter, J. C. & Hutchison, C. A., III (1999) *Bioinformatics*. 15, 72–84.
43. Morohashi, M., Winn, A. E., Borisuk, M. T., Bolouri, H., Doyle, J. & Kitano, H. (2002) *Journal of Theoretical Biology*. 216, 19–30.
44. Stelling, J., Sauer, U., Szallasi, Z., Doyle, F. J., & Doyle, J. (2004) *Cell*. 118, 675–685.
45. Angeli, D., Ferrell, J. E., Jr. & Sontag, E. D. (2004) *The Proceedings of the Natural Academy of Sciences of the United States of America*. 101, 1822–1827.
46. Stephanopoulos, G. N., Alper, H. & Moxley, J. (2004) *Nature Biotechnology*. 22, 1261–1267.
47. Srivastavawz, R., Youw, L., Summersy, J. and Yinnw J. Stochastic vs. Deterministic Modeling of Intracellular Viral Kinetics (2002). *Journal of Theoretical Biology*. 218, 309-321.
48. Klamt S, Stelling J (2006) Stoichiometric and Constraint-based Modeling. In: *System Modeling in Cellular Biology*, Szallasi Z, Stelling J, Periwal V, eds. Cambridge, Massachusetts: MIT Press.
49. Gonzalez, M.I. Stuka, R., Blazquez, M.A., Feldman, H. & Gancedo, C. (1992) Molecular cloning of C1F1, a yeast gene necessary for growth on glucose. *Yeast*. 8, 183-192.
50. Thevelein, J.M. & Hohmann, S. (1995) Trehalose synthase: guard to the gate of glycolysis in yeast? *Trends in Biochemical Sciences*. 20, 3-10.
51. Teusink, B., Walsh, M.C., Van Dam, K. & Westerhoff, H.V. (1998) The danger of metabolic pathways with turbo design. *Trends in Biochemical Sciences*. 23, 162-169.
52. Luby-Phelps, K., Castle, P.E., Taylor, D.L., Lanni, F. (1987) Hindered diffusion of inert tracer particles in the cytoplasm of mouse 3T3 cells. *The Proceedings of the Natural Academy of Sciences of the United States of America*. 84, 4910–4913.
53. Allen, R. D. (1961) in *The Cell*, ed. Brachet, J. (Academic, NY), Vol. 2, pp. 135-216.
54. Clegg, J. S. (1984) *American Journal of Physiology*. 246, 133-151.
55. Conklin, E. G. (1940) in *The Cell and Protoplasm*, American Association for the Advancement of Science, No. 14., ed. Moulton, F. R. (Sci. Press, Lancaster, PA). 6-19.
56. Crick, F. H. C. & Hughes, A. F. W. (1950) The physical properties of cytoplasm- a Study by means of the magnetic particle method.1. Experimental. *Experimental Cell Research*. 1, 37-80.
57. Frey-Wyssling, A. (1953) *Submicroscopic Morphology of Protoplasm* (Elsevier, Amsterdam).
58. Fulton, A. B. (1982) How crowded is the cytoplasm? *Cell* 30, 345-347.
59. Pollard, T. D. (1976) *Journal of Supramolecular Structure*. 5, 317-334.
60. Pollard, T. D. (1984) in *White Cell Mechanics: Basic Science and Clinical Aspects*, eds. Meiselman, H. J., Lichtman, M. A. & LaCelle, P. L. (Liss, New York). 75-86.
61. Porter, K. R. (1984) *Journal of Cell Biology*. 99, 3-12.
62. Stossel, T. P. (1982) *Philosophical Transactions of the Royal Society of London. Series. B* 299, 275-289.
63. Taylor, D. L. & Condeelis, J. S. (1979) *International Review of Cytology*. 56, 57-144.

64. Taylor, D. L. & Fechheimer, M. (1982) *Philosophical Transactions of the Royal Society of London. Series. B* 299, 185-187.
65. Minton, A.P. (2006) How can biochemical reactions within cells differ from those in test tubes. *Journal of Cell Science*. 119, 2863-2869.
66. Minton, A. P. (2001). The influence of macromolecular crowding and macromolecular confinement on biochemical reactions in physiological media. *Journal of Biological Chemistry*. 276, 10577-10580.
67. Lebowitz, J. L., Helfand, E. & Praestgaard, E. (1965). Scaled particle theory of fluid mixtures. *Journal of Chemical Physics*. 43, 774-779.
68. Minton, A. P. (1998). Molecular crowding: analysis of effects of high concentrations of inert cosolutes on biochemical equilibria and rates in terms of volume exclusion. *Methods in Enzymology*. 295, 127-149.
69. Knull, H. & Minton, A. P. (1996). Structure within eukaryotic cytoplasm and its relationship to glycolytic metabolism. *Cell Biochemistry and Function*. 14, 237-248.
70. Giddings, J. C., Kucera, E., Russell, C. P. and Myers, M. N. (1968). Statistical theory for the equilibrium distribution of rigid molecules in inert porous networks. *Exclusion chromatography. Journal of Physical Chemistry*. 72, 4397-4408.
71. Minton, A. P. (1992). Confinement as a determinant of macromolecular structure and reactivity. *Biophysical Journal*. 63, 1090-1100.
72. Cutsforth, G., Whitaker, R., Hermans, J. and Lentz, B. (1989). A new model to describe extrinsic protein binding to phospholipid membranes of varying composition: application to human coagulation proteins. *Biochemistry*. 28, 7453-7461.
73. Knull, H. R. and Walsh, J. L. (1992). Association of glycolytic enzymes with the cytoskeleton. *Current Topics in Cellular Regulation*. 33, 15-30.
74. Lakatos, S. and Minton, A. P. (1991). Interactions between globular proteins and F-actin in isotonic saline solution. *Journal of Biological Chemistry*. 266, 18707-18713.
75. Arbuzova, A., Murray, D. & McLaughlin, S. (1998). MARCKS, membranes, and calmodulin: kinetics of their interaction. *Biochimica et Biophysica Acta*. 1376, 369-379.
76. Minton, A. P. (1995). Confinement as a determinant of macromolecular structure and reactivity. II. Effects of weakly attractive interactions between confined macrosolutes and confining structures. *Biophysical Journal*. 68, 1311-1322.
77. Chandler, D. (1987) *Introduction to Modern Statistical Mechanics*. The Clarendon Press, Oxford University Press, New York.
78. Goodsell, D.S. (1993). *The Machinery of Life*. Springer, New York.
79. Kopelman, R. (1986) Rate-processes on fractals—theory, simulations, and experiments. *Journal of Statistical Physics*. 42, 185–200.
80. Luby-Phelps, K., Taylor, D. L. & Lanni, F. (1986) *Journal of Cell Biology*. 102, 2015-2022.
81. Michaelis, L., Menten, M.L. (1913) Die kinetik der invertinwirkung. *Biochemische Zeitschrift*. 49, 333–369.

82. Minton, A.P. (1981) Excluded volume as determinant of macromolecular structure and reactivity. *Biopolymers*. 20, 2093–2120.
83. Zimmerman, S.B. (1993) Macromolecular crowding effects on macromolecular interactions: some implications for genome structure and function. *Biochimica et Biophysica Acta*. 1216, 175–185.
84. Heinrich, R., Schuster, S. (1996) *The Regulation of Cellular Systems*. Chapman and Hall, New York.
85. Brooks, D.E. (2000) Can cytoplasm exist without undergoing phase separation? *International Review on Cytology*. 192, 321–330.
86. Ovladi, J., Batke, J., Bartha, F., Keleti, T. (1979) Effect of association–dissociation on the catalytic properties of glyceraldehyde 3-phosphate dehydrogenase. *Archives of Biochemistry and Biophysics*. 193, 28–33.
87. Palsson, B.O., Palsson, H., Lightfoot, E.N. (1985) Mathematical modeling of dynamics and control in metabolic networks. III. Linear reaction sequences. *Journal of Theoretical Biology*. 113 (2), 231–259.
88. Schroeder, M. (1991) *Fractals, Chaos, Power Laws*. W.H. Freeman and Company, New York.
89. Srere, P., Jones, M.E., Mathews, C. (1989) *Structural and Organizational Aspects of Metabolic Regulation*. Alan R. Liss, New York.
90. Rivas, G., Fernandez, J.A., Minton, A.P. (2001) Direct observation of the enhancement of noncooperative protein selfassembly by macromolecular crowding: indefinite linear self-association of bacterial cell division protein FtsZ. *The Proceedings of the Natural Academy of Sciences of the United States of America*. 98, 3150–3155.
91. Schnell, S. & Turner, T.E. (2004) Reactions in intracellular environments with macromolecular crowding: simulations and rate laws. *Progress in Biophysics and Molecular Biology* 85, 235–260.
92. Gershon, N.D., Porter, K.R., Trus, B.L. (1985) The cytoplasmic matrix: its volume and surface area and the diffusion of molecules through it. *The Proceedings of the Natural Academy of Sciences of the United States of America*. 82, 5030–5034.
93. Minton, A.P. (2001). The influence of macromolecular crowding and macromolecular confinement on biochemical reactions in physiological media. *Journal of Biological Chemistry*. 276, 10577–10580.
94. Laurent, T.C. (1971). Enzyme reactions in polymer media. *European Journal of Biochemistry*. 21, 498–506.
95. Savageau, M.A. (1976) *Biochemical Systems Analysis: A Study of Function and Design in Molecular Biology*. Addison-Wesley, Reading, MA.
96. Savageau, M.A. (1992) A critique of the enzymologist's test tube. In: Bittar, E.E. (Ed.), *Fundamentals of Medical Cell Biology*, Vol. 3A. Academic Press, New York, pp. 45–108.
97. Kopelman, R. (1988). Fractal reaction kinetics. *Science*. 241, 1620–1626.
98. Hornak, J.P (1997-1999). *The Basics of NMR*. www.cis.rit.edu/htbooks/nmr
99. Wilson, K. and Walker, J. *Principles and techniques of Biochemistry and Molecular Biology* 6th Edition. Cambridge University Press (2005). Chapter 13, 593-620.

100. Diehl, B.W.K., Malz, F., Holzgrabe, U. (2007) Quantitative NMR spectroscopy in the quality evaluation of active pharmaceutical ingredients in excipients. *Spectroscopy Europe*. 19, 15-19.
101. Metz, K.R., Lam, M.M. & Webb., A.G. (199) Reference Deconvolution: A Simple and Effective Method for Resolution Enhancement in Nuclear Magnetic Resonance Spectroscopy. *Concepts in Magnetic resonance*. 12, 21-42.
102. Biggler, P. (2000) *NMR Spectroscopy: Processing Strategies*. 2nd Updated Edition. Published by Wiley-VCH. 203-204.
103. Grivet, J.P., Delort, A.M. (2008) NMR for microbiology: In Vivo and in situ applications. *Progress in Nuclear Magnetic Resonance Spectroscopy*. 54, 1-53.
104. Ugurbil, K., Brown, T.R., Den Hollander, J.A., Glynn, P. & Shulman, R.G. (1978) High Resolution ¹³C NMR studies of glucose metabolism in E.coli. *The Proceedings of the National Academy of Sciences of the United States of America*. 75, 3742-3746.
105. Melvin, B.K. & Shanks, J.V. (1996) Influence of aeration on cytoplasmic pH of yeast in an NMR airlift bioreactor. *Biotechnology Progress*. 12, 257–265.
106. Navon, G., Ogawa, S., Shulman, R. G. & Yamane, T. (1977) *The Proceedings of the National Academy of Sciences of the United States of America*. 74, 888-891.
107. Hoult, D. I., Busby, S. J. N., Gadian, D. G., Radda, G. K., Richards, R. E. & Seeley, P. J. (1974) *Nature*. 252, 285-287.
108. Burt, C. T., Glonek, T. & Barany, M. (1976) *Journal of Biological Chemistry*. 251, 2584-2591.
109. Jacobus, W. E., Tayler, G. J., Weisfeldt, M. L., Nunnally, R. L. & Hollis, D. P. (1977) in *Symposium on Cellular Function and Molecular Structure (University of Missouri, Columbia, MO, May, 1977)*, Abstract. no. 13.
110. Gashan, D. G., Hoult, D. I., Radda, G. K., Seeley, P. J., Chance, B. & Barlow, C. (1976) *The Proceedings of the National Academy of Sciences of the United States of America*. 73, 4446-4448.
111. S. Ogawa, H. Rottenberg, T.R. Brown, R. G. Shulman, C.L. Castillo and P. Glynn. (1978) High Resolution ³¹P NMR study of rat liver mitochondria. *The Proceedings of the National Academy of Sciences of the United States of America*. 75, 1796-1800.
112. Sheldon, J.G., Williams, S.P., Fulton, A.M. & Brindle, K.M. (1996) ³¹P NMR magnetization transfer study of the control of ATP turnover in *Saccharomyces cerevisiae*. *The Proceedings of the National Academy of Sciences of the United States of America*. 93, 6399–6404.
113. Ma, P., Goncalves, T., Marezek, A., Loureiro Dias, M.C. & Thevelein, J.M. (1997) The lag phase rather than the exponential-growth phase on glucose is associated with a higher cAMP level in wild-type and cAPK attenuated strains of the yeast *Saccharomyces cerevisiae*. *Microbiology*. 143, 3451–3459.
114. Konrad, M. (1988) Analysis and in vivo disruption of the gene coding for adenylate kinase (ADK1) in the yeast *Saccharomyces cerevisiae*. *Journal of Biological Chemistry*. 263, 19468–19474.
115. Walsh, K. & Koshland Jr., D.E. (1984) Determination of flux through the branch point of two metabolic cycles. *Journal of Biological Chemistry*. 259, 9646–9654.

116. Den Hollander, J.A., Ugurbil, K., Brown, T.R., Bednar, M., Redfield, C. & Shulman, R.G. (1986) Studies of anaerobic and aerobic glycolysis in *Saccharomyces cerevisiae*. *Biochemistry*. 25, 203–211.
117. Szyperski, T. (1995) Biosynthetically directed fractional ¹³C-labeling of proteinogenic amino acids. An efficient analytical tool to investigate intermediary metabolism, *European Journal of Biochemistry*. 232, 433–448.
118. Marx, A., de Graaf, A.A., Wiechert, W., Eggeling, L. & Sahm, H. (1996) Determination of the fluxes in the central metabolism of *Corynebacterium glutamicum* by nuclear magnetic resonance spectroscopy combined with metabolite balancing. *Biotechnology and Bioengineering*. 49, 111–129.
119. de Graaf, A.A., Mahle, M., Möllney, M., Wiechert, W., Stahmann, P. & Sahm, H. (2000) Determination of full ¹³C isotopomer distributions for metabolic flux analysis using heteronuclear spin echo difference NMR spectroscopy. *Journal of Biotechnology*. 77, 25–35.
120. Lawson, J. W. R. & Veech, R. L. (1979). Effect of pH and free Mg²⁺ on the K_{eq} of the creatine kinase reaction and other phosphate hydrolysis and phosphate transfer reactions. *Journal of Biological Chemistry*. 254, 6528–6537.
121. Teague, W. E. J. & Dobson, G. P. (1992). Effect of temperature on the creatine kinase equilibrium. *Journal of Biological Chemistry*. 267, 14084–14093.
122. Veech, R. L., Lawson, J. W. R., Cornell, N. W. & Krebs, H. A. (1979) Cytosolic phosphorylation potential. *Journal of Biological Chemistry*. 254, 6538–6547.
123. Chance, B., Leigh J. S., Clark, B. J., Maris, J., Kent, J., Nioka, S. & Smith, D. (1985). Control of oxidative metabolism and oxygen delivery in human skeletal muscle: A steady-state analysis of the work/energy cost transfer function. *The Proceedings of the Natural Academy of Sciences of the United States of America*. 82, 8384–8388.
124. Chance, B., Leigh, J. S., Mccully, K., Nioka, S., Clark, B. J., Maris, J. M. & Graham, T. (1986). Multiple controls of oxidative metabolism in living tissues as studied by phosphorus magnetic resonance. *The Proceedings of the Natural Academy of Sciences of the United States of America*. 83, 9458–9462.
125. Chance, B., Leigh, J. S., Mclaughlin, A. C., Schnall, M. & Sinnwell, T. (1988). Phosphorus-31 spectroscopy and imaging. In *Magnetic Resonance Imaging*, vol. 2 (ed. Partain, C.L., Price, R.R., Patton, J.A., Kulkarni, M.V. & James, A.E.), pp. 1501–1520. New York: W. B. Saunders Co.
126. Golding, E., Teague, W.E.J. & Dobson, G.P. (1995) Adjustment of K' to varying pH & Mg²⁺ for the creatine kinase, adenylate kinase and ATP hydrolysis equilibria permitting quantitative bioenergetic assessment. *Journal of Experimental Biology*. 198, 1775-1782.
127. Ellington, R.W. (1989) Phosphocreatine represents a thermodynamic and functional improvement over other muscle phosphagens. *Journal of Experimental Biology*. 143, 177-194.
128. Hanekom, A.J. (2007) Personal Communications.
129. Moon, R.B. & Richards, J.H. (1973) Determination of intracellular pH by ³¹P Magnetic Resonance. *Journal of Biological Chemistry*. 248, 7276-7278.

130. Den Hollander, J.A., Ugurbil, K. & Shulman, R.G. (1986) ^{31}P and ^{13}C NMR studies of intermediates of aerobic and anaerobic Glycolysis in *Saccharomyces cerevisiae*. *Biochemistry*. 25, 212-219.
131. Den Hollander, J.A., Ugurbil, K., Brown, T.R. & Shulman, R.G. (1981) Phosphorous- ^{31}P NMR studies of the effect of oxygen upon glycolysis in yeast. *Biochemistry*. 20, 5871-5880.
132. Salhany, J.M., Yamane, T., Shulman, R.G. & Ogawa, S. (1975) High resolution ^{31}P nuclear magnetic resonance studies of intact yeast cells. *The Proceedings of the Natural Academy of Sciences of the United States of America*. 72, 4966-4970.
133. Gueron, M. & Shulman, R. G. (1975) *The Proceedings of the Natural Academy of Sciences of the United States of America*. 72, 3482-3485.
134. Brindle, K., Braddock, P., Fulton, S. (1990) ^{31}P NMR Measurements of the ADP concentration in Yeast Cells genetically Modified To Express Creatine Kinase. *Biochemistry*. 29, 3295-3302.
135. Shanks, J.V. (2001). In situ NMR systems. *Current Issues in Molecular Biology*. 3, 15-26.
136. Aime, S., Botta, M., Fasano, M. & Terreno, E. (1998) Lanthanide(III) chelates for NMR biomedical applications. *Chemical Society Reviews*. 27, 19-29.
137. NMR spectroscopy. www.cem.msu.edu/~reusch/virtualtext/spectrpy/nmr/nmr1.htm (III)
138. Larsson, C., Nilsson, A., Blomberg, A. & Gustafsson, L. (1997) Glycolytic Flux Is Conditionally Correlated with ATP Concentration in *Saccharomyces cerevisiae*: a Chemostat Study under Carbon or Nitrogen-Limiting Conditions. *Journal of Bacteriology*. 23, 7243-7250.
139. Bradford, M. (1976) A rapid and sensitive method for the quantitation of μg quantities of protein utilizing the principle of protein dye binding. *Analytical Biochemistry*. 72, 2482-54.
140. Den Hollander, J.A., Brown, T.R., Ugurbil, K., & Shulman, R.G. (1979) ^{13}C NMR studies of yeast cell suspensions. *The Proceedings of the Natural Academy of Sciences of the United States of America*. 76, 6096-6100.
141. Serrano, R., Gancedo, J.M. & Gancedo, C. (1973) Assay of Yeast Enzymes In Situ: A potential Tool in Regulation Studies. *European Journal of Biochemistry*. 3, 479-482.
142. Reeves, R. E. & Sols, A. (1973) Regulation of *Escherichia coli* phosphofructokinase 'in situ'. *Biochemical and Biophysical Research Communications*. 50, 459-466.
143. Grisolia, S. & Cleland, W. W. (1968) *Biochemistry*. 7, 1115-1121.
144. Takeshige, K. & Ouchi, K. (1995) Reconstruction of Ethanol Fermentation in Permeabilized Cells of the Yeast *Saccharomyces cerevisiae*. *Journal of Fermentation and Bioengineering*. 79, 11-16.
145. Gancedo, J. M., Gancedo, C. & Sols, A. (1967) *Biochemistry Journal*. 102, 23-25.
146. Van Aelst, L., Hohmann, S., Bulaya, B., de Koning, W., Sierkstra, L., Neves, M.J., Luyten, K., Alijo, R., Ramos, J., Coccetti, P., Martegani, E., de Magalhães-Rocha, N.M., Brandão, R.L., Van Dijck, P., Vanhalewyn, M., Durnez, P., Jans, A.W.H. & Thevelein, J.M. (1993) Molecular cloning of a gene involved in glucose sensing in the yeast *Saccharomyces cerevisiae*. *Molecular Microbiology*. 8, 927-943.
147. Bell, W, Klaassen P, Ohnacker M, Boller T, Herweijer M, Schoppink P, van der Zee P, Wiemken A. (1992) Characterization of the 56 kDa subunit of yeast trehalose-6-phosphate synthase and

- cloning of its gene reveal its identity with the product of *CIF1*, a regulator of carbon catabolite inactivation. *European Journal of Biochemistry* 209, 951–959.
148. Vuorio, O. E., Kalkkinen, N. & Londesborough, J. (1993) Cloning of two related genes encoding the 56-kDa and 123-kDa subunits of trehalose synthase from the yeast *Saccharomyces cerevisiae*. *European Journal of Biochemistry*. 216, 849–861.
 149. Van der Poll, K. W., Kerkenaar, A. & Schamhart, D. H. (1974) Isolation of a regulatory mutant of fructose-1,6-diphosphatase in *Saccharomyces carlsbergensis* *Journal of Bacteriology*. 117, 965–970 .
 150. Navon, G., Shulman, R.G., Yamane, T., Eccleshall, T.R., Lam, K.B., Baronofsky, J.J. & Marmur, J. (1979) Phosphorus-31 Nuclear Magnetic Resonance Studies of Wild-Type and Glycolytic Pathway Mutants of *Saccharomyces Cerevisiae*. *Biochemistry* 18, 4487–4498 .
 151. Van Aelst, L., Hohmann, S., Zimmermann, F.K., Jans, A.W.H. & Thevelein, J.M. (1991) A yeast homologue of the bovine lens fibre MIP gene family complements the growth defect of a *Saccharomyces cerevisiae* mutant on fermentable sugars but not its defect in glucose-induced RAS-mediated cAMP signalling *The EMBO Journal*. 10, 2095–2104.
 152. Hohmann, S., Neves, M. J., de Koning, W., Alijo, R., Ramos, J. and Thevelein, J. M. (1993) The growth and signalling defects of the *ggs1 (fdp1/byp1)* deletion mutant on glucose are suppressed by a deletion of the gene encoding hexokinase PII. *Current Genetics*. 23, 281–289.
 153. Hohmann, S., Bell, W., Neves, M. J., Valckx, D. & Thevelein, J. M. (1996) Evidence for trehalose-6-phosphate-dependent and -independent mechanisms in the control of sugar influx into yeast glycolysis. *Molecular Microbiology*. 20, 981–991.
 154. Fitts, R. H. (1994). Cellular mechanisms of muscle fatigue. *Physiological Reviews*. 74, 49–94.
 155. Hazan, R, Levine A. and Abeliovich, H. (2004) Benzoic Acid, a Weak Organic Acid Food Preservative, Exerts Specific Effects on Intracellular Membrane Trafficking Pathways in *Saccharomyces cerevisiae*. *Applied and Environmental Microbiology*. 70, 4449–4457.
 156. Holyoak, C. D., Bracey, D., Piper, P.W., Kuchler, K. & Coote, P.J. (1999). The *Saccharomyces cerevisiae* weak-acid-inducible ABC transporter Pdr12 transports fluorescein and preservative anions from the cytosol by an energy dependent mechanism. *Journal of Bacteriology*. 181:4644–4652.
 157. Basketter, D.A. & Widdas, W.F. (1978) Asymmetry of the hexose transfer system in human erythrocytes. Comparison of the effects of cytochalasin B, phloretin and maltose as competitive inhibitors. *Journal of Physiology*. 278, 389–401.
 158. Gonzalez, B., de Graaf, A.A., Renaud, M. & Sahm, H. (2000) Dynamic in vivo ³¹P nuclear magnetic resonance study of *Saccharomyces cerevisiae* in glucose-limited chemostat culture during the aerobic-anaerobic shift. *Yeast*. 16, 483–497.
 159. van Dijken, J.P. & Scheffers, W.A. (1986) Redox balances in the metabolism of sugars by yeasts. *FEMS Microbiology Reviews*. 32, 199–224.
 160. Diderich, J.A., Teusink, B., Valkier, J., Anjos, J., Spencer-Martins, I., van Dam, K. & Walsh, M.C. (1999) Strategies to determine the extent of control exerted by glucose transport on glycolytic flux in the yeast *Saccharomyces bayanus*. *Microbiology*. 145, 3447–3454.

161. Reijenga, K.A., J.L. Snoep, J.A. Diderich, H.W. van Verseveld, H.V. Westerhoff and Teusink, B. (2001) Control of glycolytic dynamics by hexose transport in *Saccharomyces cerevisiae*. *Biophysical Journal*. 80, 626–634.
162. Snoep, J.L., Mrwebi, M., Schuurmans, J.M., Rohwer, J.M & Teixeira de Mattos, M.J. (2010). Control of specific growth rate in *Saccharomyces cerevisiae*. *Microbiology*. 155, 1699-1707.
163. Gonzalez, B., Francqios, J. & Renaud, M. (1997) A Rapid and Reliable Method for Metabolite Extraction in Yeast using Boiling Buffered Ethanol. *Yeast*. 13, 1347-1356.
164. Barrow, K.D. Collins, J.G., Norton, R.S., Rogers, P.L. & Smith, G.M. (1984) ³¹P Nuclear Magnetic Resonance Studies of the Fermentation of Glucose to Ethanol by *Zymomonas mobilis*. *Journal of Biochemistry*. 259, 5711-5716.
165. Richard, P., Teusink, B., Hemker, M.B., Van Dam, K. & Westerhoff, H.V. (1996) Sustained oscillations in free energy state and hexose phosphates in yeast. *Yeast*. 12, 731-740.
166. Teusink, B., Diderich, J.A., Van Dam, K., Westerhoff, H.V. & Walsh, M.C. (1998) Intracellular glucose concentration in derepressed yeast cells consuming glucose is high enough to reduce the glucose transport rate by 50%. *Journal of Bacteriology*. 180, 556-562.
167. Yamada, E.A., Sgarbieri, V.C. (2005) Yeast (*Saccharomyces cerevisiae*) protein concentrate: preparation, chemical composition, and nutritional and functional properties. *Journal of Agricultural and Food Chemistry*. 53, 3931-6.
168. Hofmeyr, J.-H.S. & Rohwer, J.M. (2008) Control analysis of adenylate-conserving cycles in the absence or presence of adenylate kinase. In: *BioThermoKinetics in the Post Genomic Era* (Larsson, C., Pålman, I.-L. & Gustafsson, L., eds.) pp. 7-10, Chalmers Reproservice, Göteborg.